Summer 2019

Development of test methods for characterizing extrudability of cement-based materials for use in 3D printing

Jonathan Thomas Kuchem

Department:

DEVELOPMENT OF TEST METHODS FOR CHARACTERIZING EXTRUDABILITY OF CEMENT-BASED MATERIALS FOR USE IN 3D PRINTING

by

JONATHAN THOMAS KUCHEM

A THESIS

Presented to the Faculty of the Graduate School of the

MISSOURI UNIVERSITY OF SCIENCE AND TECHNOLOGY

In Partial Fulfillment of the Requirements for the Degree

MASTER OF SCIENCE IN CIVIL ENGINEERING

2019

Approved by:

Dr. Nicolas Libre, Advisor
Dr. Kamal Khayat
Dr. Mohamed ElGawady

ABSTRACT

3D printing is the process of creating three-dimensional objects using an automated additive manufacturing process. The 3D printing process has been used with materials such as metals and polymers, but application with cement based materials for the construction industry has yet to be developed. In this research, two main problems were investigated for printing cement based composite materials: extrudability and tensile reinforcement. Fiber-reinforced concrete (FRC) was studied as an internal reinforcing system to increase tensile/flexural strength. First, FRC was studied to investigate mechanical properties and use of fibers from waste tires as an environmentally friendly option. A reference mixture with no fibers, three mixtures with manufactured steel fibers, three mixtures with recycled steel fibers, and a hybrid mixture were studied. Three-point bending, compression, and modulus of elasticity tests were performed. In addition, three mixtures were made for cast and printed beams to compare the effect of printing process on fiber orientation and strength. An automated extrusion device was developed for printing and to quantitatively analyze extrusion. Test methods were developed to investigate blockage and extrusion force. Particle size, rheology, nozzle diameter, and extrusion speed were evaluated. Results showed that fibers improves flexural performance and recycled fibers provide a similar benefit to manufactured fibers. Printing fibers improved fiber orientation and post-crack properties. Different cracking mechanism were found when printing versus casting beams. The developed extrusion tests provided a successful way to quantify the extrudability. It was found that the extrusion force and energy depend on nozzle size, yield stress, and extrusion speed.

ACKNOWLEDGMENTS

First, I would like to thank my adviser, Dr. Nicolas Libre. He has provided guidance, support, and mentorship throughout my undergraduate and graduate career and encouraged me to pursue graduate school through the Greenberg Scholars program. His help within this project and other aspects of my academic career has helped me grown to the engineer I am today. I would also like to thank the other members of my committee, Dr. Kamal Khayat and Dr. Mohamed ElGawady, for their review of this document and for being great professors within my coursework.

I would like to thank Iman Mehdipour for assistance with design and making of the recycled fiber portion of the project. I would like to thank the help of Kelsey Bloom, Mustafa Abdulridha, and Jordan Pugh for help in the lab while running tests. I would also like to thank Daniel Ellerbrock for advice and help with wiring and programming the extrusion system as this area of electronics was completely new to me before starting this project. I would also like to thank the support of BCH and CIES staff including the Greg Leckrone, John Bullock, Jason Cox, and Brian Swift for help with equipment and other various items on the project. I would also like to CIES research center for use of their facilities and resources.

Finally, I would like to thank my friends and family who have helped support me throughout my academic career. A special thanks to my parents, Steve and Chris Kuchem, and my sister, Jaimie Kuchem for encouraging me throughout the pursuit of my Master's degree and supporting me in whatever way needed.

TABLE OF CONTENTS

Page

ABSTRACT iii

ACKNOWLEDGMENTS iv

LIST OF ILLUSTRATIONS ix

LIST OF TABLES xiv

NOMENCLATURE xv

SECTION

1. INTRODUCTION 1

1.1. BACKGROUND 1

1.2. SCOPE AND OBJECTIVES 3

1.3. THESIS ORGANIZATION 5

2. LITERATURE REVIEW 7

2.1. 3D PRINTING CEMENT BASED MATERIAL 7

2.1.1. Mix Design and Fresh Properties of 3D Printed Cementitious Material. 8

2.1.2. Printing with Fibers. 14

2.1.3. Extrusion of 3D Printed Concrete. 19

2.1.4. Other Studies in 3D Printing. 21

2.2. FIBER REINFOREMENT CONCRETE 25

2.2.1. General Fiber Reinforced Concrete Mechanical Behavior 26

2.2.2. Studies with Recycled Fibers 30

2.3. RHEOLOGY OF FIBER REINFORCED CEMENT-BASED MATERIALS 32

2.3.1. General Rheology of Cementitious Materials. 33

2.3.2. Fiber Effect on Rheology. 37

2.3.3. Rheology Effect on 3D Printing and Extrusion..... 41

2.4. EXTRUSION OF CEMENTITIOUS MATERIAL 45

2.4.1. Characteristics of Extruded Paste. 45

2.4.2. Measurement Methods of Extrusion. 50

3. METHODS..... 54

3.1. MATERIAL CHARACTERIZATION 54

3.2. MECHANICAL PROPRETIES OF FIBER REINFORCED CONCRETE 58

3.2.1. Mix Design 58

3.2.2. Mechanical Properties Testing 59

3.3. EXTRUSION BLOCKAGE TEST 61

3.3.1. Blockage Test Variables..... 61

3.3.2. Procedure and Test Matrix 63

3.4. RHEOLOGICAL MEASUREMENTS 68

3.5. RAM EXTRUSION TEST FOR PRINTING..... 72

3.5.1. Extruder Design..... 72

3.5.2. Testing Parameters and Materials 76

3.5.3. Testing Procedure..... 78

3.6. FLEXURAL TESTING OF PRINTED AND CAST SPECIMENS 81

3.6.1. Specimen Casting and Printing 81

3.6.2. Hardened Property Tests 85

4. RESULTS..... 91

4.1. FIBERS AS A REINFORCING SYSTEM IN CAST CONCRETE 91
4.1.1. Fiber Effect on Workability 91
4.1.2. Compressive Behavior 93
4.1.3. Flexural Behavior 96
4.2. BLOCKAGE TESTING 103
4.2.1. Effect of Max Particle Size, Workability, and Binder Content 104
4.2.2. Fiber Blockage 107
4.2.3. Evaluation of the Test Method and Future Studies 108
4.3. RHEOLOGICAL RESULTS 110
4.3.1. Transformation to Yield Stress and Plastic Viscosity 110
4.3.2. Results for Mixtures 113
4.4. EXTRUSION TESTING 115
4.4.1. Raw Results and Data from Extrusion Tests 116
4.4.2. Effect of Nozzle Size 119
4.4.3. Effect of Extrusion Rate 123
4.4.4. Effect of Workability on Extrusion 126
4.4.5. Effect of High Extrusion Pressure 128
4.5. EFFECT OF PRINTING OF MECHANICAL PROPERTIES 129
4.5.1. Compressive Strength 129
4.5.2. Flexural Results 131
5. CONCLUSION 144
5.1. SUMMARY 144
5.2. CONCLUSIONS 145

5.3. FUTURE WORK 149

APPENDICES

A. EXTRUDER DESIGN 152

B. EXTRUDER CODE 159

BIBLIOGRAPHY 163

VITA 172

LIST OF ILLUSTRATIONS

Page

Figure 1.1. Examples of 3D Printed Structures [5] 2

Figure 2.1. Layer Stability Test [10] 10

Figure 2.2. “Cylinder Stability” Test [10] 10

Figure 2.3. Printed Specimens with Various Geometries and Hierarchical Structures [18] 15

Figure 2.4. Different Extruder Types: (a) Ram Extruder [24] (b) Progressive Cavity Pump (c) Peristalic Concrete Pump [25] 19

Figure 2.5. Qualitative Extrusion Test [14] 20

Figure 2.6. Different Print Architectures [31] 24

Figure 2.7. Implementation Example of 3D Printing: Pedestrian Bridge [6] 25

Figure 2.8. Area for Evaluating Toughness and Post-Cracking Behavior of FRC [37] ... 27

Figure 2.9. ASTM C1018 Toughness Indices 28

Figure 2.10. Long versus Short Fiber Crack Mitigation [38] 30

Figure 2.11. Common Rheological Models for Cementitious Materials [51] 34

Figure 2.12. Errors Due to Structural Build-up (Top) and Plug Flow (Bottom) 35

Figure 2.13. Relative Yield Stress vs Relative Packing Fraction [57] 38

Figure 2.14. Fiber Volume Fraction Effect on Rheological Properties 39

Figure 2.15. Viscosity versus Yield Stress for Extrudability [65] 43

Figure 2.16. Forces and Flow Zones in Extruded Paste [68] 46

Figure 2.17. Schematic of Flow Cases for Extrusion [64] 48

Figure 2.18. Penetration Test Extrudability Window Example [71] 51

Figure 2.19. Ram Extrusion Test Schematic [26] 52

Figure 2.20. Squeeze Flow Test prior to Start [70] 53

Figure 3.1. Recycled Fibers (Left) vs Manufactured Fibers (Right) 55

Figure 3.2. Sand Sizes for Blockage Test 57

Figure 3.3. Sand Gradation for Sieved Sand 57

Figure 3.4. Modulus of Elasticity Test Set Up 59

Figure 3.5. Three Point Bending Test 60

Figure 3.6. Three Point Bending Schematic 61

Figure 3.7. Blockage Test Parameter Overview 62

Figure 3.8. Extrusion Syringe Dimensions 64

Figure 3.9. Flow Table Apparatus and Setup 65

Figure 3.10. Flow Table Test Before and After 25 Table Hits 66

Figure 3.11. ConTec 6 Viscometer 69

Figure 3.12. Mortar Bucket Used in the Rheometer 71

Figure 3.13. Rheometer Test Parameters 71

Figure 3.14. Extruder Test Setup 74

Figure 3.15. Schematic of Extruder 75

Figure 3.16. Electronic Schematic of the Extrusion System 76

Figure 3.17. Syringes with Modified Diameters 78

Figure 3.18. Hobart Mixer 79

Figure 3.19. Extrusion Test in Progress 81

Figure 3.20. Beam Manual Printing Process 84

Figure 3.21. Cutting Ends of Printed Beams 84

Figure 3.22. Cube Compression Test Setup..... 85

Figure 3.23. Cast Beam Three-Point Bending Setup..... 86

Figure 3.24. Manual Printed Beam Three-Point Bending Setup 87

Figure 3.25. Printed Beam Cross-Section Analysis Outline of Picture 88

Figure 3.26. AutoCAD Outline of Printed Beam Cross Section 89

Figure 4.1. Superplasticizer Demand versus Fiber Volume 92

Figure 4.2. Compression Stress vs Strain Graph for Casted FRC Specimens..... 95

Figure 4.3. Modulus of Elasticity Results- REF vs 0.25% Fibers 95

Figure 4.4. Flexural Load vs Deflection for REF vs 0.25% Fiber Mixtures 99

Figure 4.5. Flexural Load vs Deflection for REF vs 0.50% Fiber Mixtures 99

Figure 4.6. Flexural Load vs Deflection for REF vs 0.75% Fiber Mixtures 100

Figure 4.7. Flexural Load vs CMOD for REF vs 0.25% Fibers 100

Figure 4.8. Flexural Load vs CMOD for REF vs 0.50% Fibers 101

Figure 4.9. Flexural Load vs CMOD for REF vs 0.75% Fibers 101

Figure 4.10 CMOD vs Deflection..... 102

Figure 4.11. Blocking Binder Content vs Maximum Particle Size % of Nozzle Diameter..... 105

Figure 4.12. Different Blocking Mechanisms..... 106

Figure 4.13. Fiber Blockage..... 107

Figure 4.14. Conceptual Effect of improving Packing Density and Grading on Blockage 109

Figure 4.15. Torque versus Step to Check for Equilibrium..... 110

Figure 4.16. Torque versus Rotational Velocity for Rheology..... 111

Figure 4.17. Shear Stress versus Shear Rate for M-0.05 and M-0.3..... 113

Figure 4.18. Shear Stress versus Shear Rate for MF-0.05 and MF-0.3 114

Figure 4.19. Example of Raw Data graphed for Extrusion Test..... 117

Figure 4.20. Extrusion Test Load versus Displacement Parameters 117

Figure 4.21. Low Workability (M-0.05) Extrusion Force versus Displacement..... 120

Figure 4.22. High Workability (M-0.3) Extrusion Force versus Displacement 120

Figure 4.23. Average Extrusion Load versus d/D ratio 121

Figure 4.24. Maximum Extrusion Load versus d/D ratio 121

Figure 4.25. UEE versus d/D ratio..... 122

Figure 4.26. F_y versus d/D ratio 123

Figure 4.27. Extrusion Force versus Displacement for Varying Speeds 124

Figure 4.28. Average Extrusion Force versus Extrusion Speed 125

Figure 4.29. Max Extrusion Force versus Extrusion Speed..... 125

Figure 4.30. UEE versus Extrusion Speed..... 126

Figure 4.31. High versus Low Workability for 3 mm Opening..... 127

Figure 4.32. High versus Low Workability for 6 mm Opening..... 127

Figure 4.33. High versus Low Workability for 9 mm Opening..... 128

Figure 4.34. Dry Consolidated Mortar Due to High Extrusion Pressure..... 129

Figure 4.35. Cube Compressive Failure Comparison..... 130

Figure 4.36. Load versus Deflection for Printed versus Cast Beams 132

Figure 4.37. Load versus Deflection for REF (without fibers) Printed vs Cast Beams.. 133

Figure 4.38. Load versus Deflection for F-0.25 Printed vs Cast Beams 133

Figure 4.39. Load versus Deflection for F-0.50 Printed vs Cast Beams 134

Figure 4.40. First-Crack Strength Comparison for Printed versus Cast Beams 136

Figure 4.41. Printing Gaps in Cross Section 138

Figure 4.42. I_5 Toughness Comparison for Printed versus Cast Beams 138

Figure 4.43. I_{10} Toughness Comparison for Printed versus Cast Beams 139

Figure 4.44. I_{20} Toughness Comparison for Printed versus Cast Beams 139

Figure 4.45. $R_{5,10}$ Residual Strength Comparison for Printed versus Cast Beams 140

Figure 4.46. $R_{10,20}$ Residual Strength Comparison for Printed versus Cast Beams 140

Figure 4.47. Fiber Orientation Factor for Printed versus Cast Beams 141

Figure 4.48. Crack Pattern Comparison Between Cast and Printed Beams 142

Figure 4.49. Crack Pattern Schematic 143

LIST OF TABLES

Page

Table 3.1. Fiber Properties 55

Table 3.2. Mixture Proportions for FRC Study 59

Table 3.3. Blockage Test Mixture Proportion Options 68

Table 3.4. Mixture Proportions for Extrusion and Rheology Tests 77

Table 3.5. Manual and Cast Beam Mixture Proportions 82

Table 4.1. FRC Compressive Properties 94

Table 4.2. Flexural Properties of Casted FRC 97

Table 4.3. Fracture Energy 103

Table 4.4. Binder Quantity Causing Blockage 104

Table 4.5. Summary of Rheological Parameters 115

Table 4.6. Summarized Results from Extrusion Tests 119

Table 4.7. Cube Compressive Strength Results 130

Table 4.8. Printed Beam Geometric Properties from Image Analysis 131

Table 4.9. Print versus Cast Beam Flexural Properties 135

Table 4.10. Percent Change in Flexural Properties from Printing 136

NOMENCLATURE

Symbol	Description
a	Notch height
A_c	Area of concrete cross section
A_f	Area of fiber cross section
A_{lig}	Area of effective depth of beam
AFM	Atomic force microscopy
ASTM	American Society for Testing and Materials
b	Width of beam
c	Modified Bingham fitted coefficient
CMOD	Crack mouth opening displacement
d	Nozzle diameter
D	Cylinder diameter
d_f	Fiber diameter
d_i	Distance to n^{th} force measurement
dr	Initial drop in extrusion force
EE	Extrusion energy
EPA	Environmental Protection Agency
F	Fiber factor
F_{max}	Maximum extrusion force
F_{pl}	Shaping force
FRC	Fiber reinforced concrete

FR-SCC	Fiber reinforced self consolidating concrete
F_y	Initial extrusion force
g	gravitational constant
G	intercept of torque versus rotational velocity graph
G_f	Fracture energy
GUI	Graphic user interface
h	Height of mortar sheared in rheometer
H	Slope of torque versus rotational velocity graph
h_b	Height of beam
HPC	High performance concrete
I	Moment of inertia
I_5	Toughness indicie at 3 LOP
I_{10}	Toughness indicie at 5.5 LOP
I_{20}	Toughness indicie at 10.5 LOP
ITZ	Interfacial transition zone
K	Herschel Bulkley fitted coefficient
K_w	Frictional wall stress
L	Span length
L_B	Plug flow zone length
L_{dz}	Shaping zone length
L_f	Fiber length
L_E	Extrusion length
L_O	Dead zone length

LOP	Limit of proportionality
m	mass of beam
MIP	Mercury Intrusion Porosimetry
n	Herschel Bulkley power function
N	Rotational velocity
N_f	Number of fibers in cross section
n_i	n^{th} data point taken
N_t	Number of extrusion force measurements taken
N_{th}	Theoretical maximum number of fibers in a cross section
P	Peak load
PVA	Polyvinyl Alcohol
PVC	Polyvinyl Chloride
R	First crack strength
R_i	Rheometer inner radius
R_o	Rheometer outer radius
R_p	Rlug radius
R_s	Minimum of plug and outer radius
$R_{5,10}$	Residual Strength Parameter
$R_{10,20}$	Residual Strength Parameter
RTU	Rheometric workability test
SCC	Self consolidating concrete
SCM	Supplementary cementitious material
SEM	Scanning Electron Microscopy

SP	Superplasticizer
T	Torque
UEE	Unit extrusion energy
V_f	Fiber volume fraction
W_o	Area under load-deflection curve
XDR	X-ray Diffraction
$\bar{y}$	Centroid from bottom surface
α	Fiber orientation factor
δ_f	Maximum displacement at 3.5mm CMOD
$\dot{\gamma}$	Shear rate
τ	Shear stress
τ_o	Yield stress
μ	Viscosity
μ_p	Plastic viscosity

1. INTRODUCTION

1.1. BACKGROUND

3D printing is the process of creating three-dimensional objects using an automated additive manufacturing process. This process has been heavily used for designs using materials such as polymers, metals, ceramics, paper, and certain foods [1]. These areas have been widely developed and are used in many industries currently including the automotive, aerospace, medical, and many other industries [1]. In recent years, the construction and civil engineering fields have started to adopt 3D printing for the use in printing concrete structures.

3D printing concrete has the opportunity to revolutionize the construction industry [2]. By using a 3D printing process this could allow for many benefits with regards to economical, structural, environmental, and construction aspects to various types of projects [2]–[4]. Economic benefits could come from decreasing formwork and labor costs. These costs make up a high percentage of the overall concrete cost. Printing structures may also improve the productivity of the project to help save construction time. Structural benefits can come from optimized design geometry. More material can be printed in areas seeing higher stresses and material can be saved in areas of less stress. This saving of material also acts as an environmental benefit. Besides reduced labor costs and increased productivity, other construction benefits would be to help improve worker safety and quality control when building structures.

There are many possible applications for 3D printing concrete. These could include items such as printing walls, columns, precast elements, architectural structures,

stand-alone elements, panels, and much more [2], [3], [5]. Examples of some of these elements are shown below in Figure 1.1.

Figure 1.1. Examples of 3D Printed Structures [5]

One application already implemented is a 3D printed pedestrian bridge in the Netherlands [6]. This will be further discussed in the literature review in Section 2.1.4. One of the first attempts to industrialize the 3D printing concrete application is done by Contour Crafting where their goal is to implement 3D printing in building houses, multi-story buildings, wind turbine towers, bridge pylons, silos, and even construction in space [7].

Before widespread implementation, many areas of research need to be investigated to better understand 3D printing concrete. Some of these areas include solving issues of the concrete within the fresh state, hardened state, geometric conformity, and printing controls [4], [5]. Fresh properties could see issues from dealing

with the time dependent behavior of concrete changing the behavior of printing at the beginning and end of the print, issues with extrusion and print quality, the structure being able to build up properly and sustain its own weight, deformation from multiple layers, and quality control [5]. Issues with hardened properties include the bond between printed layers, tensile reinforcement, shrinkage, durability, and measuring hardened material properties [5]. Geometric issues could create problems with keeping a consistent print shape, exact dimensions being printed, printing properly with curves, creating fully dense components, and creating overhangs [4], [5]. Other items that need to be studied to create successful prints include printing control items such as pumping pressure, robot speed, nozzle geometry, and printing length [4]. Overall, there are many areas of research and questions that need to be answered to help bring this technology to the construction industry. This research will help to better define some of the areas that have not been studied in detail and are vital to better understanding 3D concrete.

1.2. SCOPE AND OBJECTIVES

The main scope of this project is to specifically investigate the extrusion process of 3D printing and use of fibers as a reinforcing system. The first step taken in the project was to study fiber reinforced concrete (FRC) and understand the effects on mechanical properties and workability. The study of FRC was done while looking at the use of recycled fibers from waste tires as a potential replacement of manufactured steel fibers. Tires from automobiles made up 3,555,000 tons of waste in 2014 according to the EPA [8]. The use of recycled materials within concrete helps improve the sustainability which can lead to reduced maintenance costs, reduced energy cost, save resources, increase

durability, reduce solid waste, and be environmentally friendly [9]. To investigate the use of the recycled fibers and properties of FRC, tests were performed to investigate the superplasticizer demand, compressive strength, modulus of elasticity, flexural strength, toughness and residual strength, and fracture energy.

Once FRC properties were better understood, the extrusion process for printing concrete was investigated. This was chosen to study as not many researchers have studied the extrusion process. The few studies and suggestions about extrusion are mostly qualitative in nature so a need for quantitative evaluation is needed. The few studies on extrusion within 3D printing concrete are described in Section 2.1.3.

With 3D printing concrete being a relatively new field, not much equipment is available. To study extrusion, a concrete extruder was designed and built to perform tests. The scope on the design of this extruder was that it would be able to attach to a printing system in the future, allow for various size extruders, allow for displacement control, and allow for the measurement of extrusion force. After creating the extrusion device, test methods were developed to characterize extrusion. Tests were designed in order to characterize blocking during extrusion, extrusion force, and extrusion energy. The effect of blocking was evaluated for different maximum particle size, two workability levels, and binder content. Extrusion was characterized to evaluate the effect of nozzle size, workability, and extrusion speed.

Finally, fibers as a reinforcing system in printing was investigated. Understanding how well fibers perform during printing is important for developing a solution to some of the issues with tensile and flexural strength of printed concrete. The effect on mechanical

properties when printing and when casting the concrete were compared as well as the effect on fiber orientation from printing.

Within this scope, the project can be broken down into several objectives for each part of the project.

- Compare the mechanical and fresh properties of recycled fibers from waste tires with manufactured steel fibers
- Develop and evaluate test methods to characterize extrusion in 3D printing cement-based materials
- Design a modular head extruder with test measurement capabilities to later be added to a full functioning 3D printer
- Investigate the effect of nozzle size, particle size, rheology, and extrusion speed on extrudability
- Compare flexural properties and fiber orientation between printed and cast beams to investigate the use of fibers as a reinforcing system in printing concrete

1.3. THESIS ORGANIZATION

Section 1 contains a background on 3D printing and the objectives and scope of the project. Section 2 covers a literature review of current studies in 3D printing concrete as well as a background on other research in fiber-reinforced concrete, rheology, and extrusion to help understand concepts within printing concrete. Section 3 explains the test methods used to study recycled fibers as a replacement for manufactured fibers and test methods developed to study extrusion and fiber reinforcement in printing. Section 4

displays and analyzes the results for the study on recycled fibers, extrusion, and printing with fibers. Section 5 describes a summary of the study, conclusions from the study and evaluation of the proposed test methods, and suggestions for future and on-going work. Appendix A contains specific drawings, schematics, and details for the extrusion system developed. Appendix B contains code used to program the extruder and load cell.

2. LITERATURE REVIEW

Additive manufacturing or 3D printing of cementitious materials is a wide ranging field with many aspects to consider before it will be implemented for a broader use in industry. It is important to understand and have a background on the concepts and current research in 3D printing concrete and cement-based materials in order to build upon some of the technology and understanding of the complex construction material itself. Not only is it important to understand the concepts, technologies, and problems in 3D printing, but, to dive into a specific problem, an understanding of other advanced concrete topics must be understood and addressed to provide an adequate background to build upon. For characterizing the extrudability of cementitious materials for 3D printing and using fibers as reinforcement, a background on concrete 3D printing, fiber reinforced concrete mechanical behavior, rheological properties and effect of fibers, and extrusion of cementitious material should first be studied in detail.

2.1. 3D PRINTING CEMENT BASED MATERIAL

3D printing of concrete has become an emerging field within construction material and concrete research. There have been a handful of studies over the past decade with a majority of the work coming out in the past few years. It is vital to understand some of the problems associated with 3D printing cement based materials to successfully study the various aspects of printing. Some of the studies that are currently published include ones that look at mix design and properties of 3D printed concrete, printing with fibers, rheological properties, printing architecture and geometry, time effects in printing

and much more. In particular, few studies have looked in depth at extrusion of 3D printing. This research has been discussed in more details in this chapter to provide a better understanding of extrudability of cement based materials. This section will provide a background on the main topics and concepts of printing and provide an overview of some of the most recent published research in literature.

2.1.1. Mix Design and Fresh Properties of 3D Printed Cementitious Material. The mix design and properties of the printed cement-based material can have an effect on all aspects of printing and is important to understand before further research can be done. These properties can affect things such as the quality of the print, how the material extrudes (extrudability), how the layers hold their own weight and stack onto each other (buildability), timing for printing, layer bond strength, and mechanical properties. The mix design will also affect items such as durability and sustainability of the mix design as well, but these have not been investigated as there is still a need to study the basic mix design and fresh properties to allow for printing to successfully happen.

Fresh properties of printed concrete fall into three main areas of study: extrudability, buildability, and open time. Studies have been done to try and develop design and performance criteria for each of these items as well as understand the effects of constituents and how traditional fresh concrete testing methods relate [10]–[12]. Test methods for extrudability are described later in detail in Section 2.1.3, but Kazemian et al. looked into developing performance-based testing criteria for the fresh properties of 3D printed concrete [10]. One criteria related to extrusion that was defined was print quality. Print quality included three separate criteria to pass the minimum quality for printing. These included looking at the surface quality, whether there were square edges,

and the dimensional conformity and consistency of the test. The dimensional conformity was defined as ok if the tested width of the print was within 10% of the design width. It should be noted that the printer used for this study used troughs and a square extruder geometry that allow for the printing with squared edges.

Fresh properties regarding buildability have been studied more including relating existing test methods to buildability and defining new test methods. Zhang et al. looked at relating existing test methods to buildability including tests methods for rheological behavior, workability, green strength, open time, and heat of hydration [11]. The tests used to study these included using a flow table, Brookfield Rheometer using a hysteresis loop, a green strength test, and isothermal calorimetry. The study was able to lead to a successful 3D printing mixture and found that thixotropy and green strength are effective ways to test the buildability. It was also found that retarder had an effect of the rate of structure rebuild with time when mixing which can affect the thixotropic increase of yield stress needed for buildability. Kazemian et al. also looked into buildability criteria, but developed test methods to evaluate buildability or "shape stability" [10]. The shape stability of the printed component was based upon the ability for a layer to hold its self-weight, weight of the layers above it, and the extrusion pressure. Two tests were developed to help analyze the shape stability of the fresh concrete. The first test was the "Layer Settlement" test [10]. This test takes an image of a printed layer next to a ruler before and after a layer is printed on it. Using an image J software from Java, the deformation of the lower layer can be calculated. Figure 2.1 shows an example of this test method.

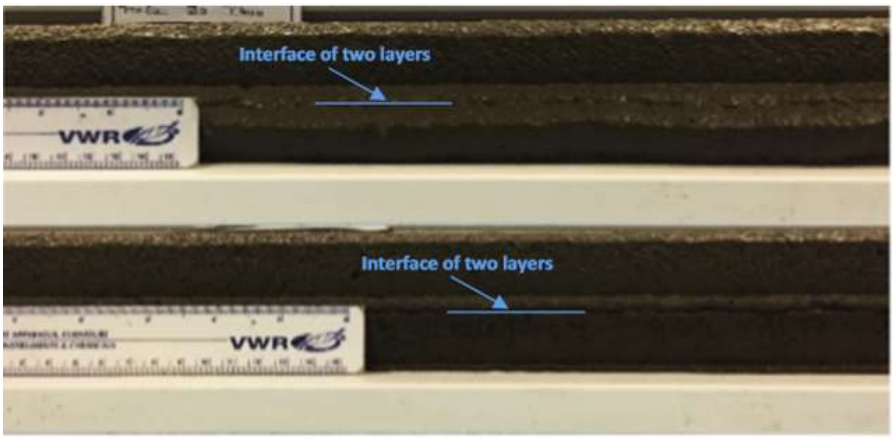

Figure 2.1. Layer Stability Test [10]

The second method developed to test shape stability was the “Cylinder Stability” test [10]. This method consisted of placing and rodding concrete in two layers within a cylinder. The sides of the cylinder are then removed carefully and any change in height from self-weight is recorded. A 5.5 kg load is then placed upon the top of the cylinder and the change in height is measured. Figure 2.2 shows this test method.

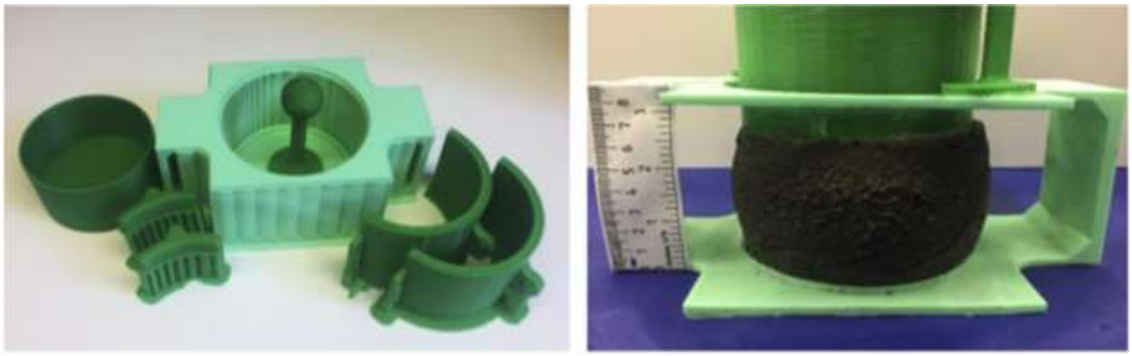

Figure 2.2. “Cylinder Stability” Test [10]

Besides current and proposed test methods being used to evaluate buildability, models were also looked into to relate strength in the fresh state to buildability. Pierre et

al. proposed a model to evaluate the structural stability and failure for printed concrete [12]. Their model considered the load on the bottom layer of the printed structure and compared the evolution of yield strength of this layer with the evolution of mechanical load with time. Their failure criteria was dependent on a geometric factor of the printed layer and the time dependent yield stress factor. They evaluated two models for the evolution of yield stress (a linear and an exponential model). This theoretical framework was then confirmed with experimental testing. The theoretical framework was found to agree with the experimental values for the multiple build rates they tested at [12].

One of the main effects of constituents described in these studies looking into fresh property relation to buildability was Nano-clay and silica fume. They were found to help increase buildability by increasing thixotropy and yield stress in the mixtures [10], [11]. This increase was due to the high specific surface area of silica fume that lead to stronger absorption and more flocculation.

Open time, or the time for acceptable printing, is a third area of fresh properties investigated. The effect of time is very important to study for 3D printing concrete. Due to the changing thixotropic and hydrating behavior of cement-based materials, the time it takes to print and the time to start printing after the initial mixing can change many aspects in the performance of the printed structure in the fresh and hardened state. One of the parameters effected by time that deals with both the fresh and hardened properties is bond strength between layers. One study looked at the effect of a time gap on the performance of the bond strength between layers [13]. They found that a major factor in bond strength due to time gap is the storage (or elastic) modulus of the initial layer at the time the next layer comes into contact. This high modulus of the initial layer can prevent

a good bond between the layers [13]. It was found that as time increased, the amount of voids at the interface increased thus weakening the bond strength. Kazemian et al. defined also developed criteria based upon printing time, but only related to fresh properties and not considering bond strength [10]. They defined this criteria as the "printability window". This window looked at two main time limits to allow for successful printing. The first is the printability limit [10]. This was measured as the longest time when a mixture can be printed with acceptable print quality. The second limit defined is the blockage limit [10]. This is the longest time that a mixture can be remain in the nozzle before blockage occurs. Taking account to these two factors is important to be able to print in a large scale as the time for printing may be long due to the size of the structure.

Two main methods of optimizing a mix design has been shown in literature. The first method was developed by Le et al. and also used by Lediga and Kruger [14], [15]. This method was done to find an optimum mix design for printing and was then verified with a full size print. For this method variable in the mix design was altered until the optimum point found and then moved on to the next constituent to optimize. This study looked at the extrudability, workability, open time, and buildability of concrete with various mix designs and then optimized their mixture based upon these results. The parameters selected to optimize were the sand content, dosages of superplasticizer, retarder, accelerator, and amount of polypropylene fibers. For extrudability the material was printed in rows until 4500 mm was printed and if the material printed without any blockage or fractures the material was considered extrudable. The mixtures with the highest sand content were found to be difficult to pass through the extruder. When

looking at workability, the effect of different dosages on the shear strength of the mixtures was evaluated for superplasticizer, retarder, and accelerator. As the superplasticizer increased, the shear strength of the fresh concrete decreased. For the retarder and accelerator, however, the workability decreased by increasing the shear strength of the mixture. For open time, the retarder and superplasticizer amounts were varied while keeping the other respective additive constant. For superplasticizer increase, it was found that with agitation, the increase in superplasticizer can help increase open time. For retarder, about a 0.5% dosage was the limit of helping increase open time while increasing the dosage further seemed to hurt the open time. For buildability, the optimum shear strength range was 0.3 to 0.9 kPa measured with a shear vane apparatus to allow for the mixture not be too stiff or to fluid. After trials with different mix designs, a 0.55 kPa shear strength was found to be optimum for buildability [14]. From all of these tests, the authors were able to pick and decide on mixture proportions that would help optimize printing and provide for a sufficient strength print. This was then verified with a full size printed bench [14]. Using this design method it was found that there were issues with segregation in the mixture due to high cement content and difficulty to pass through the pipe-pump nozzle system [15]. Lediga and Kruger also investigated the mechanical properties studied, they listed the results and were able to get compressive strengths in the range of 75-102 MPa, flexural strengths around 11 MPa, and tensile bond strengths above the minimum recommendation of 0.8 MPa [15].

The second mix design method found was based around the effect of the gradation of the sand was studied using the Fuller-Thompson method and Marson-Percy model [16]. The study looked at a mix design using the Fuller-Thompson method for a

continuous gradation system, two uniform gradation systems with varying particle sizes, two gap-graded mixtures, and a mixture with river sand where large particles (1.2 mm) were sieved out. From these results, it was found that the mixture using the Fuller-Thompson design had the best buildability with the ability to reach about 40 layers high compared to around 30 layers high for the other mix designs. The Fuller-Thompson designed mixture had a high yield stress and low plastic viscosity which can be helpful when pumping or extruding. Some of the other mix designs, especially one of the gap graded mixtures, lead to a high viscosity which makes it more difficult to print. It was concluded that the Fuller Thompson method and Marson Percy model was a successful way to design 3D printed concrete mixtures to control yield stress and viscosity for good pumpability/extrudability as well as achieve good buildability.

2.1.2. Printing with Fibers. A need for reinforcement in 3D printed concrete is vital since rebar cannot be used since the concrete is directly extruded into its final position without the use of any formwork [5]. One option to help improve the flexural and tensile strength of the printed structures is to use fibers as the reinforcement. The use of fibers in printing would also allow for better control of fiber orientation within the specimen. Fiber orientation is critical as the higher the orientation factor the better the flexural properties are in the direction of the fibers [17]. This would allow for creative use of fiber orientation and print path to come up with ideal properties for a specific geometry or application. A handful of studies has been done using fibers for 3D printing investigating the effect on fresh and hardened properties. These studies are important to understand the best use and improvement fibers can have, especially when evaluating them as the main reinforcement in 3D printed concrete.With the freedom of printing in

multiple directions and controlling fiber orientation, some studies looked at the effect on fiber and loading direction [18]–[20]. Hambach and Volkmer studied adding short fibers (3-6 mm length) to 3D printed concrete and its effect on the improvement of flexural strength [18]. They looked at how different printing paths effect the flexural strength, compressive strength, density, and porosity of the specimens. They also looked at a hierarchical structure where there was a main structure printed with a mortar infill. This idea can allow for a more economical design as the main printed structure may have a higher cost than the infill. These tests were done with carbon, glass, and basalt fibers. An example of the different print geometry and hierarchical Structure is shown in Figure 2.3 [18].

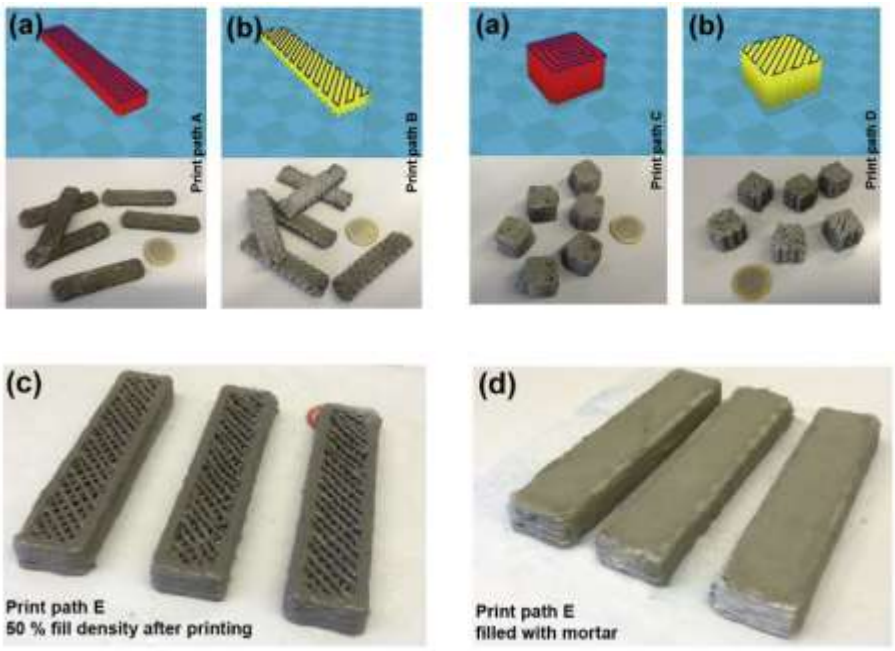

Figure 2.3. Printed Specimens with Various Geometries and Hierarchical Structures [18]

The results of this test showed that the carbon fibers at 1% volume addition had a significant effect on increasing the flexural strength while the basalt and glass fibers did not have as much of an effect. The fibers did not affect the compressive strength of the concrete. The printed path that worked best for the flexural results was print path “a” from Figure 2.3. For the hierarchical structures, the results showed that the higher percentage of fiber-reinforced printed formwork (less infill), the higher the flexural strength [18].

The modeling of the behavior was done to better understand the anisotropic properties and variation on printing/fiber direction [20]. This study looked at four different printing patterns to compare them: parallel, perpendicular, cross, and a casted specimen. They then did tensile and compressive tests to try and relate the properties to a micromechanical model. After analyzing the experimental results and the model, it showed that the performance in tension matched with the micromechanical analysis [20]. The study showed as in the others stated within this section that the best results came from the fibers oriented in the direction of the load [18]–[20]. Use of a model to understand the behavior of the fiber reinforced concrete will be needed in the future for design purposes. As shown in many of these studies, the fiber orientation and printing direction can be easily change and will have a large effect on mechanical properties due to the anisotropic nature of the material.

The loading direction and effect of fibers on the flexural, compressive, and tensile strength was done to study the anisotropic properties of the material in a study by Panda et al [19]. Glass fibers were used in this study with a geopolymer printed concrete with different length and quantities of fibers. It was found that the fibers do not have an effect

on the flexural strength, but improved the flexural and tensile strength as the fiber content increased. When looking at the different directions, it was found that the printed specimens performed best in flexure when being loaded perpendicular to the layers. The tensile strength performed best when loaded parallel to the print direction. For the tensile strength, the reason for higher strength in the parallel direction is that the perpendicular direction is controlled by the bond strength between the layers [19]. The bond strength is one issue that arises between layers as for certain concrete mix designs (highly thixotropic) can cause cold joints and weak bond. Understanding the effect of loading direction on the strength parameter is important to understand for future design of 3D printed structures.

Christ et al. looked at the addition of fibers on their effect of green strength and flexural properties for a cellulose-modified gypsum powder 3D printed mixture [21]. This study is not specifically with a cement-based material, but from this study it shows that the fibers help improve the green strength of concrete. This is important for improving buildability of concrete while printing. This test again showed an improvement in flexural properties when printing with fibers since these can take most of the flexural load away from the matrix which is in most situations brittle and weak in tension and flexure.

A manual print was done with a polymer fiber reinforced mix design to investigate workability and mechanical properties [22]. This study showed that manual printing can be used to evaluate tensile, flexural, and compressive properties of printed mixes with fibers. Important findings of this study regarding fiber reinforcement is the verification that the printed specimens had better fiber alignment which contributed to higher mechanical properties in the fiber direction. The fibers also allowed for a greater

strain capacity within the specimens. This strain capacity was also compared with a casted specimen and it was found that the printed specimen had a higher strain capacity. This again is likely due to the fiber orientation caused by to the restricted flow while extruding the fiber-reinforced concrete [22].

Ogura et al. had the goal of creating a strain-hardening cement-based composite and studying its effect on printing in terms of extrudability, buildability, and mechanical properties [23]. For evaluating the fresh properties, a flow table and ram extrusion test was used. The flow table was used to help relate a mix design to its buildability. According to their results the flow table "roughly estimates" buildability and how stable the print is [23]. With the ram extrusion test, the goal was to evaluate extrudability. Due to changing sand content in their mix design matrix, the results seemed to show a increase in extrudability with increasing fiber content. They noted, however, this change was due to the changing sand content which is controlling for extrudability compared to the fiber dosage [23]. This could be another potential topic to look into on the effect of fiber dosage on extrudability. For mechanical properties, a uniaxial tension test was performed on printed and cast specimens. Fiber content as low as 1% using a high density polyethylene microfiber showed strain hardening behavior when testing and a multiple crack failure method [23]. The printed specimens outperformed the casted specimens in testing as in previous studies noted to be due to increased fiber orientation. The author also added that a decreased air content due to the extrusion forming process could have also benefited the mechanical properties of the printed specimens versus the cast specimens.

2.1.3. Extrusion of 3D Printed Concrete. Depending on the type of printer, there are various methods for extruding concrete. Some printers will use a pumping process to extrude the concrete. Others will use a direct extrusion or syringe type method. Some large scale 3D printers use a screw pump or progressive cavity pump to push the material out while constantly shearing the material. Figure 2.4 shows an example of each of these extrusion methods.

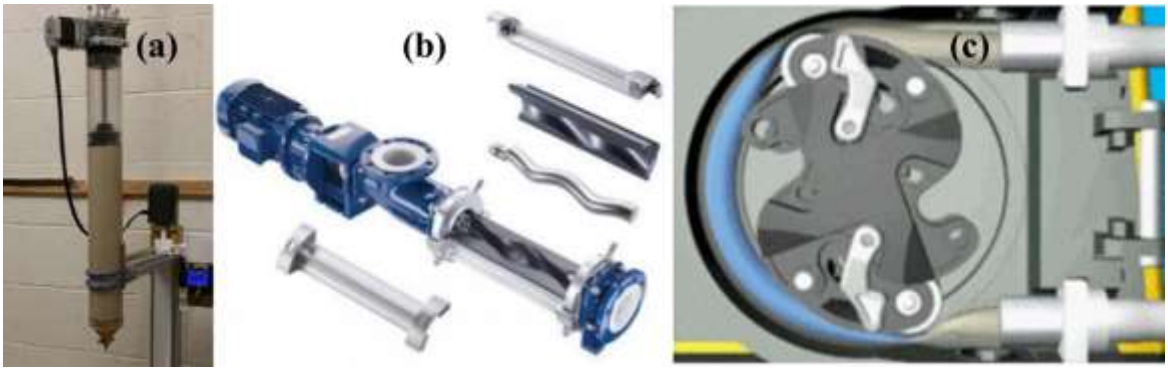

Figure 2.4. Different Extruder Types: (a) Ram Extruder [24] (b) Progressive Cavity Pump (c) Peristalic Concrete Pump [25]

Aside from the extrusion method, the nozzle size and geometry will also have an effect on extrusion (see Section 2.4 for more details). Not as many studies have been done on defining and characterizing the extrusion of 3D printed concrete. Most studies find a mix design that is extrudable and characterize it as a “yes” for extrudability. The following test method will be described that is used in multiple papers to qualitatively define extrusion. One study will also be described that proposes a quantitative test for defining extrudability and looks more in depth.

One test method that multiple researchers have used is a qualitative test looking at extruding multiple layers horizontally and checking for defects [14], [15]. This test

method specifically consists of extruding with a 9 mm filament five groups from one to five filaments each 300 mm long for an overall length of 4500 mm. If there is no blockage or fracture in the extruded layers then the mix design is listed as ok and is extrudable. This test is shown in Figure 2.5 below.

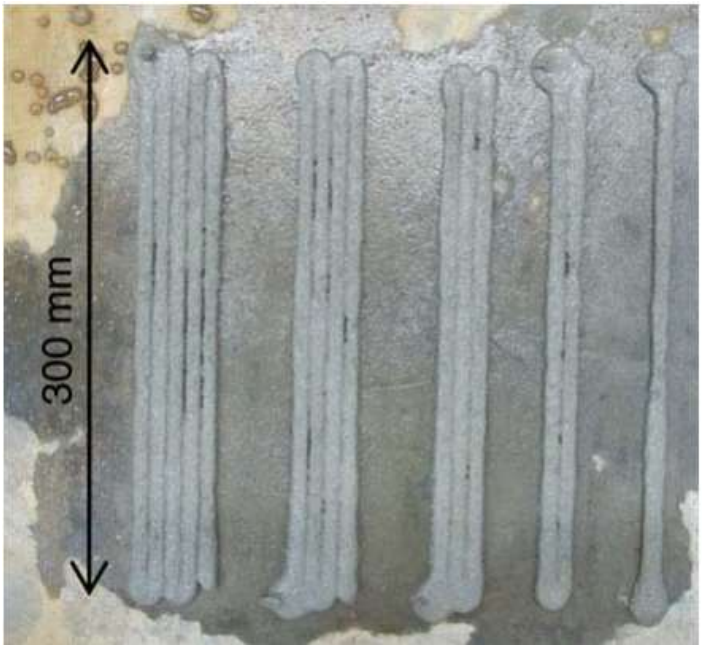

Figure 2.5. Qualitative Extrusion Test [14]

To quantitatively study extrusion, on study used the ram extrusion test while also developing a test called the “3D-printer extrudability test (3DPET)” [26]. The ram extrusion test is described in greater detail in Section 2.4. The test was done for a printer with a progressive cavity pump extruder. In this test, the rotational velocity of the progressive cavity pump was used to relate the voltage needed used to extrude the concrete based upon the known maximum voltage and know maximum rotational velocity. Using an electrical power measuring device, the total electrical power from the

extrusion process was able to be measured. Simultaneously while testing, the flow rate was calculated. This was done by determining the weight of the concrete extruded and turning it into a volume by using the extruded concrete density. Using the power and flowrate, they define an "extrudability index UEE" which is measured in Joules per cubic centimeter [J/cm^3]. This is related to the amount of energy it takes to extrude a unit volume of material [26]. This test method was compared with the ram extrusion results. The test method did not line up exactly with the ram extrusion test. The UEE seemed to align better with the results measured from the rheological analysis. The authors stated that this test method is not the easiest to directly apply to another printing system, but the overall concept of measuring electrical power and the flow rate can be used to theoretically describe how extrudable a concrete mixture is [26].

2.1.4. Other Studies in 3D Printing. With 3D printing of concrete and cement-based materials being relatively new, many aspects other than the ones already covered are being studied. 3D printing is a concrete is a complex process that involves many avenues of study besides the fresh material behavior. Other studies are presented here to get an understanding of the overall current work and research in 3D printing cement-based materials.

An area to overcome in printing concrete is actually creating or designing a printer. This can involve many different mechanical, electrical, and computer programming aspects. If not done properly, even with a well designed and robust concrete mix design, the printing could fail due to poor calibration and bad accuracy when printing layers. A group from the Loughborough University built a 5.4 x 4.4 x 5.4 m frame with the ability to print various three-dimensional shapes [27]. In their paper

they describe the general process in building their printer, issues they had, and the results of their finished product.

One area of 3D printing concrete that is currently being developed is finite element modelling. In one study, a finite element model was created to analyze the fresh concrete within the first 90 minutes after printing [28]. This study used various geotechnical tests to evaluate the material properties of the fresh concrete in order to develop a Mohr-Coulomb failure criterion. This was used to help evaluate the time-dependent material properties so a model could be developed in ABAQUS. The model created was found to accurately model the failure-deformation mode but overestimated the amount of layers that could be printed. The difference in this overestimation was said to be due to not taking into consideration geometric and material imperfections and having issues obtaining material properties without compacting concrete. Modelling as such can be a useful tool when designing a structure to be printed to make sure it would not fail in the fresh state before hardening.

With the freedom of design that comes with printing, interlocks can be designed into a print. One study looked at how these interlocks can affect the bond strength between printed layers [29]. The interlocks printed in between layers were varied in size from no interlock up to a 0.75” interlock in increments of 0.25”. A splitting and compression bond test was done to evaluate the bond strength gain from the different interlocks. From this test, it was found that for both the compression and splitting bond tests, the interlock increased the bond strength with size up to 0.5” where then the 0.75” interlock tested the same as no interlock. This shows that through the creative use of

interlocks to a certain length, bond strength can improve which is a common issue for highly thixotropic materials.

Study of the microstructure of printed concrete can also be useful in better understand many of the problems and phenomena that occur. An in depth study was done to look at the microstructure as well as compare this microstructure with equivalent casted specimen [30]. Moini et al. used X-ray Micro-CT scans to evaluate the microstructure. Four main features were noted and discovered from the CT-scans. They included the presence of macropores, micropores at the interface of filaments creating micro-channels, “self-rearrangement of filaments”, and accumulated anhydrous cement particles near the pores [30]. The pore network described was aligned with the direction of printing. Knowing this information, innovative solutions can be developed from a material or print design standpoint to help overcome the issues with bond strength caused by these pores.

With 3D printing comes the freedom to print in different architectures that was not easily able to cast before. Taking advantage of this can provide a new perspective on design of structures not just architecturally, but also structurally. A study was done to evaluate the ability of different print architectures [31]. An example of some of the innovative architectures that can be printed and studied is shown in Figure 2.6 [31]. This study looks at and tests the different architectures to evaluate their failure mechanism and properties. Some of the architectures exhibit different failure modes and behavior compared to the normal behavior expected from a cement-based printed composite.

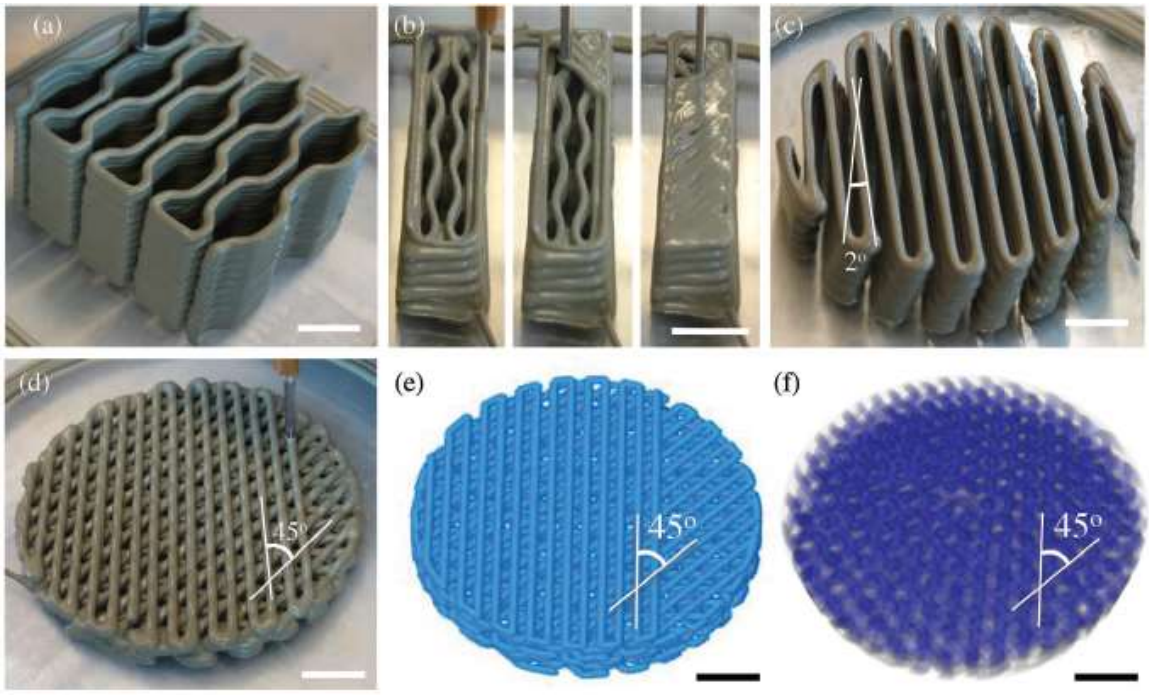

Figure 2.6. Different Print Architectures [31]

With all of the different studies out there, field implementation is something that will be looked at very closely and some of the next steps for implementing this technology. One example of an implementation of 3D printing concrete is a pedestrian bridge that was designed, printed, and implemented in the Netherlands [6]. This bridge spans 6.5 meters and is 3.5 meters wide and designed for a uniformly distributed load of 5.0 kN/m^2. The first step was material testing in the design to evaluate a mix design that would allow for printing and also meet the proper compressive strength, modulus of elasticity, shrinkage requirements, and creep requirements. The bridge was then evaluated using a finite element model. The print path was then designed and the specimen was tested using a four point bending test in the lab. The reinforcement used was a post tensioning system. After verification of all structural parameters in the lab, the structure was reprinted and brought to the field. Once installed in the field, the bridge

then underwent an in-situ test to evaluate the safety of the bridge. The full-scale test passed and the 3D printed bridge project was opened to the public. An image of the completed bridge is shown in Figure 2.7 [6].

Figure 2.7. Implementation Example of 3D Printing: Pedestrian Bridge [6]

Overall this is an example of a successful 3D printed structure that is implemented. As mentioned in this section, there is still a lot more ongoing research to better understand printing cement-based materials. With this increase in knowledge, the frequency of real world use of 3D printing concrete will expand vastly.

2.2. FIBER REINFOREMENT CONCRETE

Fibers have been used as a reinforcement system and for crack control in concrete over the past couple decades. Fibers present themselves as a potential reinforcement for 3D printing due to the fact that they would be homogenously mixed with the concrete and

could be extruded with the paste. Fiber reinforced concrete (FRC) has been widely studied in conventional concrete and other specialty concretes. Getting an understanding of the benefits, testing, and effects of different fiber reinforcing systems in concrete will allow for an implementation for 3D printing and the expected effects on mechanical properties. The mechanical behavior of FRC as well as the use of recycled fibers from waste tires is further presented to create a background knowledge for the tests on FRC for conventional concrete in the current project and its future application within printing.

2.2.1. General Fiber Reinforced Concrete Mechanical Behavior. The main use of fiber reinforcement in concrete is to benefit the flexural and tensile behavior of the brittle concrete matrix [32]–[44]. This improved behavior includes improving the flexural and tensile strength, the post cracking properties, and energy absorption of the concrete. The fibers improve this brittle behavior by acting transferring and taking the load in tension, which the brittle concrete matrix performs poorly at. When high strength and modulus fibers (such as steel) are used, this then increases the capacity of the member in both flexural and tensile loading as the fibers can take a high amount of the load before it is transferred to the matrix. Compressive strength is less effected by the addition of fibers. Multiple researchers have shown that the effect of fibers on compressive strength is small or negligible [33], [42], [43]. Even though the compressive strength is not greatly affected, the failure mode is slightly different. With the addition of fibers, the failure mode still becomes more ductile than brittle [33].

Once the concrete matrix is cracked, the fibers help to bridge the cracks and keep them from propagating. This allows the concrete to still sustain load and control crack widths within structures. Depending on the fiber type and volume, this can make the

concrete behave more ductile. It has been stated in multiple studies how fibers improve ductility [32], [33], [38]. The concrete composite can show signs of strain hardening, elasto-plastic response, or strain softening depending on the fiber volume, fiber type (modulus and strength), and fiber aspect ratio.

Evaluating the post cracking behavior is heavily studied when looking into FRC mechanical properties as this is where most of the benefits of the fibers are. This can be analyzed using a three-point bending test with a notched beam. One way to evaluate the post-crack behavior is to analyze the toughness of the concrete. This can also be related to the energy absorption of the concrete. This is done by evaluating the area under the load versus deflection curve after the concrete first cracks. A graphical representation of this is shown in Figure 2.8 [37].

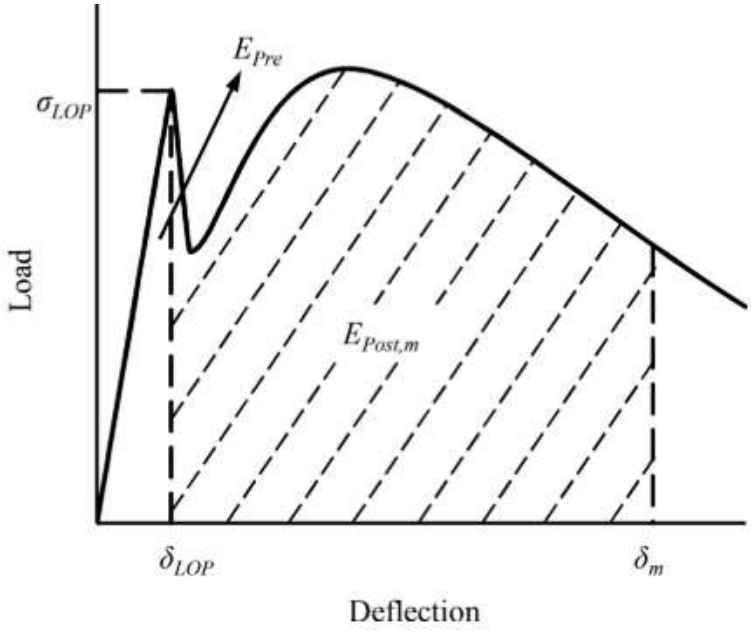

Figure 2.8. Area for Evaluating Toughness and Post-Cracking Behavior of FRC [37]

ASTM C-1018 provides guidance on this test method and some of the calculations for evaluating this behavior [45]. The toughness can be evaluated at different intervals of deflection once the first crack or limit of proportionality is found. This is graphically shown in Figure 2.9 along with a range of toughness values for FRC compared to plain concrete and elastic-plastic materials. For each toughness value, if the experimental toughness is above the elastic-plastic material it is considered strain hardening, and if it is below the elastic-plastic material and above plain concrete then it exhibits strain hardening.

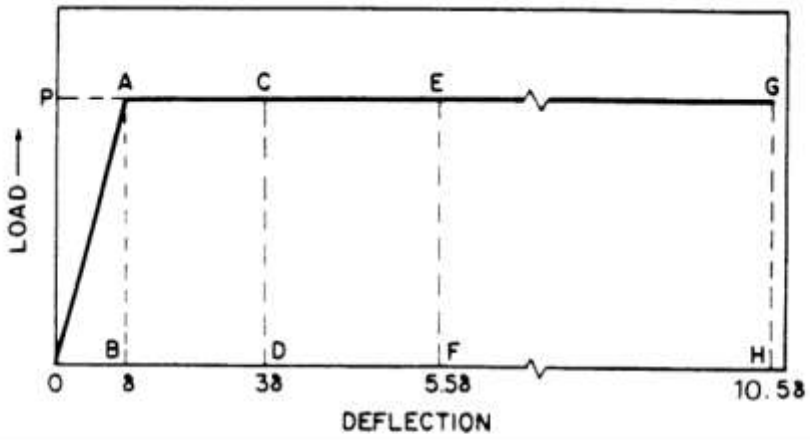

Area Basis[A]	Index Designation	Deflection Criterion	Values of Toughness Indices		
			Plain Concrete	Elastic-Plastic Material	Observed Range for Fibrous Concrete
OACD	I_5	3δ	1.0	5.0	1 to 6
OAEF	I_{10}	5.5δ	1.0	10.0	1 to 12
OAGH	I_{20}	10.5δ	1.0	20.0	1 to 25

[A] Indices calculated by dividing this area by the area to the first crack OAB.

Figure 2.9. ASTM C1018 Toughness Indices

Improving the toughness indices and post-crack properties is not only vital in crack propagation, but can help increase the safety and load carrying capacity in seismic and impact loading.

There are many different types of fibers that have been used and studied in FRC. Many studies include the use of steel fibers for their high strength and modulus. Other studies use polymer type fibers such as polypropylene fibers [32]. Other types of fibers such as natural fibers and modified-olefin-fibers have been used and studied [37], [38]. The use and selection of fiber type should be chosen based on a number of factors including desired strength, post-cracking behavior, workability implications, durability, cost, and availability.

The proportioning, size, and modulus can have a large impact on the performance of FRC. All of the previous mentioned studies have shown that with an increase overall fiber volume, the flexural, tensile, and post-cracking properties increase. Changing the fiber length (or aspect ratio) can also affect the performance of the FRC. Some studies have looked at this effect while incorporating hybrid systems of multiple types of fibers [38], [39]. In [38] it was found that higher modulus fibers helped improve the strength while lower modulus fibers helped improve ductility. Creating a hybrid mixture of different modulus fibers can exhibit the benefits of both of these properties. They also illustrated graphically how the difference in long and short fibers can mitigate different types of cracks within the concrete matrix as shown in Figure 2.10 [38].

In Mohammadi et al. they also verified that the longer fibers are better at mitigating macros-cracks while short fibers are better at mitigating micro and meso-cracks [39]. They also found that short fibers provided better workability than long fibers. They were looking to investigate an optimum mixture of long and short fibers, but they found that there was not one mixture that was optimum for all mechanical properties and workability.

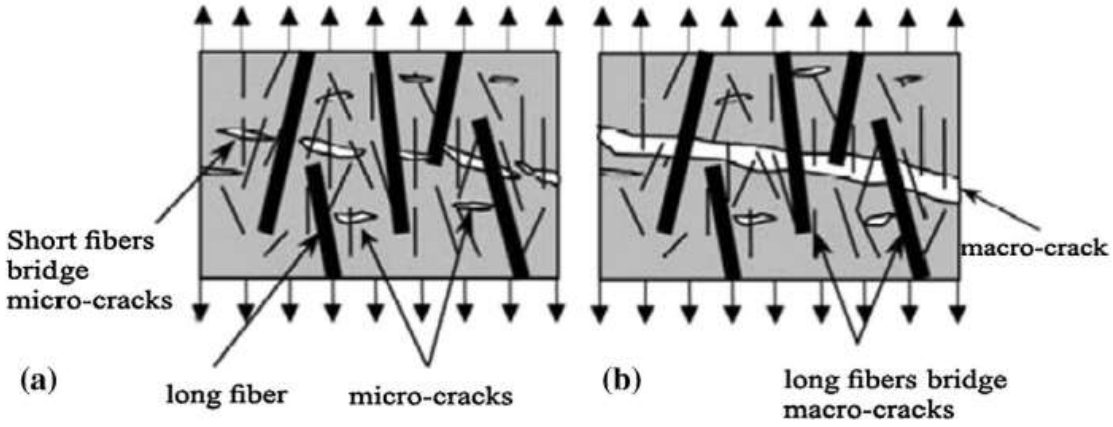

Figure 2.10. Long versus Short Fiber Crack Mitigation [38]

Finally, it should be noted that the fiber orientation has a large effect on the mechanical properties. With normal cast-in-place concrete the fiber orientation is random which can cause variations in results. One study found that stiffer fibers had a greater variation due to less likely spread out during casting [40]. The random fiber orientation may hinder use of FRC in certain applications This potentially presents an opportunity in 3D printing as the print direction and extrusion may have an effect on fiber orientation.

2.2.2. Studies with Recycled Fibers. A handful of studies have also been done using recycled fibers from waste tires. Some studies were done investigating the mechanical behavior of the fibers [41]–[43]. From these studies it was found that the recycled fibers were comparable to industrial used steel fibers for the mechanical properties. It was found by [42] that the addition of the recycled fibers seemed to decay the post-peak crack behavior compared to the steel fibers. The splitting tensile strength

and flexural strength of the fibers seemed to be comparable. The failure mechanism for beams and slabs tested throughout these experiments were the same as well.

One study investigated the pullout behavior of the recycled and steel fibers [44]. This study created a numerical model using an incremental plasticity based formulation first to estimate the pullout strength of the fibers. An experimental investigation was then used to validate this model in which they found good agreeance. From this experimentation it was found that the recycled fibers had a similar bond strength to industrial steel fibers, but a lower peak load. The recycled fibers needed a greater crack opening to be pulled out but did not reduce crack width as much compared to the industrial steel fibers.

The fatigue resistance of the recycled fibers was also studied [34]. The use of fibers was shown to increase the endurance life of the concrete composite. The recycle fibers were found to also help restrain the micro and meso-cracks better while the steel fibers used in comparison helped better with the macro cracks. The study on fatigue resistance with recycled fibers was for use in concrete pavement. With the improvement of fatigue resistance with the recycled fibers, it was stated that up to 26% of the pavement thickness could be reduced.

A stress-strain relationship was investigating noting that the neutral axis changes with the load [35]. The RILEM equation estimating the strength was then compared using the stress-strain relationship for the fibers and it was found to be an overestimate. A similar study was then done to adjust the RILEM model for design and use of the recycled fibers [36]. The new model was found to be more conservative and accurate than the RILEM model.

2.3. RHEOLOGY OF FIBER REINFORCED CEMENT-BASED MATERIALS

Rheology is the science that describes the relationship between flow and deformation of a material. For cement-based materials rheology is important in understanding the properties and performance in the fresh state. This relationship has to deal with how the shear stress, shear rate, and time dependent behavior of a material are related. This can be rather complex for concrete and other cementitious materials as the behavior is a complex fluid of suspended particles that also has time dependent properties [46]. Due to cement-based materials having a time dependent rheological behavior, they are considered thixotropic. Thixotropy in cement based materials is the structural breakdown and build up of the internal structure of cement paste with constant shear and then rest [47]. This can also be looked at as the variation of viscosity at a constant shear rate. Understanding the rheological and thixotropic properties is vital to the performance of the concrete in the fresh state. Rheology of cement based materials is used to define and design mixes such as self-consolidating concretes (SCC), shotcrete, underwater concrete, pumping concrete, high-performance concrete (HPC), and much more [48], [49]. Not designing for or considering the rheological properties can cause issues with segregation, blockage, passing ability, filling ability, formwork pressure, shaping of concrete, and much more. For 3D printing understanding these properties is important for characterizing material properties such as extrudability, buildability, bond strength between layers, and much more. The following sections go into more detail on the basics of rheology for cementitious materials, the effect of adding fibers to cement based materials and its effect on rheology, basics of how rheology affects 3D printing, and basics of how rheology can affect the extrusion process.

2.3.1. General Rheology of Cementitious Materials. To accurately measure and study the rheological properties of cementitious materials, often times rheometers are used. There are a variety of different types of rheometers with various geometries with a concentric cylinder and parallel plate being the most common for cement pastes [50]. In general, rheometers will measure the torque at different rotational velocities. These points can then be transformed based upon known geometries to come up with fundamental values of shear stress and the shear rate the material undergoes.

From the graph of shear stress versus shear rate, also known as a flow curve, different models can be applied to look at the yield stress of the material and the effect of viscosity at different shear rates. The most common model used is the Bingham Model which is a linear model. This model is described by Equation (1):

$$\tau = \tau_o + \mu_p \dot{\gamma} \quad (1)$$

where τ is the shear stress, $\dot{\gamma}$ is the shear rate, τ_o is the yield stress, and μ_p is the plastic viscosity. Depending on the specific material, sometimes a nonlinear behavior can occur. When this nonlinear behavior occurs, two common models used are the Modified Bingham and Herschel Bulkley models show in Equation (2) and Equation (3) respectively.

$$\tau = \tau_o + \mu\dot{\gamma} + c\dot{\gamma}^2 \quad (2)$$

$$\tau = \tau_o + K\dot{\gamma}^n \quad (3)$$

The c value in the Modified Bingham model is a fitted coefficient that is used to describe the nonlinear behavior and whether the material has a shear-thinning or shear-thickening behavior. The K value in the Herschel Bulkley model is a fitted coefficient and the n value is a power function of the shear rate. The selection of the model should be chosen

carefully as the selection of the models can provide significant differences in the evaluation of rheological properties such as yield stress and viscosity as shown in Figure 2.11 [51].

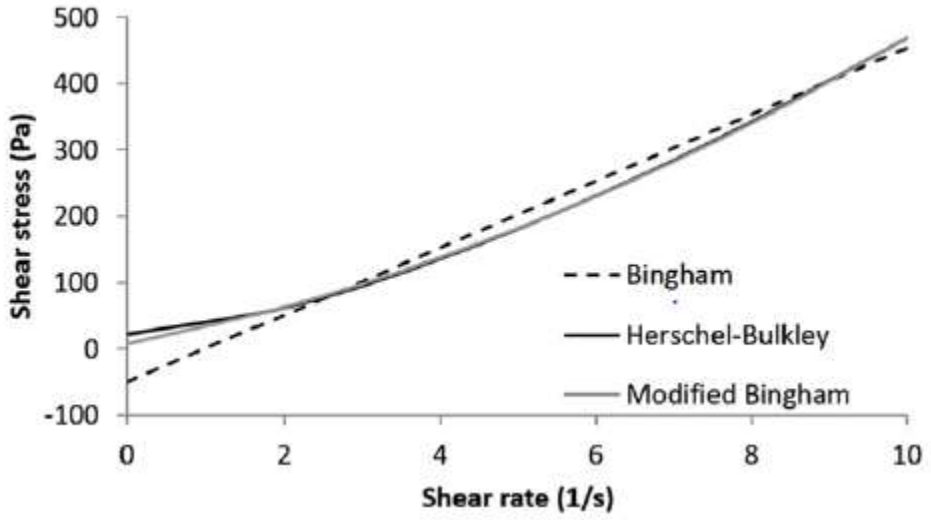

Figure 2.11. Common Rheological Models for Cementitious Materials [51]

The models shown are three common models, but many other models have been developed [52]. Some of these models provide more accurate results for certain types of cement based materials, but also add complexity by having more terms than the models presented in Figure 2.11.

Rheological measurements can be tricky and difficult to interpret as many measurement errors can be hidden in the results. Since cement-based materials are thixotropic in nature, this can cause false interpretations of measured torque values. If the structure of the material is not completely broken down, the torque value recorded will appear higher since the structure has not reached equilibrium yet for a given shear rate [51]. This can also be affected by the mixing procedure as it has been shown that the

mixing energy or shear history can change the initial rheological parameters measured [50]. Plug flow is also a phenomena that can occur when measuring that needs to be corrected for to get accurate results especially in concentric cylinder rheometers [50], [51]. Plug flow occurs when not all of the material in the rheometer is sheared. This can cause inaccurate results since the equations to calculate the yield stress and plastic viscosity use the entire outer radius in calculations rather than the plug radius. Errors due to structural buildup and plug flow are shown in Figure 2.12.

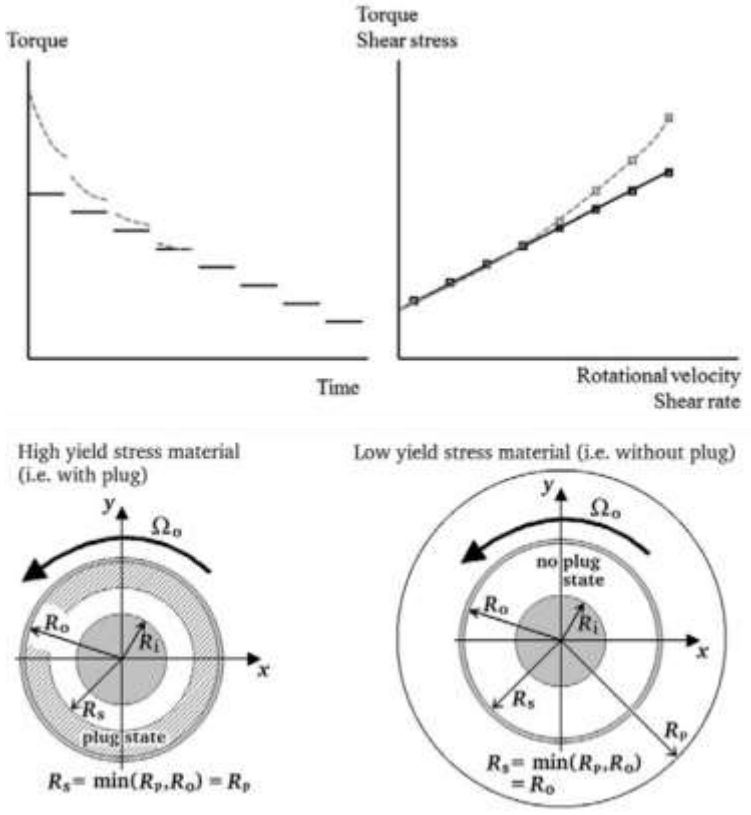

Figure 2.12. Errors Due to Structural Build-up (Top) and Plug Flow (Bottom)

A third common error that can effect results is due to particle migration and slip in the rheometer. This error is due to particles moving away from the high shear zones.

This causes lower rheological measurements since there would be less particles where the measurement of torque is occurring [50], [51].

Two tools that can be used to help evaluate the rheological properties of various concrete mixes is a rheograph and a workability box [48]. A rheograph is a graph of the yield stress (x-axis) versus the plastic viscosity (y-axis) to compare different mixes. This can be used to evaluate the effect different changes on a mix design. For example, changing the water to cement ratio will change both the yield stress and plastic viscosity so a rheograph will be able to show the change in rheological properties for the different ratios [48]. Rheographs can then be extended to a workability box. A workability box is a two-dimensional polygon area within a rheograph [48]. A workability box can be used to define combinations of yield stress and plastic viscosities that represent a certain type of concrete or workability in concrete. This can be useful when trying to come up with a mix design for different high performance concretes which require adapted rheology to be most effective.

When rheometers are not available to precisely measure and study the rheology of cement-based materials, other alternatives can be used to study and correlate yield stress and plastic viscosity. Many empirical tests are used to evaluate workability and rheology of cement-based materials, but two main tests are discussed here. One test to relate to the yield stress is the mini-slump tests for cement paste and mortars [53], [54]. One of the studies also provided a correlation to an Abram's cone as well. Roussel has shown through analytical and empirical tests that the slump flow diameter measurement from these tests can link to yield stress of a mix. To study viscosity, one test that can be done for cement paste is the use of a Marsh cone. This test involves the measurement of time

for a cement paste to travel through a cone and fill a volume of 1000 mL. The time is recorded every 100 mL. Through analytical modeling, it has been shown that the time to fill the volume relates to the viscosity of cement paste [55]. These two methods are alternative and less expensive ways to evaluate rheology if a rheometer is not available.

2.3.2. Fiber Effect on Rheology. For use of fibers as a reinforcing system within 3D printed concrete, the effects of the fibers on the fresh properties and rheology should be well understood. Fibers will change the rheological properties of the mixture, and this will affect both the buildability and extrudability of the printed concrete.

Khayat and Roussel [56] looked at the testing and performance of Fiber Reinforced-Self Consolidating Concrete (FR-SCC) and several conclusions were able to be made from their study on how fibers effect concrete rheology. Some of the tests in their study included slump flow, V-funnel, Filling Box, and use of an IBB concrete rheometer. The study also looked at the effect of fiber volume on the workability, rheological properties, and flow characteristics of the concrete. They found that the addition of fibers increased the yield stress with an increase in fiber volume. For the constant yield stress and slump values, as the fiber content increased this increased the measured plastic viscosity.

Martinie, Rossi, and Roussel [57] also performed work to look at the rheology of fiber-reinforced concrete. They specifically looked at the effect of fibers on yield stress, how the packing fraction of the fibers related to the rheology, and came up with a criteria to define the difference between a rigid and flexible fiber used in the mix. Their rheological tests were performed with a Haake viscotester VT550 and a Vane test was performed. When looking at what defines a fiber as rigid or not, they found that it was

based on a couple of factors: Young's Modulus and the aspect ratio. The fiber rigidity is important because rigid fibers will have increase the yield stress more than flexible fibers (less rigid) once they reach a critical volume fraction of fibers. When they reach this volume the network of fibers will be able to withstand an external load due to contact of the rigid bodies with the material. The higher the Young's Modulus the greater increase in rigidity and if the fibers become longer (thus increasing the aspect ratio) then this will make them less rigid. It was shown that steel fibers are rigid and long carbon fibers are not even though they have similar Young's Modulus. The paper also looks at how the relative packing fraction effects the yield stress of the cement paste with fibers. A fiber packing fraction above 0.8 caused the yield stress to spike significantly. This is shown in Figure 2.13 where the packing fraction is on the x-axis and the y-axis is the relative yield stress of the mixture. The relative packing fraction is the ratio of the yield stress of the paste containing fibers versus the yield stress of the paste without fibers.

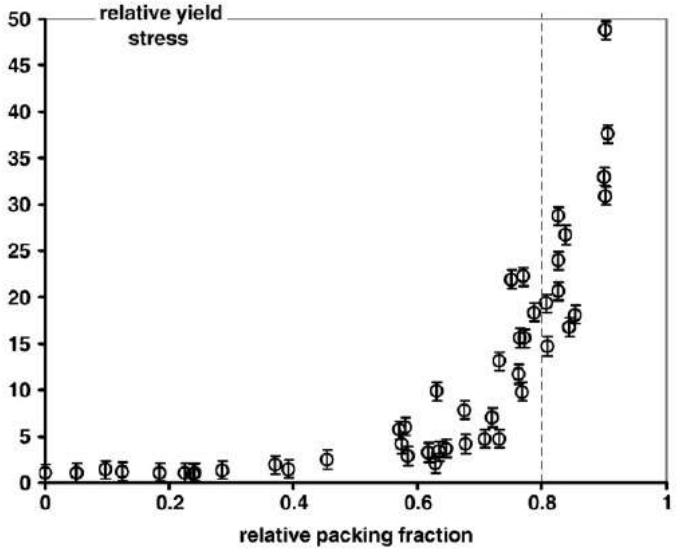

Figure 2.13. Relative Yield Stress vs Relative Packing Fraction [57]

This matches work from Emdadi et al. and Mehdipour and Libre [58], [59]. Both compare the fiber factor, $F = \frac{V_f L_f}{d_f}$, to the effects on workability of paste, mortar, or concrete. Similar to Figure 2.13, they show that the yield stress increases exponentially, but rather than comparing relative packing fraction, fiber factor is compared. By looking at the fiber factor, a critical fiber factor F_c, and a dense fiber factor F_d were found. The critical fiber factor is the point where workability starts to reduce for a mixture. The dense fiber factor is where the workability rapidly decays with a higher chance of fiber clumping, segregation, and reduced mechanical properties. This effect of volume fraction of particles on the rheological properties, which is directly related to the fiber factor, is shown in Figure 2.14. The three regions shown correspond to being under the critical fiber factor, in between the critical fiber factor and dense fiber factor, and above the dense fiber factor.

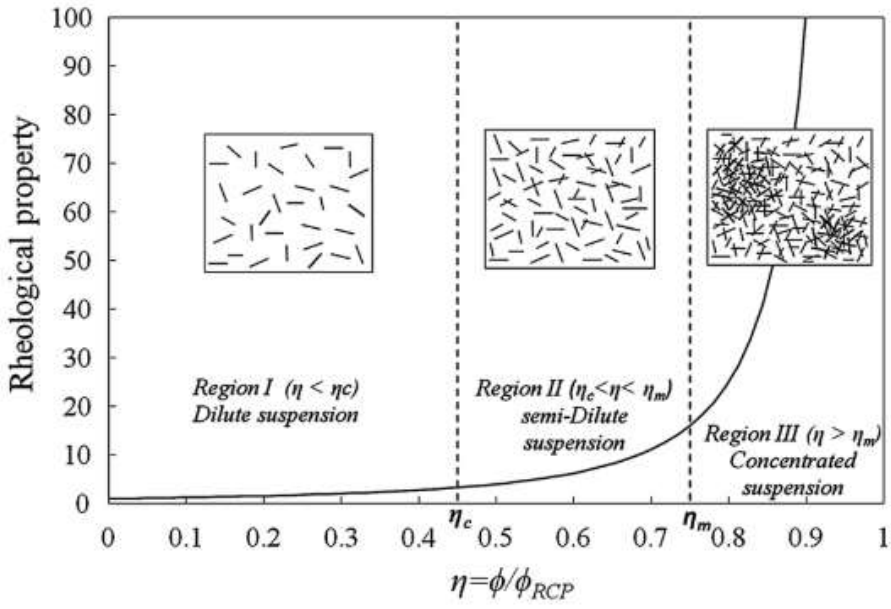

Figure 2.14. Fiber Volume Fraction Effect on Rheological Properties

Malaszkiewicz [60] investigated the rheological properties of polymer fibers. He investigated the yield stress and plastic viscosity of three different types of polymer fibers at 10, 40, and 80 minutes after mixing. He performed these tests by using a Viskomat XL rheometer to measure the mortar properties. The three types of polymer fibers studied was a fibrillated isotactic polypropylene fiber, a fibrillated refined polypropylene fiber, and a copolymer-profiled fiber. The results from these tests show that even when comparing polymer fibers to each other, the results are dependent on the fiber type. The author concluded that the workability of the monofilament fiber was found to be better than the fibrillated fiber. The fibers had the highest impact on yield stress. The increase in plastic viscosity was increased with fiber content. Fibrillated fibers developed their spatial structure during mixing and increased the yield stress as the content increases. Increase in content of profiled fibers did not affect the yield stress. Viscosity increase over time was slower for fibrillated fibers than fiber free mix. Finally, the efficiency of the superplasticizer over time increased which meant that the yield stress increase was slower with time compared to the fiber free mix.

Similarly a study was done on polymeric synthetic macro fibers to study the rheological effects [61]. As in the case of polypropylene fibers, the yield stress and plastic viscosity both saw linear increases with increasing fiber content. One important finding was that the rate of the increase in yield stress and plastic viscosity was dependent of the mixture design as three different mixture designs with varying amount of silica fume.

Ding et al. [62] did a study on the workability of various kinds of polymer and steel fibers. They investigated the rheological properties and workability for mixtures

with micro-fibers and macro-fibers. For the micro-fibers they used a rheometer to find the yield stress and plastic viscosity of the micro-fiber mixes. They also compared this with a flow channel. For the macro-fibers, the rheometer was not able to be used so a slump test, J-ring, and L-box was used to evaluate the workability. From completing these tests they found that for the micro-fibers, the smaller dosages (1 kg/m^3 for polypropylene fibers and 10 kg/m^3 for steel fibers) do not have negative influence on workability. At a higher dosage of 2 kg/m^3 the polypropylene micro-fibers had a negative effect. When comparing the flowability results from the flow table, they agreed with the results found from the rheometer.

Ponikiewski and Katzer [63] also have done a study on the rheological effects of different types and geometries of fibers on FR-SCC. They tested the slump, T50, and yield stress of the fresh concrete mixtues. The yield stress was found using a Rheometric workability test (RTU) with the rheometer BT-2. The study was done on steel, basalt, and polypropylene fibers with the steel fibers having various geometries. The yield stress of all the different types of fibers increased with fiber volume increases as previously shown by [56]. As far as looking at the different geometries, the different fiber geometries can somewhat effect the value of different rheological properties but overall have the same behavior as the main fiber type.

2.3.3. Rheology Effect on 3D Printing and Extrusion. The rheological properties of cement paste and mortar can have a large impact on many of the requirements for 3D printing and extrusion of cement based materials. Optimization of rheological properties is also difficult due to the many conflicting needs in the rheological properties throughout the printing process in order for all aspects to be

successful. Roussel described various parameters that rheology has to play in 3D printing concrete [64]. He describes several areas that the rheological behavior effects including extrusion/pumping, layer stability, geometry control, and layer interface strength. [65] also looked into the effect of rheology, but specifically on extrusion.

For extrudability/pumpability of concrete, an initial fluidity is required to pump or extrude which is based upon a lower yield stress and plastic viscosity [64]. Depending on the extrusion system, these specific values needed for extrudability change and even the process to which the way extrusion behaves is effected (see Section 2.4.1). The rheological properties of the material is one of the parameters will effect whether the material behaves as a plug or if the material will be sheared throughout the extrusion process depending or not whether the rheology allows for an lubrication layer [64].

Another method to look into the rheological properties was to use capillary rheology with a ram extruder to help define extrudability based upon rheology [65]. This method used the known value of extrusion pressure, diameter of the extrusion tube, length extruded, and extrusion rate to calculate the apparent shear stress and apparent shear rate. From this criteria, there was not a good relation to yield stress or plastic viscosity and extrudability when looking at each criteria alone. The authors did find that there was an interaction between the two parameters that allowed for extrudability to be defined. This interaction between yield stress and plastic viscosity is shown in Figure 2.15 where whether a mix design was defined as not extrudable if it had poor shape stability, phase migration, excessively high extrusion pressure, or surface defects [65]. It should be noted that this experiment was not studying extrudability for 3D printing, but the criteria used is still relevant and necessary in extrusion of 3D printing.

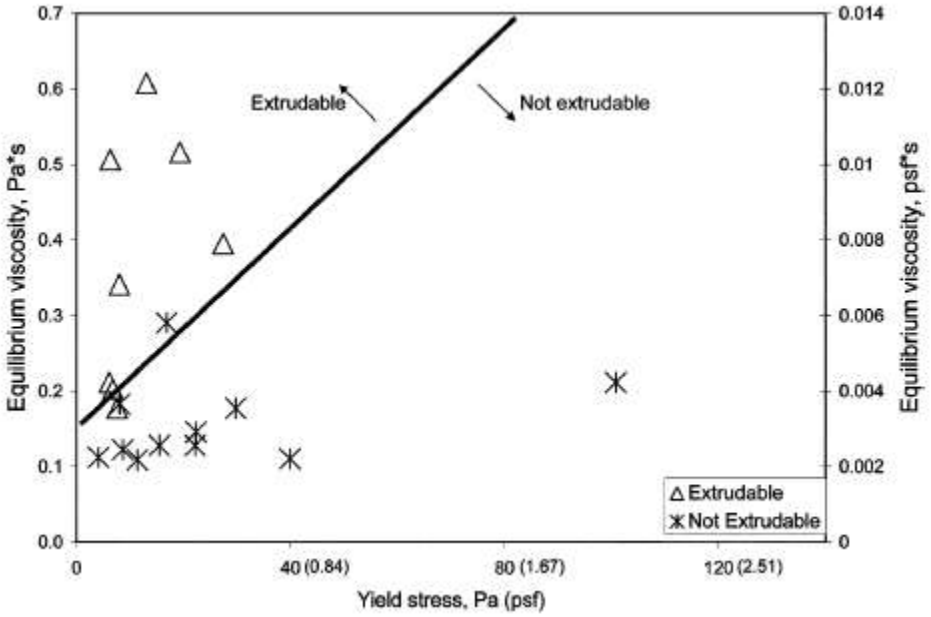

Figure 2.15. Viscosity versus Yield Stress for Extrudability [65]

Rheology also has an important role once the material has been extruded. The stability of the layers (printability), individually and as a whole, are affected by rheological properties. Roussel discussed the stability of layers in terms of both single layer stability and multiple layer stability [64]. For a single layer printed, the concrete must have a sufficient yield stress after deposition to be able to hold its own weight under gravity. Other factors that could add to the initial yield stress needed by a material would be the speed and layer height of the material [64]. If the speed of printing is fast, then this will create an inertial stress that the concrete yield strength must be above to hold. For a thin layer, surface tension could contribute to control the shape of the printed layer.

For the stability of multiple layers, many rheological and physical factors play a role. The thixotropic properties effect the stability since the more thixotropic the material, the higher the yield stress build up will be. The yield stress will be important to control as time increases due to the strength of the lower layers needing to be able to withstand not

only its own weight, but the weight of the above layers which will continue to increase as printing continues [64]. Due to the thixotropic buildup of the material, this then shows that the speed and length of printing for each layer matters as this will affect the structuration time, or time for structural build up, for the material. The overall stability of the printed structure then comes into play. Since the printed structure is a slender element, issues with buckling or overall stability failure of the structure can become an issue. Also, settlement of the layers can cause the structure to not be printed properly even though the yield strength might suffice [64]. They are affected by the elastic properties of the printed material below its yield stress.

Bringing the different aspects of stability into printing shows in detail the first conflict between rheological properties of printing concrete. For stability, a higher yield stress is preferred to allow for more layers and faster printing to occur. For extrusion, this higher yield stress could cause a material to become difficult to extrude or require high extrusion pressure.

Geometric control of layers is also affected by rheology. One issue that can occur while printing is a cracking behavior of the deposited layer especially around curves when printing. This cracking behavior can be due to an initially high yield stress material especially for high solid fractions and strong particle interactions [64]. Other factors contributing to the cracking of layers include the radius of curvature from extrusion, material tensile strength, and critical strain. It is also suggested that polymer or organic fibers could help mitigate this issue.

Finally, rheology can control the layer interface strength. The layer interface strength can be affected by how thixotropic a material is. Highly thixotropic materials can

form cold joints between layers as has been studied in self consolidating concrete [66]. This puts an upper limit on the structuration rate available for concrete. This puts two main constraints on printing: longer print time leading to weaker layers and higher thixotropy leading to weaker layers [64]. Again this leads to another conflict of fresh properties. High thixotropy can help increase the stability of the printed layers, but also can increase the chances of a cold joint or weak interlayer bond. Overall the rheological parameters of cement-based materials have a large effect on every aspect of extrusion and 3D printing.

2.4. EXTRUSION OF CEMENTITIOUS MATERIAL

Extrusion of cementitious material was not first used in 3D printing. Extrusion of cementitious materials has also been used for making curbs, hollow core slabs, and wall panels to name a few. Understanding the behavior of extrusion in the fresh state is important as it undergoes widely different forces and processing than typical cast in place or even self-consolidating concrete. With respect to 3D printing, understanding how this can affect fresh properties and the different parameters within extrusion is vital. The tribological and rheological behavior of the paste has been previously studied by several authors and is further discussed.

2.4.1. Characteristics of Extruded Paste. One of the first items to understand about extruded paste is the behavior of the paste flowing through the extruder and the different forces on the paste/mortar. Perrot et al. looked at creating a frictional plastic prediction model for extruding paste and in doing this studied the physical mechanisms governing the forming process [67]. In this study they described the flow as a plug with

slip and friction along the walls of the extruder. The type of extruder used in this study was a ram extruder which pushed the paste out of a cylinder through a die at the end of the cylinder. Both [67], [68] described the overall force needed to create the plug flow as a combination of the frictional force and shaping force. Figure 2.16 shows the different forces described by the two studies. F is the total force needed to extrude the paste, K_w is the frictional stress along the walls of the extruder, F_{pl} is the shaping force of the material, D is the diameter of the cylinder, and d is the diameter of the opening. Three zones of flow were described and are shown in Figure 2.16: the plug flow zone of length L_B, the sheared flow in the shaping zone of length L_{dz}, and the dead zone of length L_O.

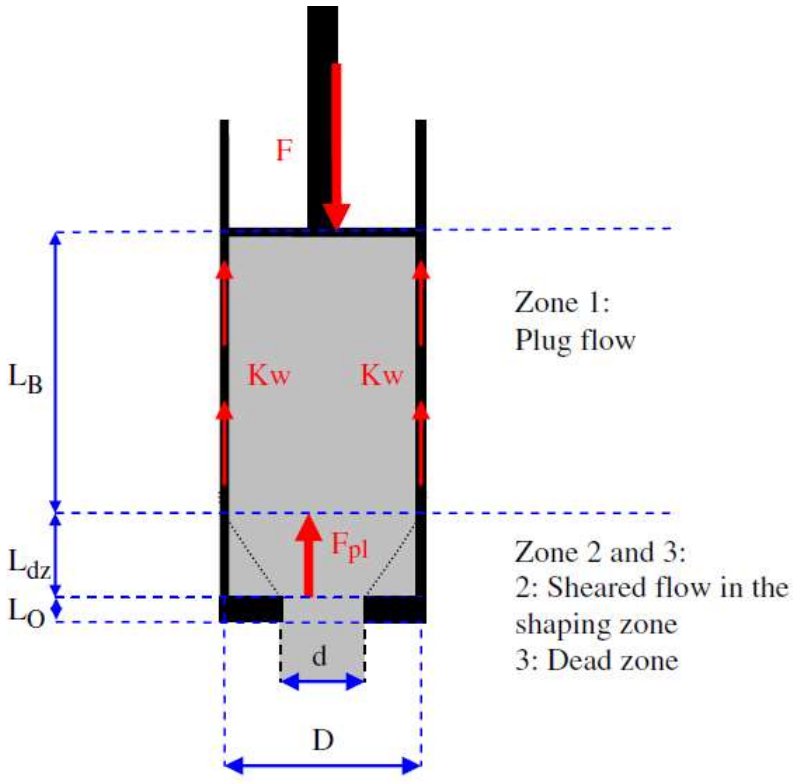

Figure 2.16. Forces and Flow Zones in Extruded Paste [68]

Several researchers have stated that liquefaction can occur within the paste due to the loading previously described [67], [69], [70]. Due to the friction on the walls of the cylinder, a high-pressure gradient forms within the extruder. This causes water or cement paste to filter through the granular skeleton of the mortar [67]. This can be compared to the effect of consolidation in soils and can lead to an increased pressure near the end of the extrusion process. If there is a lot of filtration or bleeding due to this pressure gradient, the solid volume fraction and water-cement ratio will change in addition to the increased extrusion force needed [69]. This can also change the local rheological and tribological properties within the paste [67].

According to [70] two different mechanisms can be considered to control the extrusion behavior and they are related to the way the paste or mortar will behave. One mechanism considers the material as perfectly plastic. If the material is perfectly plastic, then the yield stress and ratio of the opening to the cylinder width (d/D) will control and be linked to the pressure needed for extrusion. The other mechanism considered is for non-yielded frictional materials. In this mechanism, friction is speed dependent and related to frictional energy dissipation. This increases as the frictional zone, or length of the cylinder, increases. Toutou et al. found that the speed of extrusion effected how the material behaved- perfectly plastic versus non-yielded frictional [70]. Their results showed that a higher extrusion speed led to a cohesive plastic behavior, while lower speeds led to a drained frictional plastic behavior.

Another similar criteria was described for extrusion and pumping for applications for 3D printing. This criteria also gives two cases of behavior that can occur: 1) pure extrusion of an unsheared plug flow that deposits a flocculated material and 2) material is

sheared and spreads on the support or layer and then builds structure [64]. These two cases are caused by whether or not a “lubrication layer” forms. The “lubrication layer” is a layer around the edge of the extruder where only water and fine particles are sheared and the extrudability (or pumpability) is dependent on this layer rather than rheological properties [64]. This layer does not form as well for lower water to cement ratio or high yield stress and viscous mixes. The formation and transition of these two cases are dependant on the material rheology, extrusion rate, and nozzle geometry [64]. These layers are illustrated in Figure 2.17. It was also noted, however, that for extrusion with a screw pump, these cases do not exist since the material is sheared in the nozzle thus changing rheological property requirements for printing.

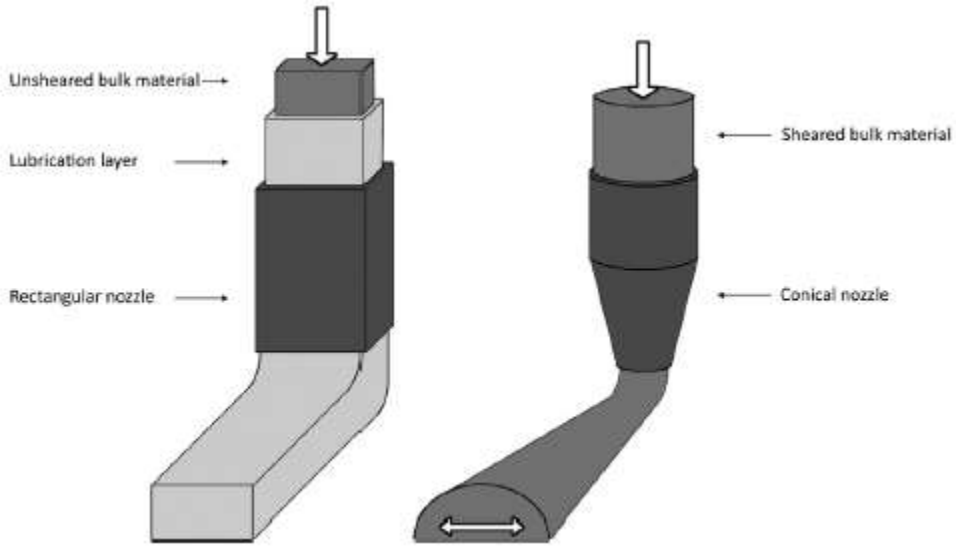

Figure 2.17. Schematic of Flow Cases for Extrusion [64]

Speed is not the only physical testing parameter that effects the behavior of the extruded material. It is well known that the extrusion ratio (d/D) and shape of the nozzle effects the extrusion force needed [67], [68], [70], [71]. Having a larger d/D ratio would

allow for easier extrusion and less force. For direct comparisons between mixes in terms of their extrudability, the d/D ratio should be kept constant unless this is under investigation within the experiment.

Aside from the understanding of the characteristics of flow during extrusion, the extruded paste can have other changed properties due to the extrusion process compared to cast-in-place concrete. According to [69] extrusion helps improve the mechanical properties by limiting the water content and voids within the specimen. Another study looked at the porosity of the extruded paste compared to cast in place concrete [72]. This study did various tests such as Scanning Electron Microscopy (SEM), Mercury Intrusion Porosimetry (MIP), Atomic Force Microscopy (AFM), and X-Ray Diffraction (XRD). They also found that extrusion decreased the porosity making a more dense and compacted product. Decreasing the porosity can have a positive effect on mechanical and durability requirements of the concrete.

Not as many studies looked into the effect of extrusion of fibers. One study that looked into fibers compared the results of the tests with cast-in-place concrete and looked at how the specimens performed on a microscale as well as macroscale [72]. This test used polyvinyl alcohol (PVA) fibers and acrylic fibers of varying lengths of 2 mm and 6 mm. The study concluded that the shorter fibers had improved flexural strength than the longer fibers in the extruded composite. This had to due with the mechanism of failure in the fibers. For the longer fibers, the fibers would fracture and not pullout. For the shorter fibers, they would pull-out. This difference in mechanism was noted to be due to the difference in matrix bond to the different fibers. They also found that the extruded composite had better bond to the 6 mm fibers compared to the cast-in place specimens.

This could be due to the decreased porosity and increased density of the extruded paste compared to the cast in place paste. There is still a need to define how the fibers affect extrudability from a workability, rheological, and extrusion standpoint.

2.4.2. Measurement Methods of Extrusion. Three main methods have been suggested in literature for characterizing the extrudability of concrete. These methods include a penetration resistance test, ram extrusion test, and squeezing tool test [67], [68], [70], [71]. These tests have been used to characterize and quantify some of the behavior described previously for extruded cementitious material. The squeeze test and penetration resistance tests are indirect test methods while the ram extrusion test directly measures the extrusion process. The following paragraphs will describe each of these test methods as well as the information they provide on characterizing extrusion for cement-based materials.

The penetration resistance test was used by Chen et al. to help understand the extrusion time window [71]. This test follows ASTM C403 [73]. In this test, fresh concrete is penetrated with a needle and the amount of force needed to penetrate the sample is measured. This is done after a suggested initial time period of three to four hours and then measured at half to one hour intervals thereafter for samples without an accelerator [73]. This is done until a penetration resistance of 4000 psi [27.6 MPa] is reached. This allows for a penetration resistance versus elapsed time plot to be graphed. Outside of extrusion testing, this testing method is used to find the initial set and final set of concrete by finding the time it takes to reach 500 psi [3.5 MPa] and 4000 psi [27.6 MPa] respectively.

For the use of characterizing extrusion, the zone in which the material was extrudable was first defined in terms of penetratition resistance. This allowed for the upper limit (too stiff to extrude) and the lower limit (too wet to extrude) to be defined [71]. Then using the penetration resistance test, a graph could be plotted and the extrudability window was found for which the penetration resistance was in between the upper and lower limits. An example of this graph is shown in Figure 2.18.

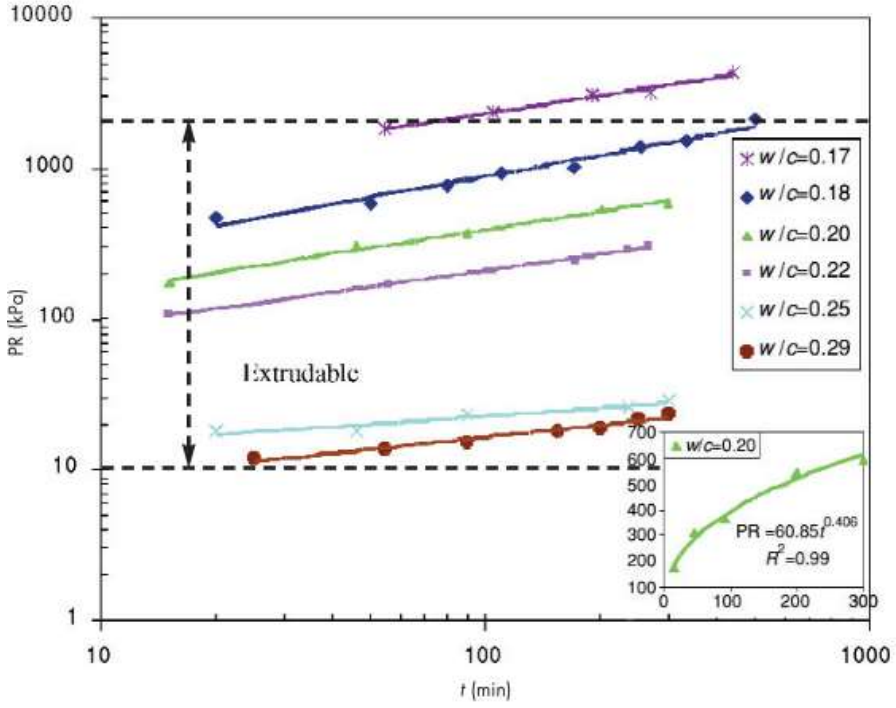

Figure 2.18. Penetration Test Extrudability Window Example [71]

In Figure 2.18 PR stands for penetration resistance and t is the time of hydration. This test is helpful in defining the extrudability limits and the time range for extrudability. The study noted that the results will be different for each extrusion system

based on the type of die or cross-section being extruded and the amount of extrusion force that can be applied [71].

The ram extrusion force is a common method for evaluating extrudability and studying the characteristics of cementitious materials being extruded [26], [67], [68]. This test consists of pushing or extruding mortar through a cylinder with a piston pushing it. While the piston is pushing the material, the force can be measured along the distance of the tube. This allows for a detailed study of the mechanisms and mechanics behind extrusion as mentioned and studied in Section 2.4.1. There are no standards for testing procedures for this test currently. Various velocities and geometric configurations have been used for testing. In Figure 2.19 a schematic of a ram extrusion test is shown [26].

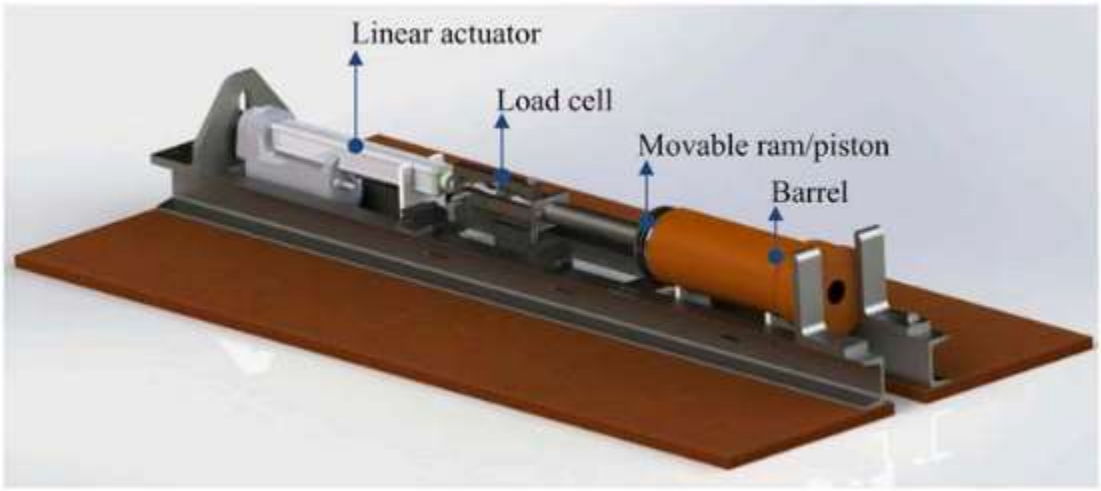

Figure 2.19. Ram Extrusion Test Schematic [26]

In one study [68], the ram extrusion test was used and expanded on to also allow for a measurement of the frictional force. This allows for a study of the frictional effects

on the extruded mortar and the ability to compare its effects with the overall force on the mortar.

The third method found to study extrudability is the squeeze flow test [70]. This method uses a press with parallel circular plates to compress a cylindrical sample of fresh mortar. The sample is compressed at a constant velocity and the force is measured. This force causes a radial flow. The reduced compression load can then be plotted against the sample height over the plate radius. This data can be used to find certain rheological parameters that effect the extrusion quality and machine processing [70]. One of the main findings from doing this test is to understand if the material will have a perfect plastic behavior or a drained frictional plastic behavior. Figure 2.20 shows an image of a test on a clay paste sample before the test start tests by [70].

Figure 2.20. Squeeze Flow Test prior to Start [70]

3. METHODS

Characterizing extrudability of cement based materials for 3D printing is challenging due to the lack of standard test methods and procedures. In this chapter, the test methods to evaluate the performance of fibers as a reinforcing system and the test methods developed to characterize extrudability are described. First, the test methods to investigate the effect of fibers as a reinforcing system and comparing with an environmentally friendly option are described. Then test methods are described in detail to evaluate extrudability and to analyze the printing extrusion process quantitatively and qualitatively. The tests developed are extended to printing with and without fiber reinforcement. The developed tests are designed to characterize the extrusion process in terms of blockage, extrusion force and energy, and rheological properties. A final verification and comparison of mechanical properties through manual printing is described as well.

3.1. MATERIAL CHARACTERIZATION

The descriptions of the materials for both the concrete and mortar mixtures used in the FRC and printing studies are further described in this section. For the concrete mixtures in Section 3.2, a Type I Portland limestone cement with five percent silica fume replacement was chosen as the binder for the experiment. Natural river sand, intermediate, and coarse aggregate were used in the concrete mixtures all in compliance with ASTM C33 [74]. The manufactured fibers are a straight fiber with a length of 13 mm and 0.20 mm thickness. These fibers are copper coated and have a tensile strength of

2160 MPa. The recycled fibers come from shredded up tires so the geometry, length, and diameter have some variance. The geometric properties of the fibers are shown in Table 3.1.

Table 3.1. Fiber Properties

	Density (kg/m^3)	Length (mm)	Thickness (mm)	Aspect Ratio
Recycled Tire Fibers	6800	22.50	0.30	75
Manufactured Steel Fibers	7800	13.00	0.20	65

The length and thickness of the recycled fibers varied due to the randomness of being shredded from the tires. The values for recycled tire fibers in Table 3.1 are based on an average. Shown in Figure 3.1 is the recycled fibers (left) compared to the manufactured fibers (right).

Figure 3.1. Recycled Fibers (Left) vs Manufactured Fibers (Right)

The materials used in the printed mortar consisted of Type I Portland Cement, Missouri Natural River Sand, MasterGlenium 7500 full-range water reducing admixture, fibers, and tap water. The Type I cement was sieved with the No. 100 size. MasterGlenium 7500 meets ASTM C494 [77] criteria for both a Type A and Type F water-reducing and high range water reducing chemical admixture. The fibers used were the Dramix OL 13/.20 steel fiber which is the same as the manufactured fiber type previously discussed. The physical properties of these fibers are shown previously in Table 3.1 and are shown in Figure 3.1.

The sand was evaluated using a sieve analysis to help understand the particle distribution. With particle size effecting the blockage point for extrudability, understanding the amount of each particle size and the gradation of the particles is important for analyzing blocking. The sieve analysis was done in accordance with ASTM C136 [78]. Three different maximum sand sizes were used for investigating blockage: No. 8, No. 16, and No. 30 sieved sand. Figure 3.2 shows an image of each of the size sands. The gradation for each of the mixtures from the non-sieved Missouri Natural River Sand to the No. 30 sieved sand is shown below in Figure 3.3. From this it shows that the gradation becomes less evenly distributed as the sand gets sieved with a large gap in particle size. For the No. 30 sieved sand the sand almost becomes mono-sized. This difference in gradation and sand size changes the specific surface area in the mixtures which has an effect on water demand. This finding will briefly be described when discussing the findings from the Blockage Test.

Figure 3.2. Sand Sizes for Blockage Test

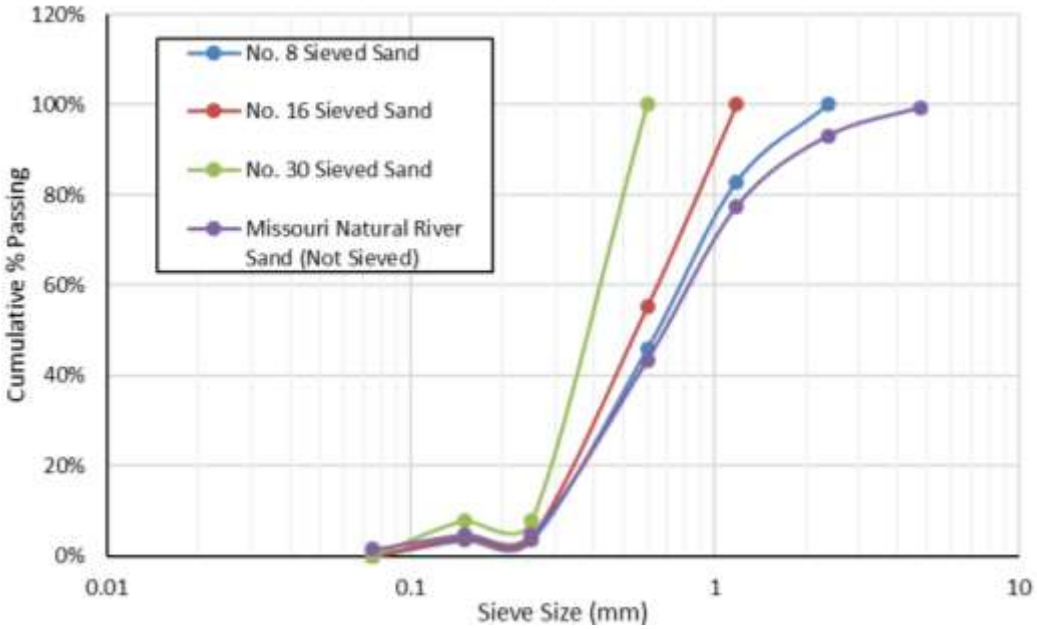

Figure 3.3. Sand Gradation for Sieved Sand

.

3.2. MECHANICAL PROPRETIES OF FIBER REINFORCED CONCRETE

Eight different mixtures were chosen to look at the differences in fiber effect on fresh and mechanical properties. A reference mixture (REF) with no fibers was made to compare how the fibers improve the mechanical properties of the concrete. Three mixtures of recycled tire fibers as a sustainable replacement to manufactured fibers were chosen with a 0.25, 0.5, and 0.75 percent by volume (RF-0.25, RF-0.50, RF-0.75). Three mixtures of the manufactured steel fibers with the same percent volumes as the recycled fibers were also studied (F-0.25, F-0.50, F-0.75). The eighth mixture was a hybrid mixture (HF) with 0.25 percent volume of recycled fibers and a 0.25 percent volume of steel fibers.

3.2.1. Mix Design The properties and proportions of the concrete mix design were kept constant throughout all the mixtures with the volume of fibers and amount of superplasticizer (SP) being the only changes. The water to cementious material ratios were kept constant but SP dosage was adjusted in order to achieve the same workability in all mixtures. The water-cementitious material ratio was held constant at 0.40. The proportions for all of the eight mixtures are shown in Table 3.2.

The amount of SP varied to try and keep a target slump of 17.5 ± 2.5 cm. Three beams with cross section dimensions of 76.2 x76.2 mm and two cylinders with a diameter of 101.6 mm and length of 203.2 mm were made for each mix. The beams were made with a 25.4 mm deep notch. The samples were cured in lime saturated water and tested at 28 days.

Table 3.2. Mixture Proportions for FRC Study

Mixture	w/cm ratio	Cement (kg/m^3)	Silica fume (kg/m^3)	Coarse Aggregate (kg/m^3)	Intermediate Aggregate (kg/m^3)	Sand (kg/m^3)	Manufactured Fiber %	Recycled Fiber %	SP Wt. % of binder
REF	0.40	285	15	580	390	965	0	0	0.90
RF-0.25	0.40	285	15	580	390	965	0	0.25	1.00
RF-0.50	0.40	285	15	580	390	965	0	0.50	1.10
RF-0.75	0.40	285	15	580	390	965	0	0.75	1.15
F-0.25	0.40	285	15	580	390	965	0.25	0	1.20
F-0.50	0.40	285	15	580	390	965	0.50	0	1.40
F-0.75	0.40	285	15	580	390	965	0.75	0	1.50
HF	0.40	285	15	580	390	965	0.25	0.25	1.25

3.2.2. Mechanical Properties Testing. A compression test, modulus of elasticity test, and a three point bending test were performed on the specimens. The compression test was performed on two samples to find the compressive strength of the concrete according to ASTM C39 [75]. A modulus of elasticity test [76] was then performed where the cylinders were tested to 40% of the ultimate compressive strength. The set up for the elastic modulus test is shown in Figure 3.4.

Figure 3.4. Modulus of Elasticity Test Set Up

Flexural properties were tested using a three point bending test [45]. The beam was set up over a span of 304.8 mm with the point load being placed over the center of the span. An extensometer was attached to metal strips that were placed at the end of the notches on the beam and measured the crack mouth opening displacement (CMOD) versus the load in the experiment. The load versus deflection was also measured in the experiment which allowed for the measurement of toughness and residual strength by finding the area under the load versus deflection curve. The three point bending test also allowed for calculations of first crack load, maximum bending stress, and fracture energy. The machine loaded the beams at a constant rate of 1 mm/minute and was done for a minimum of ten minutes. The set up for the three point bending test of the notched beam is shown in Figure 3.5 and a schematic of the test is shown in Figure 3.6.

Figure 3.5. Three Point Bending Test

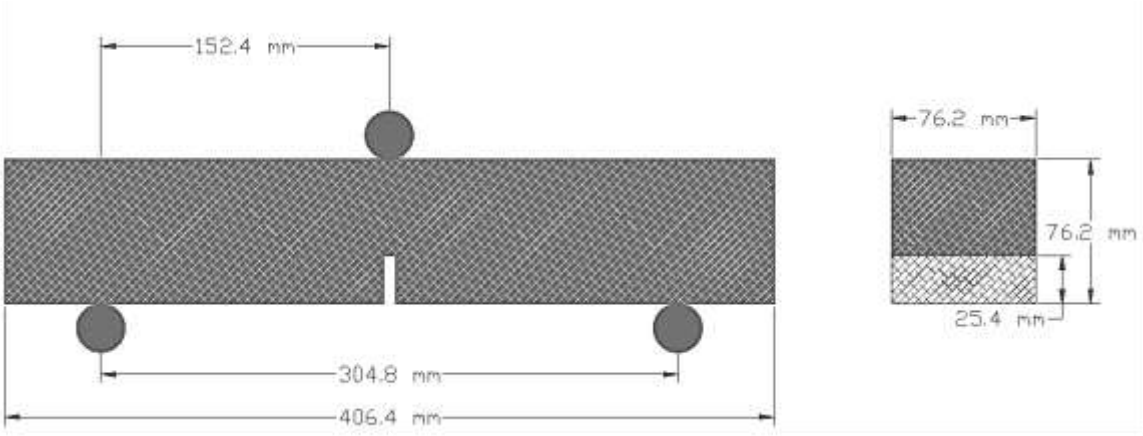

Figure 3.6. Three Point Bending Schematic

3.3. EXTRUSION BLOCKAGE TEST

Blockage in terms of extrusion refers to the interlocking and accumulation of particles that stops the paste or mortar from being able to flow through an extruder. Blockage can cause extrusion to completely stop and if using a mechanical system with a motor could then cause excessively high load on the motor which in turn could damage or burn out the motor. Depending on the constituents, blockage can occur initially causing no extrusion to occur, or can happen as extrusion continues and there is a buildup of particles near the opening of the extruder. Understanding the causes of blockage and developing tests to characterize extrudability are critical in creating a successful mix design for printing.

3.3.1. Blockage Test Variables. Many factors influence blockage of a system. The following tests look at four factors that can change whether a mixture causes blockage during extrusion. These factors include 1) maximum particle size, 2) workability, 3) binder content, 4) and fiber content. Mortar was investigated in this study.

The same factors could apply to larger and smaller systems if chosen to study (paste and concrete level). An overview of the study of blockage is shown in Figure 3.7.

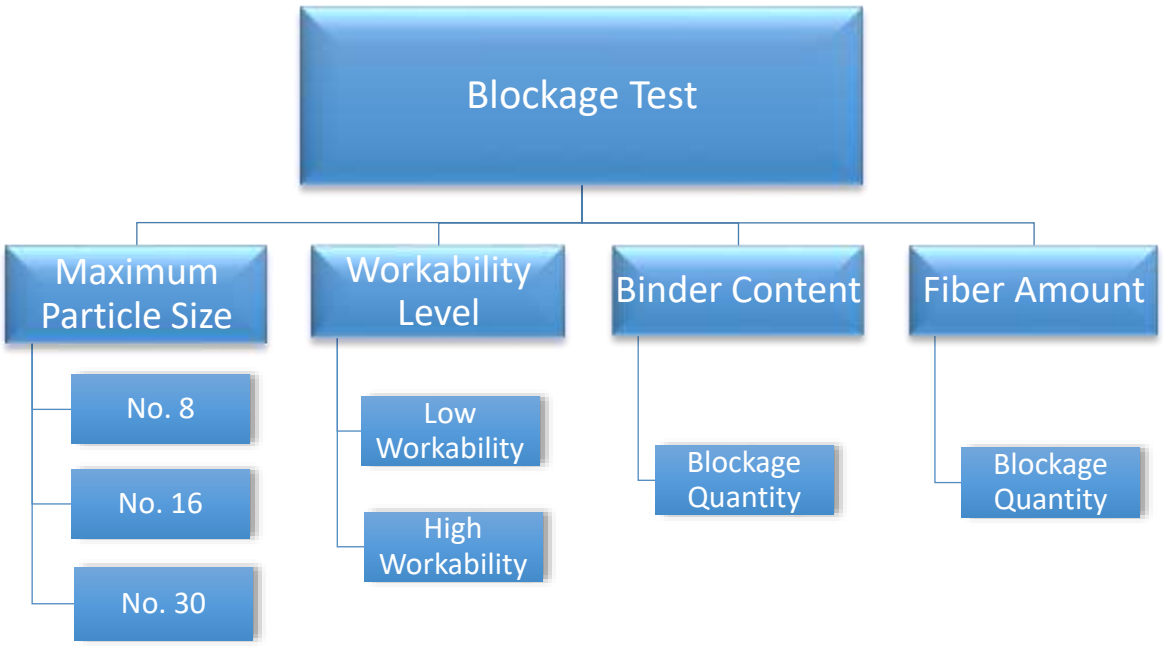

Figure 3.7. Blockage Test Parameter Overview

For looking into the effect of the maximum particle size, three different maximum sand sizes were evaluated. These included sands sieved with a No. 8 (3.26 mm), No. 16 (1.18 mm), and No. 30 (0.6 mm) sieves. All the different size sand was sieved from the same Missouri natural river sand.

To study the workability, two different workability levels were chosen for each sand size. A less workable mixture was tested not using any water-reducing admixtures thus resulting in a mini-slump that did not flow and needed to use the flow table. A more workable mixture was tested using a superplasticizer (water-reducing admixture) to allow for a slump flow without using a flow table. For the No. 8 and No. 16 sieved sands 0.3%

of the binder content of superplasticizer was used. For the No. 30 sieved sand, 0.5% superplasticizer was used instead of 0.3% due to the increased specific surface area of using smaller particles causing a higher water demand which decreased workability.

Binder content was studied by altering the amount of binder to allow for extrusion. By adjusting the binder content, a blockage point, or minimum binder content that is needed in the mixture to provide enough lubrication between coarser particles and allow for flow of the mixture through the nozzle, could be found. This blockage point would allow for an understanding of when a mixture goes from extrudable to blocked for a given sand size and workability level. Identifying a minimum required binder content is important for an extrusion system for developing proper experimental test matrices that verifies all the tested mixtures will not block and can be analyzed for the intended study.

Fiber content can be analyzed by taking a known extrudable mixture and increasing the fiber content until the blocking point is found again. This was done by varying the fiber content in each mixture until it blocks. This allows for a critical fiber volume fraction of fibers to be found. This would also vary with each specific extruder depending on the geometric properties of the fibers and nozzle.

3.3.2. Procedure and Test Matrix. The blockage point was tested using a 150 mL syringe to extrude the mortar mixes. This syringe size chosen is the same as what is used for some of the ram extrusion tests for printing later described in Section 3.5. The syringe had an internal diameter of 39.5 mm and a nozzle diameter of 3.71 mm. The length of the syringe as measured from the 150 mL mark to the end of the of the syringe

is 119 mm and the total length of the cylindrical portion of the syringe is 148 mm. This syringe is shown in Figure 3.8.

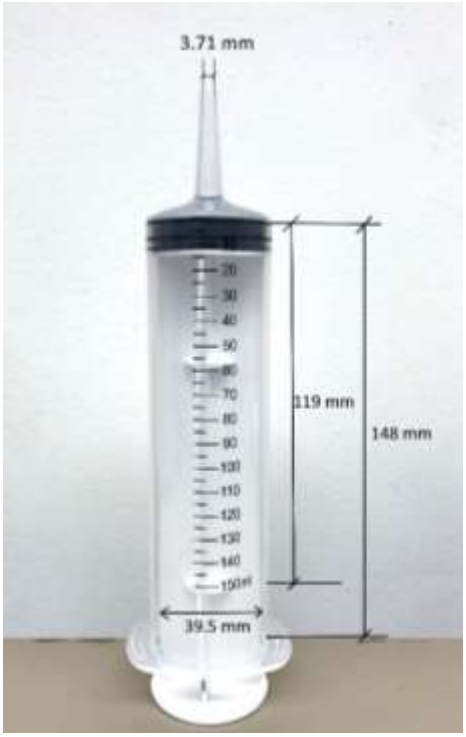

Figure 3.8. Extrusion Syringe Dimensions

First, before blockage was tested, the mortar mixture was tested using a mini slump. For the less workable mixture this was done using a flow table in accordance with ASTM C1437 [79]. The mortar was placed in two layers of the mini slump and rodded 20 times after each layer. The size of the mini slump was 70 mm diameter circle at the top of the cone and a 100 mm diameter opening at the bottom of the cone. The top of the mini slump was then scraped off to be level with the top. This can be shown in Figure 3.9.

The mini slump was then pulled and 25 table drops was applied to the mortar. This then caused the mortar to spread out into a circular shape. This circular shape was

then measured in both directions and averaged to get the slump flow reading. Figure 3.10 shows the slump flow after pulling the mini slump and after 25 hits.

Figure 3.9. Flow Table Apparatus and Setup

For the more workable mixtures, the flow table was not needed to create a slump flow. For this test, once the slump cone was pulled the mortar flowed into a circular shape similar to what is shown on the right in Figure 3.10. The diameter of this slump flow was also measured in both directions and averaged for each mixture created.

An initial maximum particle size was chosen to test. For this maximum particle size a certain binder content was chosen to try with a low binder content. The mortar was then mixed and filled to the 150 mL mark on the syringe. For the less workable mixtures, the material was rodded to get rid of any air pockets. For the more workable mixtures, the mortar was able to fill the syringe easily without rodding.

Figure 3.10. Flow Table Test Before and After 25 Table Hits

The syringe was then manually pushed to see if the mortar would extrude. If the mortar blocked the nozzle, the binder content was then increased by 100 kg/m^3 and tried again. Blocking the nozzle was considered for both the case where it initially blocked or when the nozzle blocked partially through the extrusion process before the 150 mL of mortar was extruded. Once a mixture was able to extrude the full length without blocking, a mixture with a 50 kg/m^3 less binder content was then tried (intermediate point). This was done in order to validate the minimum required binder content to within 50 kg/m^3. If the intermediate point passed, then this was defined as the minimum binder content for extrusion. If the intermediate point blocked, the previous binder content that passed was considered the minimum binder content for extrusion. This process was repeated for all three maximum particle sizes to find the binder content that was the blocking point for both the more and less workable mixtures.

It should be noted that the process above would also work in the reverse manor. If the initial binder content selected passed, then the binder content would be lowered by 100 kg/m^3 until the nozzle blocked. An intermediate point would then be tested to increase the accuracy of the specific blocking point. For the syringe used the following mixtures were chosen from to help identify the blocking point for the different sand sizes and workability levels as shown in Table 3.3.

For testing the fibers, the syringe from Figure 3.8 was modified to have a nozzle diameter of 9.2 mm. This larger diameter nozzle was chosen to decrease the chance for blockage. For the fiber blockage test, the same process as above was followed for a constant sand size of No. 16 max size. The binder content chosen to test the fiber blockage was 900 kg/m^3 based upon results from the initial blockage tests without fibers. Fibers were then added to the mixture starting at a low fiber content of 0.25% by volume. This fiber content was chosen because it was the lowest fiber content used in the FRC study. If the mixture was able to extrude, the fiber content was then increased and mixture was attempted to extrude again. This was repeated until nozzle was blocked. Since the binder content had already been investigated as extrudable, this would then give the fiber content that would cause blockage. This test was done with a higher workability mixture with a 0.3% superplasticizer content and lower workability mixture with a superplasticizer content of 0.05%. Testing both low and high workability mixtures allowed for the fibers to be isolated for studying blockage and keep workability from having an effect on the results.

Table 3.3. Blockage Test Mixture Proportion Options

Mixture Options	**w/c ***	**Binder Content (kg/m^3)**	**Fine Aggregate (kg/m^3)**
1	0.35	600	1390
2	0.35	650	1323
3	0.35	700	1255
4	0.35	750	1188
5	0.35	800	1120
6	0.35	850	1053
7	0.35	900	985
8	0.35	950	918
9	0.35	1000	850
10	0.35	1050	783
11	0.35	1100	715
12	0.35	1150	648

*SP Content for Higher Workability Mixes 0.3% for No. 8 and 16 Sand and 0.5% for No. 30

No SP used for the Lower Workability Mixes

3.4. RHEOLOGICAL MEASUREMENTS

The rheological measurements were performed on a ConTec 6 Viscometer. This is a large gap coaxial rheometer made for paste and mortar measurements. The ConTec 6 measures the torque values for varying rotational velocities that can go from 0 to 1

revolution per second (rps). The rheometer has an inner radius (R_i) of 5 centimeters and an outer radius (R_0) of 6 centimeters. The ConTec 6 is shown below in Figure 3.11.

Figure 3.11. ConTec 6 Viscometer

The test method developed was used to measure the yield stress and plastic viscosity of the mortar mixtures. A descending curve was used to measure these properties. A descending curve measurement consists of measuring the torque and rotational velocity points starting from the highest rotational velocity and stepping down in equal increments until the lowest rotational velocity is reached. For this test, a maximum rotational velocity of 0.5 rps was chosen and a minimum rotational velocity of

0.025 rps was chosen. Ten equal increments were spaced out including these points. The range of this rotational velocity was selected based upon the intended use of the mortar it was testing. Since the mortar would not experience a high shear rate during extrusion or printing, the maximum rotational velocity of 0.5 rps would well cover the behavior the mortar would experience. The lower end rotational velocity was chosen to as close to zero as the rheometer would allow. This allows for less of an interpolation back to the yield stress (y-intercept) which increases the accuracy of that value.

The mortar was tested directly after mixing before the ram extrusion test. The mixing procedure was kept constant to avoid a difference in shear history when the measurements were taken. The mixing procedure is described in detail in Section 3.5. Once the mortar was mixed, it was placed in a bucket around two-thirds full. The bucket was then taken directly to the rheometer and placed in the machine to test immediately. The bucket used is shown next to the coaxial head of the rheometer in Figure 3.12.

To start the test, a pre-shear of 25 seconds was applied at the highest shear rate of 0.5 rps. The reason for using a pre-shear is to break down any structural build-up due to thixotropy. After the pre-shear, the rheometer would start at the highest shear rate of 0.5 rps and work its way down to the next rotational velocity every five seconds. Fifty sampling points was taken for every rotational velocity. This happened during the last four seconds at each specific rotational velocity since a one-second transient interval was used to allow for breakdown of structure and a non-thixotropic response to be measured. Figure 3.13 shows a summary of the testing parameters as input into the rheometer.

Figure 3.12. Mortar Bucket Used in the Rheometer

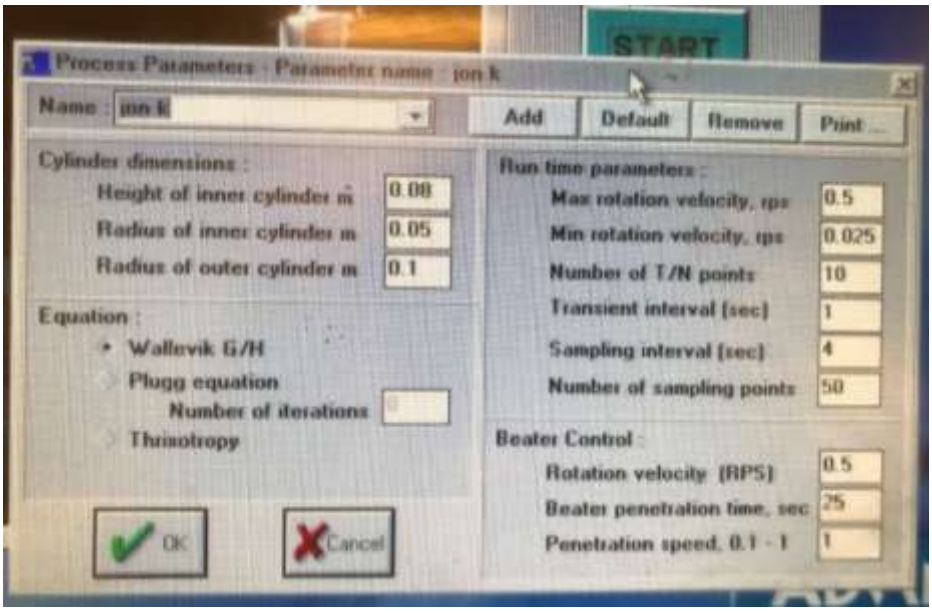

Figure 3.13. Rheometer Test Parameters

After the measurements were finished, the height of the mortar on the coaxial blade was measured. This measurement was taken at a minimum of two spots and averaged to calculate the height of the mortar that was sheared. After the tests on the rheometer, a mini-slump test using a flow table was used. Before doing this test, the mortar was remixed for 30 seconds at a medium speed on a Hobart mixer to break up any thixotropic build-up. This test procedure was the same as previously described following ASTM C1437 [79]. All of these tests were performed on the same mixtures made for extrusion discussed in Section 3.5.

3.5. RAM EXTRUSION TEST FOR PRINTING

A ram extruder was designed to be used as a modular head for a 3D printer. The extruder and test method was used to evaluate a mortar that had a high workability (semi-flowable) and low workability (buildable). It was also attempted to extrude with fibers for the low and high workability mixtures. In the following sections a ram extrusion test is described similar to that in Section 2.4.2, but modified for use in 3D printing. This test will provide data that allows the extrusion force and energy of a specific mixture to be monitored and help define what is extrudable for mortar.

3.5.1. Extruder Design. An extruder is a tool used for pushing material out through a nozzle using a piston, auger, or pump as shown in Section 2.1.3. The extruder chosen to design was similar to the ram extruder tests using a piston and cylinder to push the material through the nozzle. The extruder was designed to implement features such as being displacement controlled, flexible for different size extruders for printing cement paste and mortar, robust and durable, and portable to allow for implementation in the

future to be attached to a medium size printer (1x1 meter). The extruder type is similar to that which is used in the Discov3ry Paste Extruder attachment for an Ultimaker printer [80] which is used at research at Purdue [30], [31] and that shown in an experiment at U.C. Berkeley [24]. The extruder designed consists of a top and bottom plate that connects bearings to a threaded rod. A screw nut is attached to the threaded rod and a motor which causes rotation thus bringing the screw nut up and down based upon the direction of rotation. Two steel plates are bolted to the screw nut. Attached to these steel plates is the pancake load cell and this is what is used to push the syringe described in Figure 3.8 down and allows for the measurement of force versus displacement. On the outside of the bottom and top plate, four linear rail shafts are connected to provide structure to the two plates. The moving plates are also attached to the linear rail shafts using four linear bearings. This allows for a guided motion to keep the motion perfectly linear while also providing support to the threaded rod and screw nut from any bending forces due to the eccentric loading. The height in between the top and bottom plates is 27.9 cm and the usable height after accounting for the height of the plates and coupler is around 24.1 cm. On the bottom plate a 44.5 mm slot is cut out to allow for multiple diameters of syringes easily be used for extrusion. Specific drawings and dimensions of the extruder are shown in Appendix A (note that drawing units are in inches). A picture of the extruder test setup is shown in Figure 3.14 and a schematic of the extruder is shown in Figure 3.15.

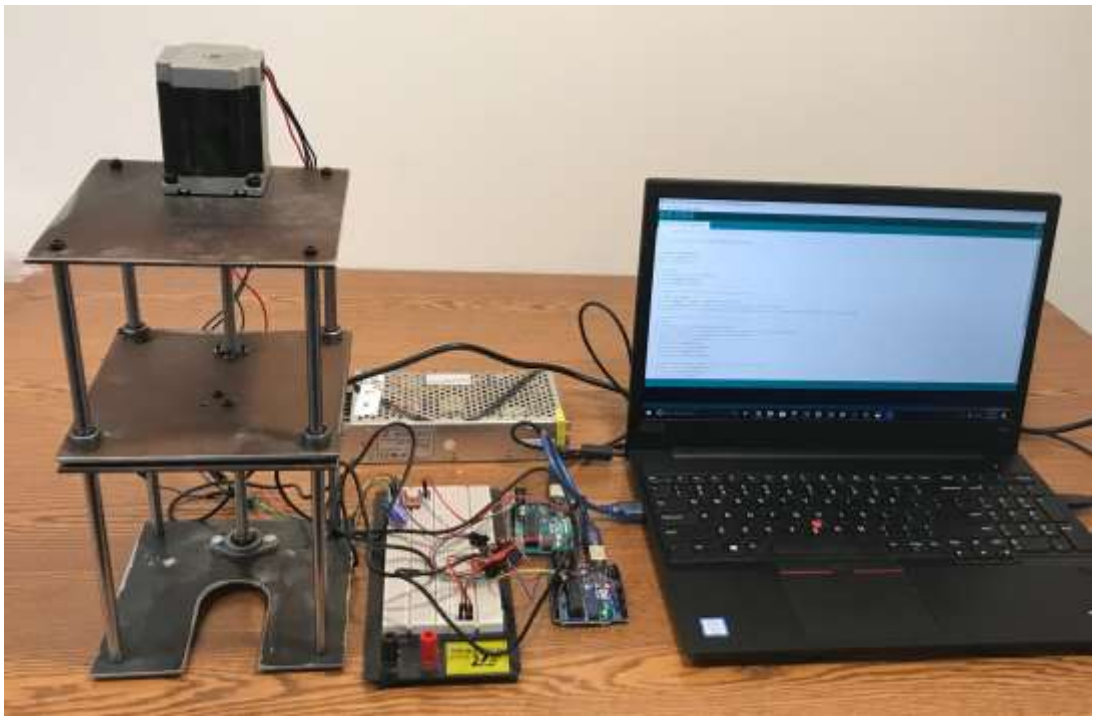

Figure 3.14. Extruder Test Setup

The motor is a Nema 23 stepper motor that uses 2.8 Amps of current and can provide a holding torque up to 1.9 N.m. It has a 1.8^{o} step angle which allows for 200 steps per revolution. The motor is connected to a circuit board that uses an A4988 Stepper Motor Driver Chip to control the motor with an Arduino. A twelve volt power source is also connected to power the motor. Code can then be uploaded from the computer to the Arduino to control the motor. Schematics of the circuits and the code used to control the motor are shown in Appendix A and B respectively. The motor was tested within the current system to find out the linear amount of force it could handle before it would lock up. An initial motor (Nema 17) was used and found to reach up to 40 N of linear force. The Nema 23 motor was then used to replace the Nema 17 to increase the capacity of the motor. Through testing, it was found that the Nema 23

provided a working limit of 80 N. Increasing above this point started causing the motor to lock up and non-continuous rotation of the threaded rod. The maximum total linear force found was 100 N as this was near the maximum value ever recorded during a test while the motor was locking up.

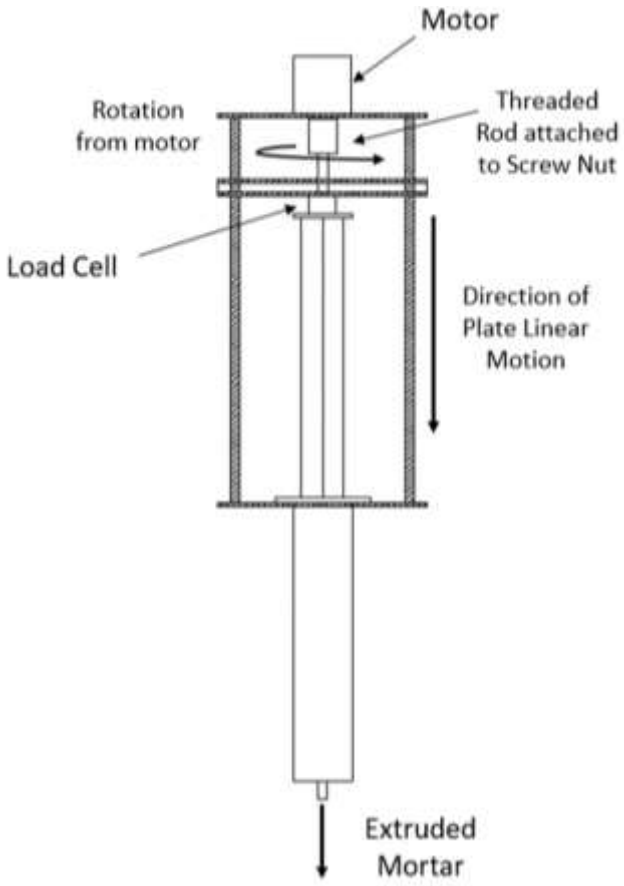

Figure 3.15. Schematic of Extruder

The load cell used is attached to the bottom of the moving plates and is rated up to 50 kg (490 N). The load cell pushes against the syringe and reads the load throughout the test. The load cell is connected to a separate Arduino which allows the data to be recorded on the Serial Monitor on the computer. The load cell was calibrated with a five

pound load and verified with a one pound load up to the hundredths of a pound. The load cell is currently programmed to take a reading every three tenths of a second. The dimensions and specifications of the load cell are shown in Appendix A and the code for calibrating and running the load cell are in Appendix B. Figure 3.16 shows a schematic of how the load cell, motor, extruder, and computer are all connected.

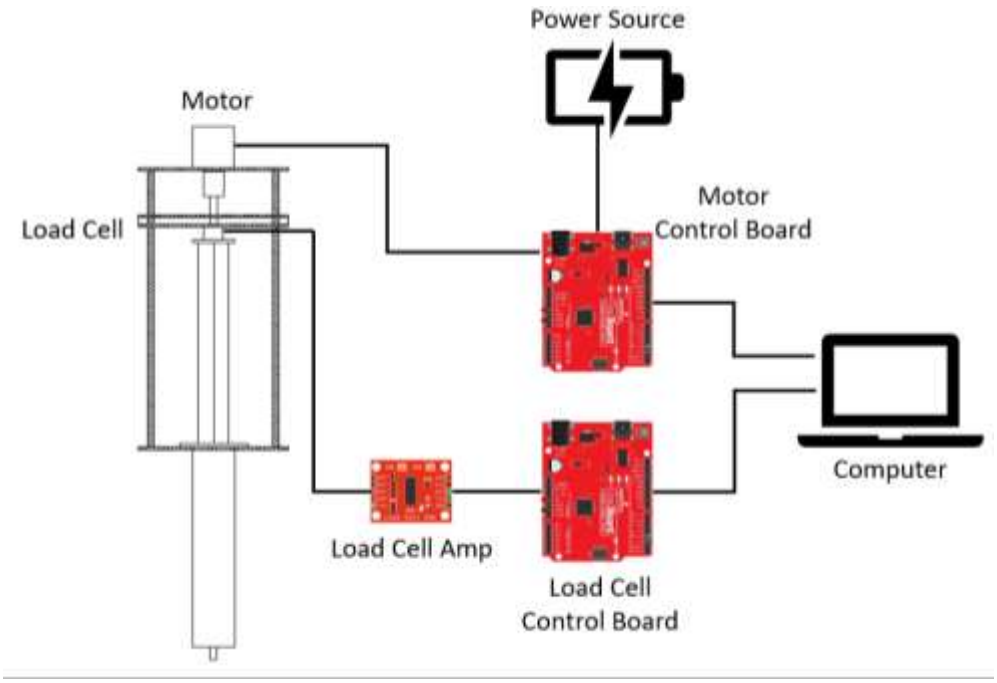

Figure 3.16. Electronic Schematic of the Extrusion System

3.5.2. Testing Parameters and Materials. The extrusion test was done at a rate of 1.39 mm/s. This was selected as it was towards the slower end of what the motor could control. The slower speed was needed for a reasonable extrusion force since a higher speed would create issues with the maximum torque on the motor due to limited amount of volume being extruded out of the small nozzle opening. The slower speed also simulates a speed that would be close to what is used once the extruder is attached to a

3D printer. This constant rate was applied over a distance of 116 mm. This distance allowed for almost 150 mL to be extruded and stopped just before the plunger would hit the end of the barrel of the syringe.

The materials used were similar to the blockage test. Type I Portland cement was used and sieved with the No. 100 sieve. The sand used was the No.16 sieved Missouri Natural River Sand. The manufactured fibers were attempted to be printed as shown in Figure 3.1 and whose properties are shown in Table 3.1. The same Superplasticizer (SP) was used as the blockage test as well. The mixture proportions are shown below in Table 3.4. All the constituents add up to 2200 kg/m^3. The sand was kept at a constant ratio compared to all the constituents to keep a ratio that had shown to work from the blockage tests.

Table 3.4. Mixture Proportions for Extrusion and Rheology Tests

Mixture	**w/b ratio**	**Portland Cement (kg/m^3)**	**Aggregate (kg/m^3)**	**Steel Fiber (vol %)**	**SP (% of binder)**
M-0.3	0.35	900	985	0	0.3
M-0.05	0.35	900	985	0	0.05
MF-0.3	0.35	900	985	0.25	0.3
MF-0.05	0.35	900	985	0.25	0.05

The syringe shown Figure 3.8 was modified to have 6.32 mm and a 9.13 mm opening as well. All three of these syringe sizes was tested for each mixture to investigate the effect on nozzle diameter and the d/D ratio on extrusion. The three different nozzle types are shown below in Figure 3.17.

Figure 3.17. Syringes with Modified Diameters

One other set of tests was done on the M-0.3 mixture. After all the tests were performed, the mortar was remixed and tested again at the 1.39 mm/s speed for the 9.13 mm syringe. The speed was then increased to 1.51 and 1.64 mm/s and tested with the 9.13 mm syringe. The large syringe was the only tested since the initial test at 1.39 mm/s was near the top of the motors working capacity. After the tests the mini slump was taken again to evaluate any structural buildup from the long time taken to do all of the tests.

3.5.3. Testing Procedure. First the empty syringes were each tested in the extruder. The syringes were first oiled up to decrease any frictional buildup from previous use. They were then placed in the extruder and tested to get the extrusion force necessary for an empty extruder.

After the empty syringes were tested, the mortar was then mixed in a Hobart mixer. The mixing procedure followed ASTM C305 [81]. Binder was added to the water and superplasticizer at a mixing speed for 30 seconds. After that the sand was added and

mixed at a mixing speed for 30 seconds. The speed was then increased to a medium speed for 30 seconds. The mixer was then at rest for 90 seconds and during the first 15 seconds the mortar was scraped from the sides of the mixer. After the rest period, the mortar was mixed at a medium speed for 60 seconds. For mixes with the fibers, the fibers were added after the sand at a stirring speed for 30 seconds. A picture of the Hobart mixer used is shown in Figure 3.18.

Figure 3.18. Hobart Mixer

Immediately after mixing, rheological properties of the mortar was measured with a rheometer and mini-slump test on the flow table. This is described in detail in Section

3.3. For the low workability mixtures, the diameter of the top of the cone was measured compared to the 70 mm initial opening. The high workability mixtures were taken as described in Section 3.3. After the rheological measurements were taken, the mortar was remixed again for 30 seconds at a medium speed to break up any thixotropic build-up. The mortar was then taken to the extruder for testing.

Three syringes were tested to measure the extrudability: normal syringes with the 3.71 mm opening, one modified syringe with the 6.32 mm opening, and one modified syringe with a 9.13 mm opening. Each of these tests were done twice on each nozzle size to get an average. The syringes were either cleaned out or another syringe with the same dimensions was used for the second trial in order that the first test did not have any effect on the first test. The mortar was placed into the syringes and rodded in three layers to take out any air pockets in the syringe for the low workability mixtures. The high workability mixtures were able to fill the syringes without being rodded. The syringes were filled up to the 150 mL mark and placed in the extruder such that the load cell was centered on the syringe plunger. Once the syringe was set, the serial monitor on the Arduino program was opened to start reading data. The reset button was then hit on the Arduino controlling the motor which starts the motor. The motor then runs at the testing parameters as described in the previous section while the load cell is recording data. After the test ends, the data is copied and saved to a text file. This process is repeated for all three syringes tested. Figure 3.19 shows a picture of the test in progress.

Figure 3.19. Extrusion Test in Progress

3.6. FLEXURAL TESTING OF PRINTED AND CAST SPECIMENS

A few samples were made and tested to study the effect of ram extruder printing on the fiber orientation and mechanical properties of concrete. The following sections describe the manual printing process used to create the printed beams and their comparison with cast beams. The testing of mechanical properties including compressive strength, flexural strength, and post-crack properties will also be described. This investigation will allow for an initial investigation on the use of fibers in printing and the effect of printing on fiber orientation.

3.6.1. Specimen Casting and Printing. To compare the effects of printing on flexural properties and fiber orientation of the hardened concrete, three mixtures were used to compare casting and printing. One reference mixture without fibers and mixtures

with 0.25% and 0.50% fibers by volume were investigated. The mixture proportions were selected based on the results of the lower workability mixture of the blockage test. This was chosen to stay consistent for comparing the results even though extruder used had a larger opening than the syringe used in the blockage tests. The SP dosage was also held constant to reach the same workability as the blockage test. The fibers used were the same as the manufactured fibers used in Figure 3.1. Table 3.5 below shows the mixture proportions used in the investigation.

Table 3.5. Manual and Cast Beam Mixture Proportions

Mixture	**w/b ratio**	**Cement (kg/m^3)**	**Aggregate (kg/m^3)**	**Steel Fiber (vol %)**
REF	0.35	900	985	0
F-0.25	0.35	900	985	0.25
F-0.50	0.35	900	985	0.50

The mixing procedure was the same as described in Section 3.5.3. Once mixed the mini slump was taken for each mixture. For compressive strength, three specimens were cast normally in 50 x 50 mm cube molds. The cast beam size was modified from the normal 75 x 75 mm cross section to be 75 x 50 mm. This beam size was modified to allow for the printed beams to be easier to match the cast beams since buildability was not studied in detail throughout this study. Two cast beams were made for each mixture.

Two manually printed beams were also made for each mixture. The beams were printed using a manual extruder made from 2” PVC with a coupler to attach to a 0.5” PVC bushing. A pushing rod, or plunger, was made to fit the inside diameter of the pipe closely to allow for the mortar to be pushed out. The print was three layers wide by three layers tall. This was chosen on the first print as the first REF specimen was close to the 75 x 50 mm target dimensions. All of the layers were printed longitudinally to allow for the fiber orientation between printing and casting beams to be investigated.

The following procedure was used to print the beams. After the mortar was mixed, the mortar was placed in the into the extruder. This was done in three separate layers. In between each layer of placing into the extruder, the mortar was rodded five to ten times to make sure there were not any air pockets or gaps inside the extruder. The bottom layer is then extruded by manually pushing the mortar with the pushing rod. The layer was printed a little longer than 300 mm measured with a meter stick. This allowed for the beams to be cut to the length of 300 mm once all of the layers were printed. The second layer was then extruded directly above the first layer. This process was repeated for the third layer. The printing process is shown below in Figure 3.20.

After the beams were printed, to get a more uniform length the ends were both cut using a concrete scraper. This also allowed for the ends to have a more uniform section. This process is shown below in Figure 3.21.

The cast beams were demolded after 24 hours. The manually printed beams were easily able to move to the curing tank due no use of formwork. All of the specimens were moved to a limewater tank to cure for 28 days.

Figure 3.20. Beam Manual Printing Process

Figure 3.21. Cutting Ends of Printed Beams

3.6.2. Hardened Property Tests. The tests performed on the hardened specimens included a cube compression test, three point bending test, and image analysis and fiber characterization of the failed beam specimens. The first test done was the compression test on the 50 x 50 mm mortar cubes. This compression test was done according to ASTM C109 using a load rate of 200 lb/s load rate [82]. All three cubes were tested at 28 days and the compressive strength was taken as the average of the three specimens. A figure of the test setup is shown below in Figure 3.22.

Figure 3.22. Cube Compression Test Setup

The beams were tested using a three-point bending test. The span length tested was 200 mm. A constant displacement of 1 mm/min was applied while the load and displacement were measured with a data acquisition system on the Instron 4469 machine. The beams with fibers were tested a minimum of ten minutes due to the fibers preventing failure of the specimen. The reference beams were tested until total failure which occurred well before the ten-minute (10 mm) mark. The cast beams were tested with the 75 mm side as the width and 50 mm side as the height. The cast beam test setup is shown below in Figure 3.23.

Figure 3.23. Cast Beam Three-Point Bending Setup

The manually printed beams were first measured across the length to better define the geometry of the beam. Approximately 11-13 measurements were taken from end to end approximately 25 mm apart from each other. A measurement was taken of the height,

the width of the base, and the top width using a dial calipers. The two widths were taken due to some specimens having shown signs of slight settlement of the bottom layer and the variability in placing the layers with the manual printing process. A top, side, and isometric view picture was taken as a reference before testing as well.

Once the specimen has been measured it was placed on the supports for the bending test. The specimen was adjusted slightly in the supports until the most even surface along the center of the specimen was found in order to decrease chances for stress concentrations due to the uneven top surface geometry. Once set, the printed beams were then tested with the same testing method as the cast beams. Figure 3.24 shows the test setup for the printed beams.

Figure 3.24. Manual Printed Beam Three-Point Bending Setup

Due to the printed specimens not having a clear geometric shape, the moment of inertia, centroid, area, and other geometric properties could not be easily calculated by hand. An image analysis was done on the cross section where the specimen broke in

order to calculate the geometric properties to accurately calculate the stresses through the section. A picture of the broken cross section was first taken next to a ruler. It is important when taking the image that the photo be taken on a plane parallel to the cross section. It was also important that the ruler be level with the top surface of the cut section so that the image could properly be scaled. AutoCAD was then used to analyze the cross-section properties which is shown in Figure 3.25 and 3.26.

Figure 3.25. Printed Beam Cross-Section Analysis Outline of Picture

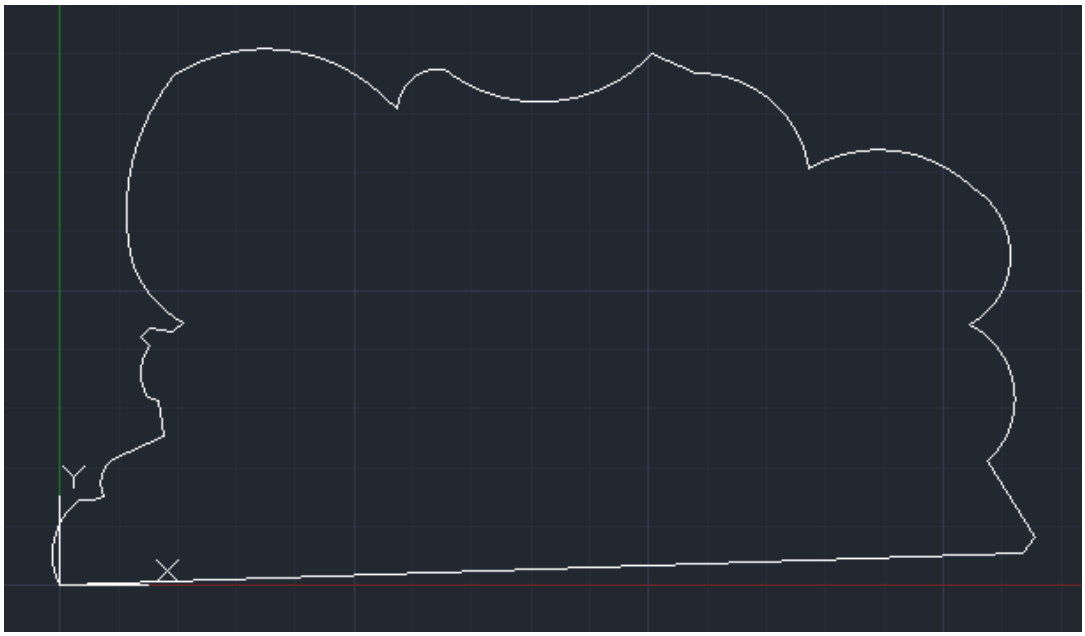

Figure 3.26. AutoCAD Outline of Printed Beam Cross Section

The last test done on the broken cross-sections from the flexural test was finding the orientation factor, α. The procedure followed that done by [17]. For the broke cross sections for both printed and cast specimens, the number of fibers sticking out of the face was counted. Counting the fibers gives a look into whether they orient in the longitudinal direction of the beam and would allow for the study of whether printing can help improve fiber orientation. The fiber orientation factor ranges from 0 to 1 with 0 being no fibers oriented perpendicular to the broke cross section and 1 being that all the fibers would be oriented perpendicular to the cross section. Improving the fiber orientation would help improve flexural and tensile performance of the beams since more fibers would be aligned in the direction of tension to contribute to load sharing. The fiber orientation factor is described by equation 4:

$$\alpha = \frac{N_f}{N_{th}} = N_f \frac{A_f}{V_f A_c} \quad (4)$$

N_f is the number of fibers counted in the cross section and N_{th} is the theoretical maximum number of fibers that would be in the cross section if all of the fibers were oriented perpendicular and evenly distributed throughout the specimen. A_f is the area of the fibers which is divided by A_c, the area of the cross-section, and V_f, the fiber volume fraction. This means that the area of the fibers in the section is divided by the theoretical area of the fibers in the section if that volume fraction would appear. When calculating the fiber orientation factor, multiple different people counted the number of fibers and then this value was averaged due to the large amount of fibers in the cross-section and the small size of the fibers making it difficult to count.

4. RESULTS

In this chapter, the experimental results are presented and discussed in detail. In Section 4.1 the study on FRC and the use of recycled fibers from tires is described. Following that in Section 4.2, blockage test results are described. The results from the rheometer and the extrusion test are then discussed in Section 4.3 and 4.4 respectively. Finally, in Section 4.5 the mechanical properties of the printed beams are presented and effects of the printing process are analyzed.

4.1. FIBERS AS A REINFORCING SYSTEM IN CAST CONCRETE

The study of the effect of fibers as a reinforcing system in cast concrete shows the effects and benefits of using fibers in concrete. Mechanical properties of FRC that are made with two types of fibers are compared to study the feasibility of applying recycled fibers as an environmentally friendly option to replace manufactured fibers. First the effect of workability, specifically superplasticizer demand is presented. Then the effects on compressive strength, flexural strength, and post-crack performance of the concrete samples are discussed.

4.1.1. Fiber Effect on Workability. The slump of the concrete mixtures was kept consistent by varying superplasticizer dosage to allow proper compaction of concrete samples and ensure uniform distribution of fibers in the consolidated mixture. The superplasticizer demand to obtain the required workability is an indicator of the effect of fibers on workability of concrete mixtures. Figure 4.1 shows a comparison to see

the effect of the type and amount of fibers on the superplasticizer demand of concrete mixtures.

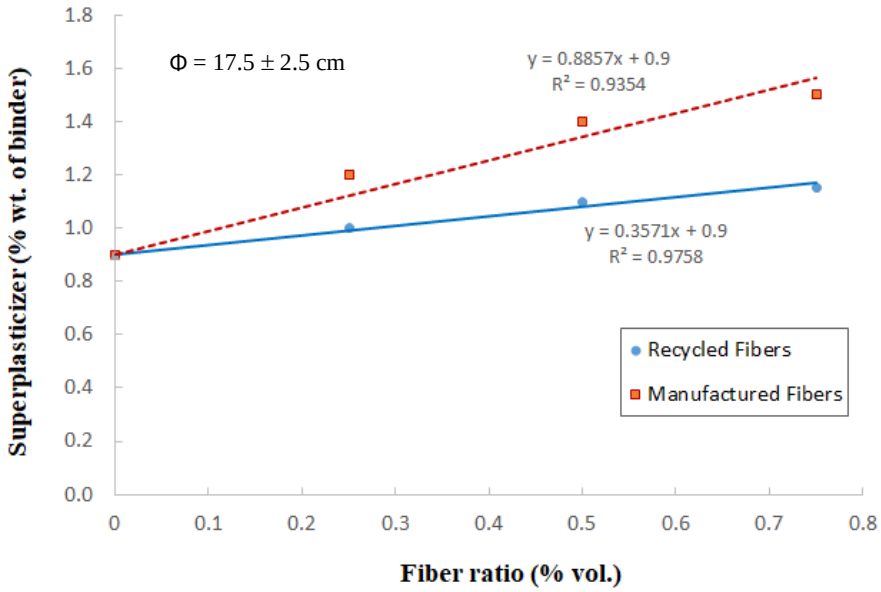

Figure 4.1. Superplasticizer Demand versus Fiber Volume

The comparison between the fiber amount shows that with an increase in fiber amount the amount of superplasticizer (SP) needed increases linearly. All FRC mixtures required more SP dosage to achieve the same workability of the reference mixture (mixture without fibers). This increase could be due to increased internal friction and an increase in the particle interaction in the mix. These would cause the mixture to be less workable and require the higher amount of SP. The manufactured fibers showed a higher demand of SP needed than the recycled fibers. One reason that the manufactured fibers might have required more SP than the recycled fibers is due to the higher stiffness of those fibers. The recycled fibers vary in length and thickness and some of the fibers are less stiff that could cause less internal friction and more flexibility in the mixture

compared to the manufactured fibers. With the steel fibers being straight and consistent in geometry and the recycled fibers having a more variable geometry, this could affect the workability of the concrete as geometry has an effect on workability [43]. Another reason for the recycled fibers requiring less superplasticizer could be that there is a greater number of manufactured fibers per a given volume of concrete. The higher number of fibers per concrete volume would cause greater inter-particle friction as there would be more contact specific surface area from the fibers causing the friction. One other aspect of workability that was noticed during mixing was fiber clumping. This could cause issues in fiber distribution due to clumping and entanglement, which makes the mixture difficult to flow. This issue was dealt by allowing the fibers to break apart in the coarse aggregate when mixing and also checking the samples for clumps when consolidating the concrete. The mild fiber clumping was observed mixtures with higher amount of fibers (0.75% volume) for both the manufactured and recycled fibers.

4.1.2. Compressive Behavior. The results of the compression tests are summarized in Table 4.1. The pre-peak energy is found from the area under the load-deflection curve up to the maximum (or peak) load. The total-energy is found similarly from the area under the entire curve until failure. The results of the modulus of elasticity test, pre-peak energy, total energy, and compressive strength is shown in Table 4.1.

Findings from this table show that the fibers do not provide much of an improvement in compressive strength. One reason why the fibers have not increased the compressive strength is that the fibers are mainly effective for bridging cracks in the concrete. The results are consistent with previously reported findings in literature [33], [37], [40], [42], [43].

Table 4.1. FRC Compressive Properties

	Compressive Strength		Pre-Peak Energy		Total-Energy		Elastic Modulus	
	Average (MPa)	**Change from REF**	**Average (kN.mm)**	**Change from REF**	**Average (kN.mm)**	**Change from REF**	**Average (Mpa)**	**Change from REF**
REF	56.7	-	282	-	542	-	45700	-
RF-0.25	51.8	-8.6%	246	-13%	437	-19%	45900	0.44%
RF-0.50	41.6	-27%	233	-17%	452	-17%	42900	-6.1%
RF-0.75	56.3	-0.71%	320	13%	551	1.7%	46400	1.5%
F-0.25	64.7	14%	312	10%	551	1.7%	46400	1.5%
F-0.50	50.9	-10%	285	0.80%	507	-6.5%	51000	12%
F-0.75	58.3	2.8%	367	30%	643	19%	44100	-3.5%
HF	49.7	-12%	268	-5.2%	464	-14%	43600	-4.6%

*RF: Recycled Fibers
F: Manufactured Fibers
HF: Recycled/Manufactured Hybrid

The stress-strain properties of the concrete specimens are shown in Figure 4.2. This shows that the fibers did not affect the overall shape of the graph and did not provide significant benefit in regard to compressive strength.

Figure 4.3 shows the graphical results of the modulus of elasticity test. Just the 0.25% fiber mixtures and reference mixture is shown to give an easier comparison. The same trend was observed in all other mixtures

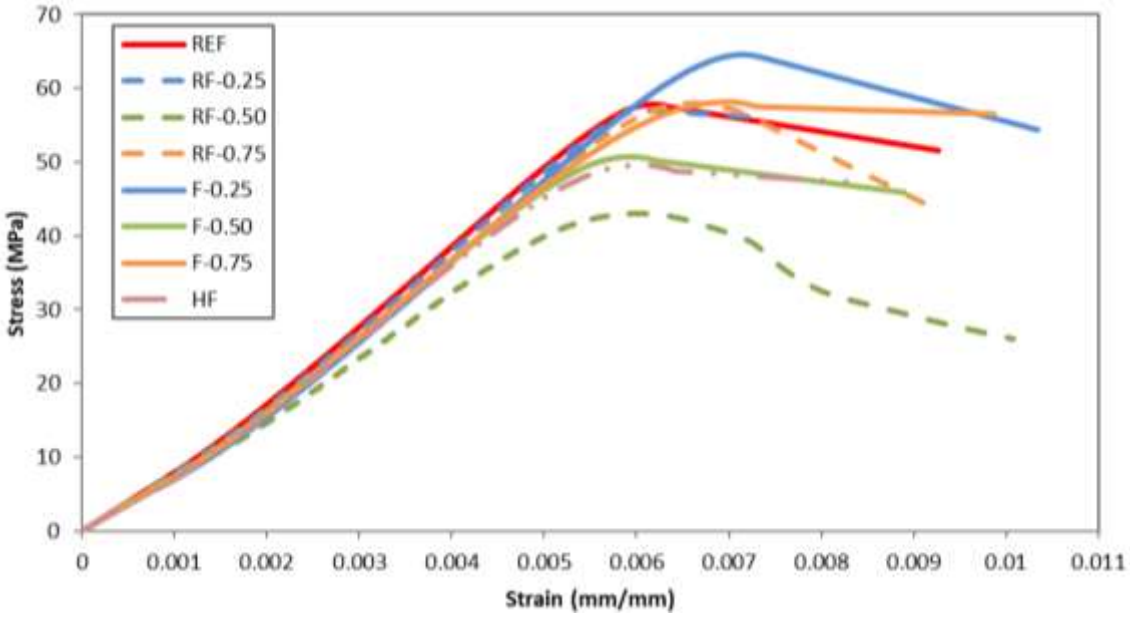

Figure 4.2. Compression Stress vs Strain Graph for Casted FRC Specimens

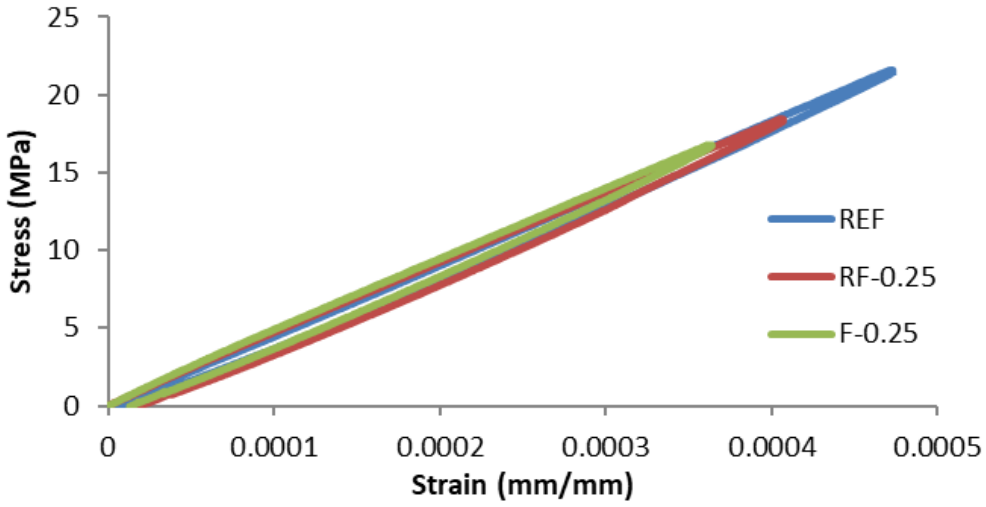

Figure 4.3. Modulus of Elasticity Results- REF vs 0.25% Fibers

The fibers show to not have much of an effect on the elastic modulus as most of the concrete mixtures were either slightly higher or lower than the reference. This is because the fibers constitute a small portion of the concrete ingredients and are used for

bridging the cracks which has a minimal effect on the elastic part of the stress-strain curve. As the fiber content increases, the modulus still remains constant as well. All of these results show that the main constituents of the concrete matrix are still the controlling factor on the elastic modulus.

Even though the fibers did not have much of a positive effect on the compressive strength, the expected behavior of the fibers was to improve the toughness of the concrete. Since the modulus of elasticity is the same in different mixtures, the pre-peak energy results was effected by the compressive strength results. If there was a lower compressive strength, this would noticeably affect the area under the curve before the peak. All of the steel fiber results had higher pre-peak energy than the reference and the recycled fiber mixtures with the same amount of fiber content. The recycled fibers did not show much of an improvement on compressive toughness for pre-peak and total toughness with the RF-0.75 mixture being the only one with a slightly higher toughness.

4.1.3. Flexural Behavior. A summary of all the flexural properties found from the three point bending test is shown in Table 4.2. The pre-peak energy in Table 4.2 is calculated as stated in Section 4.1.2. The first-crack strength (or flexural strength) is calculated according to ASTM Standards [45], [83] according equation (5):

$$R = \frac{PL}{b(h_b - a)^2} \tag{5}$$

where R is the first-crack strength (MPa), P is the peak load (N), L is the length of the span (mm), b is the width of the beam (mm), h_b is the height of the beam (mm), and a is the height of the notch in the beam (mm). The toughness indices and residual strength of the beam was also found according to ASTM C1018-197 [45]. The I_5, I_{10}, and I_{20} are toughness indices that can be used to compare toughness between different beams in the

experiment. I_5 is the area under the curve of the load deflection graph at 3 times the peak deflection or limit of proportionality (LOP) divided by the area under the curve before the first crack. I_{10} and I_{20} are the same calculation but at 5.5 and 10.5 times the LOP deflection respectively. The different toughness indices also are a representation of how ductile the beam behaves after the first crack rather than the regular brittle failure. The residual strength $R_{5,10}$ and $R_{10,20}$ are found by taking $20(I_{10} - I_5)$ and $10\ (I_{20} - I_{10})$.

Table 4.2. Flexural Properties of Casted FRC

	First-crack strength (MPa)	**Pre-Peak Energy (N*m)**	**I_5**	**I_{10}**	**I_{20}**	**$R_{5,10}$**	**$R_{10,20}$**	**Total-Energy (N*m)**
REF	3.70	0.46	1	1	1	0	0	0.57
RF-0.25	3.82	0.37	2.76	4.27	6.66	30.1	23.9	-
RF-0.50	3.66	0.60	3.98	7.58	12.4	72.0	48.0	-
RF-0.75	4.85	0.64	5.06	9.47	16.67	88.2	72.0	-
F-0.25	4.25	0.43	3.33	5.35	7.78	40.4	24.2	-
F-0.50	3.50	0.58	4.26	7.14	10.8	57.5	36.7	-
F-0.75	4.48	0.76	4.65	7.67	11.3	60.5	35.7	-
HF	4.27	0.65	4.09	6.75	9.90	53.3	31.5	-

Comparing the REF first-crack strength to other mixtures, all the mixtures show an increase in strength except RF-0.50 and F-0.50. The increase in first-crack strength varied from 3% to 31% with the higher fiber content providing higher strengths. The manufactured steel fibers had slightly higher first crack strength values compared to the recycled fiber mixtures. The hybrid fibers showed high first-crack strength in outperforming the reference and both 0.5% fiber mixtures. Generally the addition of fibers seem slightly increase the first-crack strength.

The increased toughness and residual strength is one of the main reasons for adding fibers to concrete mixes. The results show all of the toughness indices increase with an increasing amount of fiber content. When comparing steel and recycled fibers, the recycled fibers showed greater $R_{5,10}$ values for all except the 0.25% fiber mixture. The recycled fibers seemed to have greater later residual strength, $R_{10,20}$, than the manufactured fibers as well. This could be due to recycled fibers needing greater crack openings to be pulled out [44]. The improved first-crack strength, toughness, and residual strength of the hybrid mixture could be due to the steel and recycled fibers each being better at bridging different kinds of cracks such as micro and macro-cracks in the concrete.

Figures 4.4-4.6 shows the fibers ability to sustain a load after the initial crack. This is vital in increasing the safety and sustained load of a beam, specifically against cyclic loads. The graphs also show that the recycled fibers and manufactured fibers have a similar behavior. This similar behavior is promising for the potential replacement of the manufactured fibers as this increased toughness, sustained load, and crack control is the main reason for adding the fibers to the concrete.

The CMOD versus load graphs in Figures 4.7-4.9 show that the crack mouth opening between the recycled and manufactured fibers were very similar. This shows that recycled fibers are as effective as manufactured fibers in controlling crack opening and mitigating crack propagation.

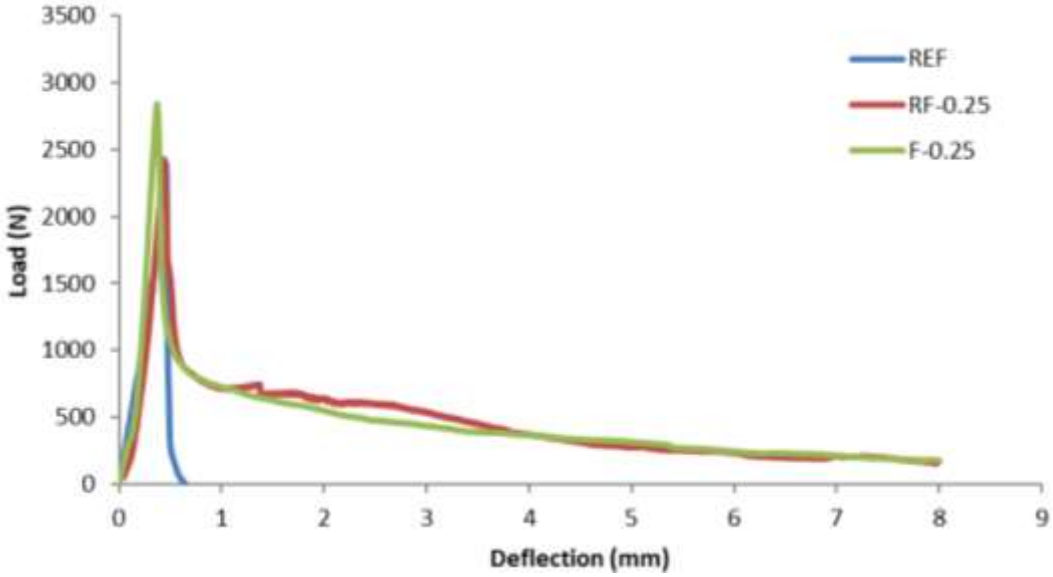

Figure 4.4. Flexural Load vs Deflection for REF vs 0.25% Fiber Mixtures

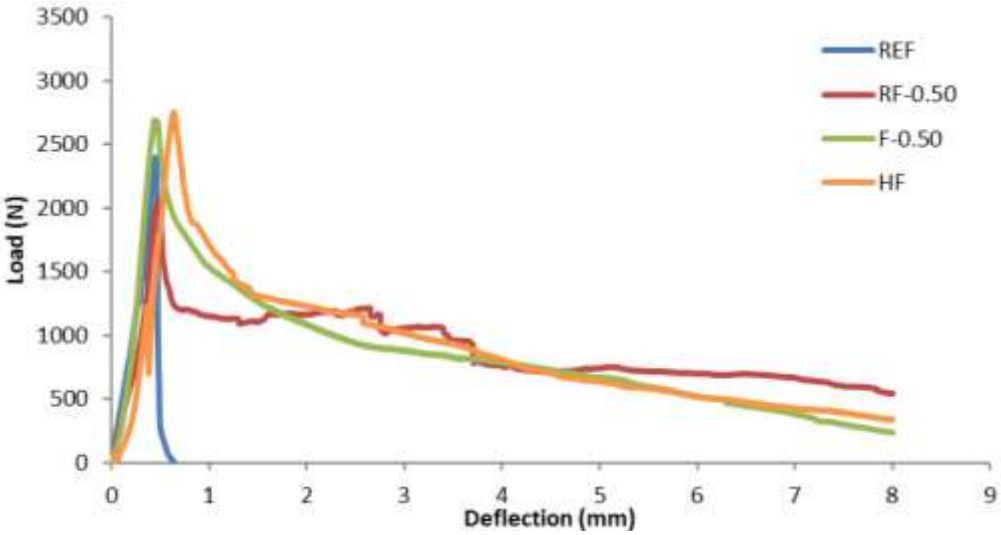

Figure 4.5. Flexural Load vs Deflection for REF vs 0.50% Fiber Mixtures

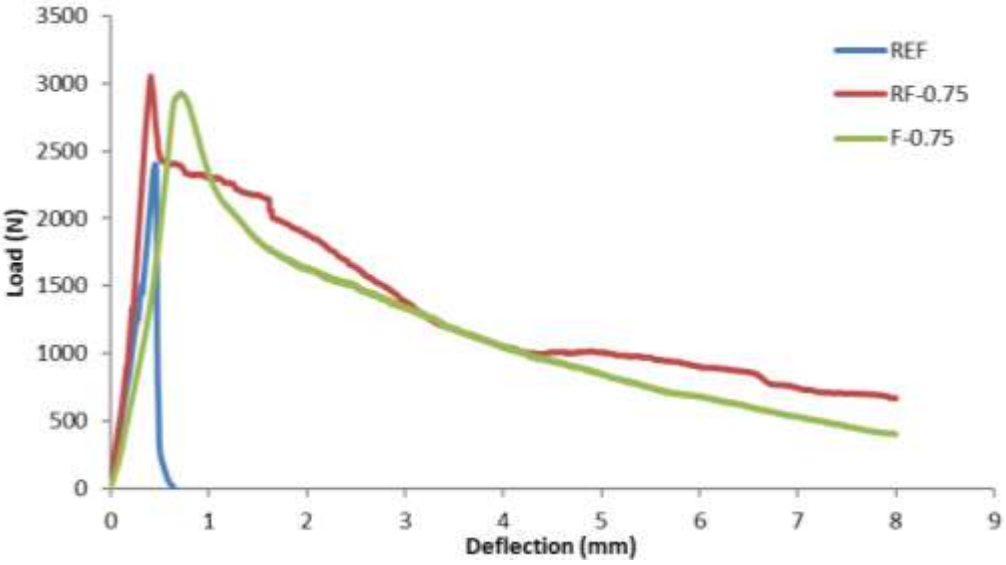

Figure 4.6. Flexural Load vs Deflection for REF vs 0.75% Fiber Mixtures

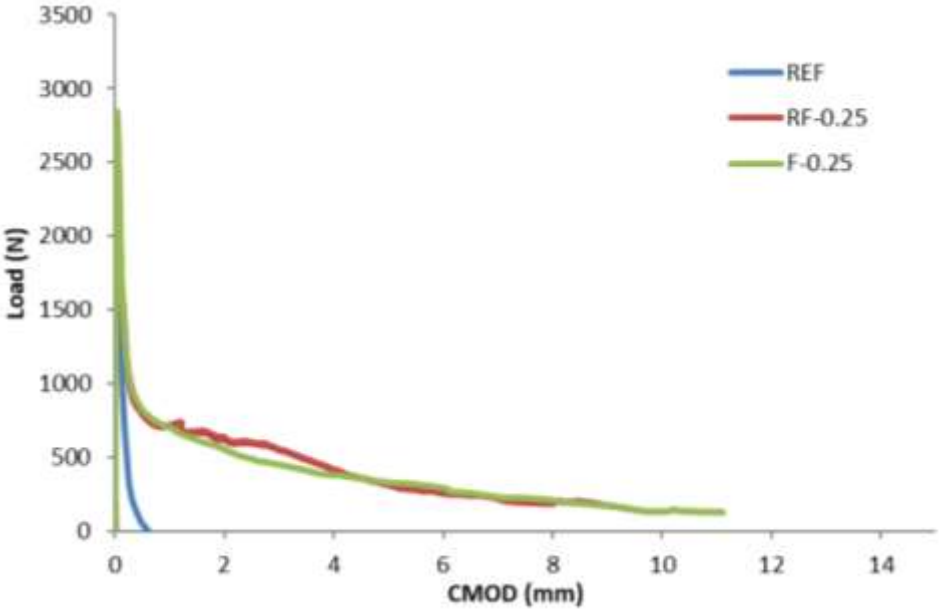

Figure 4.7. Flexural Load vs CMOD for REF vs 0.25% Fibers

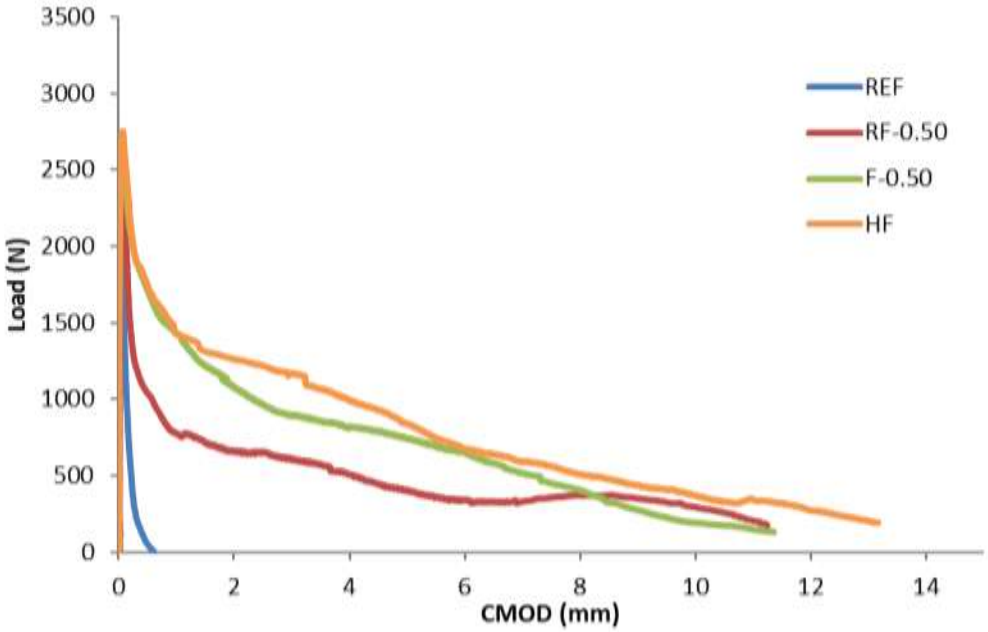

Figure 4.8. Flexural Load vs CMOD for REF vs 0.50% Fibers

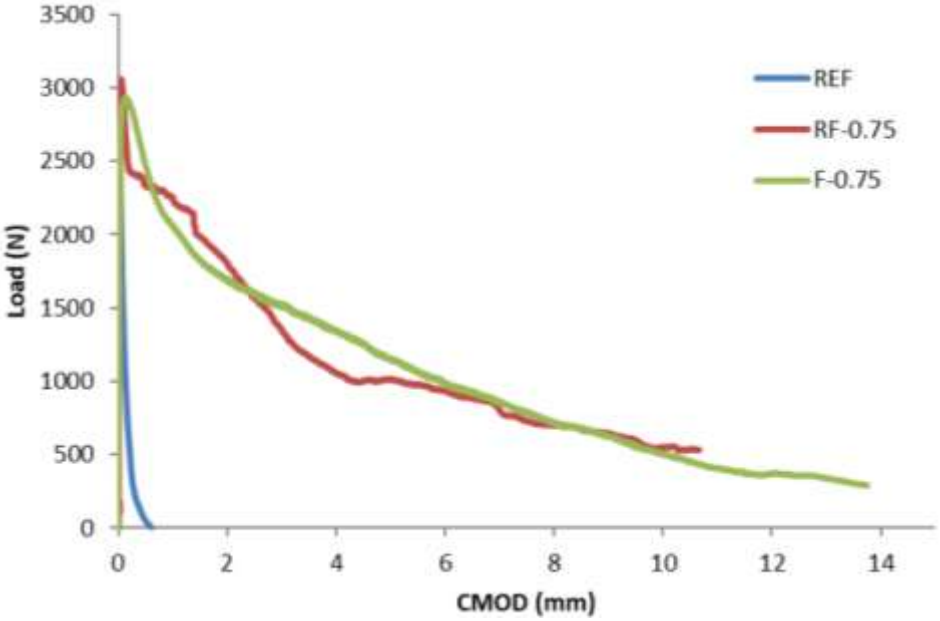

Figure 4.9. Flexural Load vs CMOD for REF vs 0.75% Fibers

Figure 4.10 shows the relationship between deflection and crack mouth opening displacement. The relationship shows that the recycled fibers are more efficient at reducing the crack opening for a given amount of deflection. This could be due to the difference in fiber geometry between the two types of mixtures. Since the recycled fibers are longer, this could help decrease the crack mouth opening due to there being a greater bond strength that is needed to completely pull out the fibers in bending.

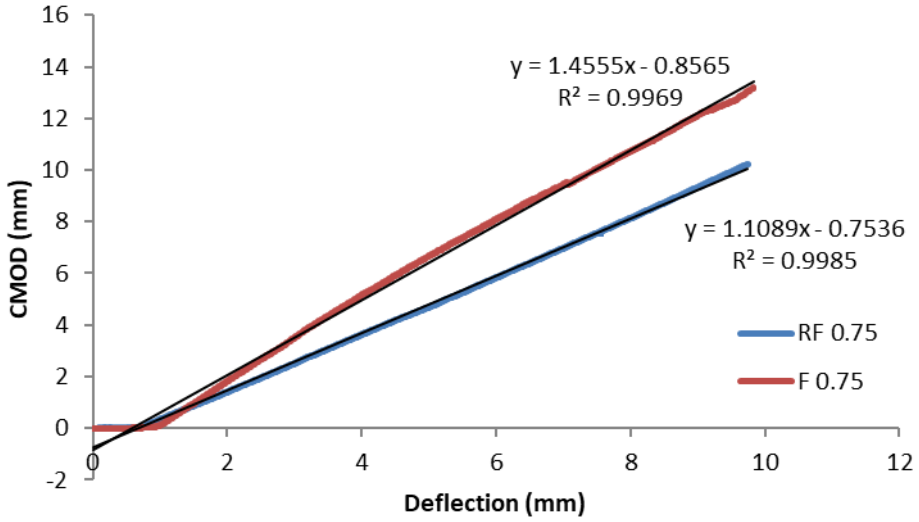

Figure 4.10 CMOD vs Deflection

Table 4.3 shows how the fracture energy varies for each of the mixtures. Fracture energy is calculated using equation (6) according to RILEM [84]:

$$G_f = \frac{W_0 + mg\delta_f}{A_{lig}} \quad (6)$$

where G_f is the fracture energy (N/mm), W_0 is the area of the load-deflection curve, mg is the weight of the beam, δ_f is the maximum displacement at the 3.5 mm CMOD value, and A_{lig} is the area of the effective depth of the beam- A_{lig} = b(h-a).

Table 4.3. Fracture Energy

Mix	Fracture Energy (N/mm)
REF	0.187
RF-0.25	1.006
RF-0.50	1.603
RF-0.75	3.027
F-0.25	0.913
F-0.50	1.902
F-0.75	2.414
HF	1.703

Fracture energy allows the cracking resistance and toughness to be compared between the mixtures [85]. Table 4.3 shows that the fibers greatly increase the fracture energy and cracking resistance. The recycled fibers helped improve the fracture energy more than the manufactured most likely due to the shape of the fibers. Since the geometry of the recycled fibers is inconsistent and more hooked like, the fibers had a better bond and pullout resistance thus helping improve the fracture energy.

4.2. BLOCKAGE TESTING

The following sections discuss the results from the blockage test, the different items that can be analyzed, qualitative and quantitative findings, and an evaluation of the test method. The gradation and analysis of the fine aggregate used is first described followed by results of the test.

4.2.1. Effect of Max Particle Size, Workability, and Binder Content. The blockage test results were then analyzed after characterizing the sand size and gradation. The blockage point was found for each sand size for both the high and low workability mixtures as described in Section 3.3. This data is shown below in Table 4.4.

Table 4.4. Binder Quantity Causing Blockage

	High Workability	Low Workability
Sieve Size (mm)	Binder Blocking Point (kg/m^3)	Binder Blocking Point (kg/m^3)
2.36	1100	1150
1.18	850	800
0.6	800	700

The blocking point could then be plotted against the maximum particle size as a percentage of the nozzle opening. This allows for the blockage to be normalized for applications of different nozzle sizes. This is shown in Figure 4.11.

This figure shows how as the particle size increases the required binder content also increases as expected. From this data, a sand size and binder quantity could be chosen for further experiments. The 900 kg/m^3 binder content for the No. 16 sieved sand was selected for further extrusion tests. This is the minimum binder required in the mixture to provide enough spacing between aggregates and lubricate them in order to pass through the smallest nozzle used. The No. 16 sand was selected because the No. 8 sand would have a much higher binder content than the others. This high binder content could cause more issues with high heat of hydration and shrinkage problems, but the concrete equivalent to the mortar would have a lower binder content and cause less

issues. The No. 30 sieved sand was not selected due to the high water demand at this level.

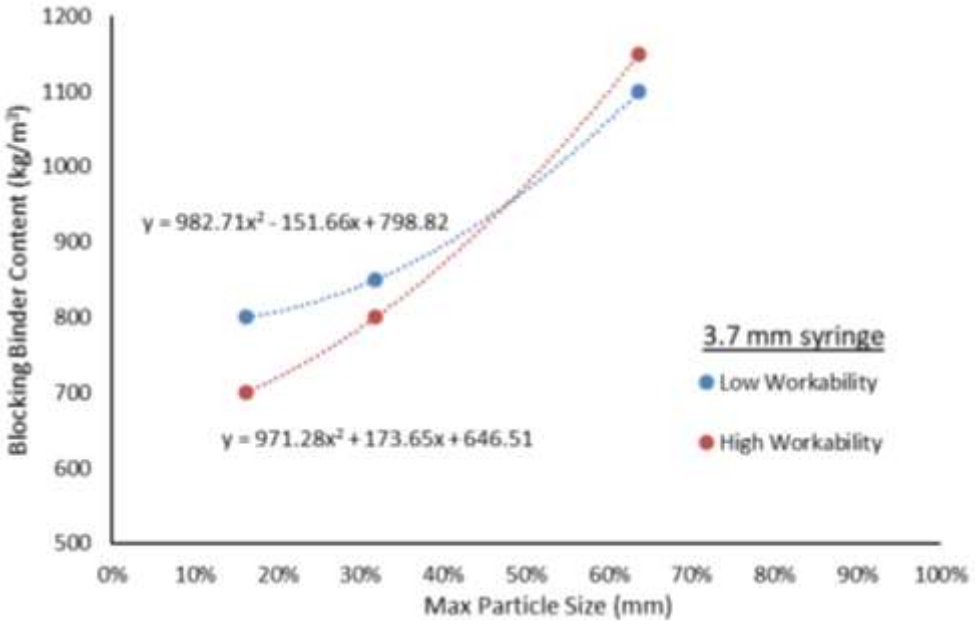

Figure 4.11. Blocking Binder Content vs Maximum Particle Size % of Nozzle Diameter

Using a higher quantity of superplasticizer could be used to bring it to a similar level, but this also comes with the risk of higher amounts of bleeding and segregation of the particles. The selected binder content and sand sized proved to be successful for later experiments as no issues with blockage occurred.

From visual observation and conceptual study of the blocking phenomena, two main blocking mechanisms were interpreted. The first blocking mechanism would be a Homogenous Blocking Mechanism. This mechanism would occur for smaller maximum particle sizes compared to the nozzle diameter. In this mechanism, the accumulation of multiple particles coming together at the nozzle would interlock until the entire mixture

could not pass through the nozzle. The second mechanism would be the Large Particle Mechanism. In this mechanism, large particle sizes close to the nozzle diameter could cause blocking and a large reduced area for the rest of the mortar to extrude from leading to total blockage of the mixture. This causes the blockage risk to increase greatly as the random chance that a few of the larger particles coming together would be high throughout the process. This is shown in Figure 4.11 by the large (nonlinear) increase once the particle size is around 64% of the nozzle opening. Also if sand particles are non-spherical or elongated they might be passing through the sieve size on a shorter side. This could create larger length particles that reaches closer to the nozzle diameter that must pass through while extruding. The two different blocking mechanisms are schematically shown below in Figure 4.12.

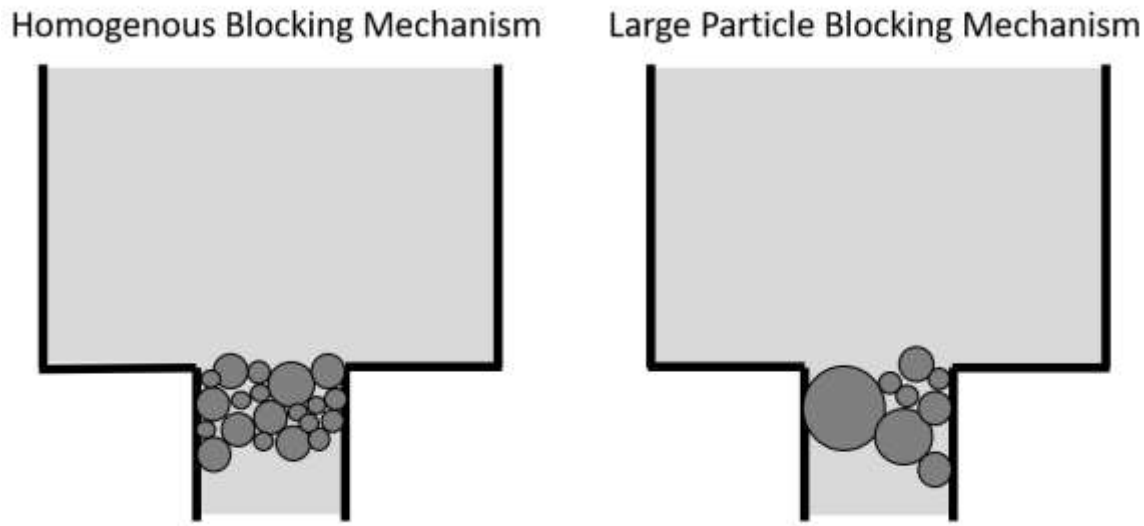

Figure 4.12. Different Blocking Mechanisms

4.2.2. Fiber Blockage. The fibers were then tested to find the blocking point with the 9.13 mm nozzle. This was tested with the low and high workability mixtures. These two mixtures resulted in a mini slump of 245 mm and 104 mm. The mixtures tested at a fiber volume of 0.25%. For both of these mixtures, the fibers blocked on every trial. The blockage is shown below in Figure 4.13.

Figure 4.13. Fiber Blockage

The fibers show that they are oriented in multiple directions. With the fibers being longer than the opening of the syringe, if the fibers are being extruded parallel or partially parallel to the nozzle then they might not pass through the it. The fibers also show that even at the low quantity of fibers multiple fibers were being extruded at once. A lower fiber content was not further investigate because below 0.25% would have very little benefit on the mechanical properties of the concrete. Thus, for the current system and for

the current fibers used, fibers cannot be extruded with the extruder and the nozzle configurations. For future optimization of this system, a larger syringe or custom made "syringe" could be developed to allow for extrusion of fibers. A reducer could also be incorporated so there is not such a harsh change in size from the tube diameter to the nozzle diameter. This might also help align the fibers as they are being extruded which has benefits for not only reduced blockage and increased fiber content, but also improved mechanical properties if the fiber alignment can be well controlled. This would give engineers a lot more freedom of design and creativity to allow for fiber alignment in directions that experience high bending and tensile stresses.

4.2.3. Evaluation of the Test Method and Future Studies. When looking at the particle distribution from Figure 3.3 the poor gradation of the lower sized particles would theoretically lead to a lower packing density. The concept of packing density in blocking leads to a future area of research to understand the effect of packing density and how optimizing the packing density would benefit the extrusion and blockage for printing concrete. Theoretically if the particles have better packing they would be able to have a less chance of blocking due to the increased packing and decreased void space in the mixture. If the lower two sieved sands had a better particle distribution then this might lower the amount of binder content needed to extrude. This would have environmental benefits in reducing the cement content, benefits on shrinkage and heat of hydration, and benefits in increasing the buildability of the printed concrete as it has been shown that increasing the sand content increases buildability. A conceptual graph of the benefit of

improving packing density is shown below in Figure 4.14 (Note: the graph is conceptual and the values are just to show the behavior, not actual magnitudes).

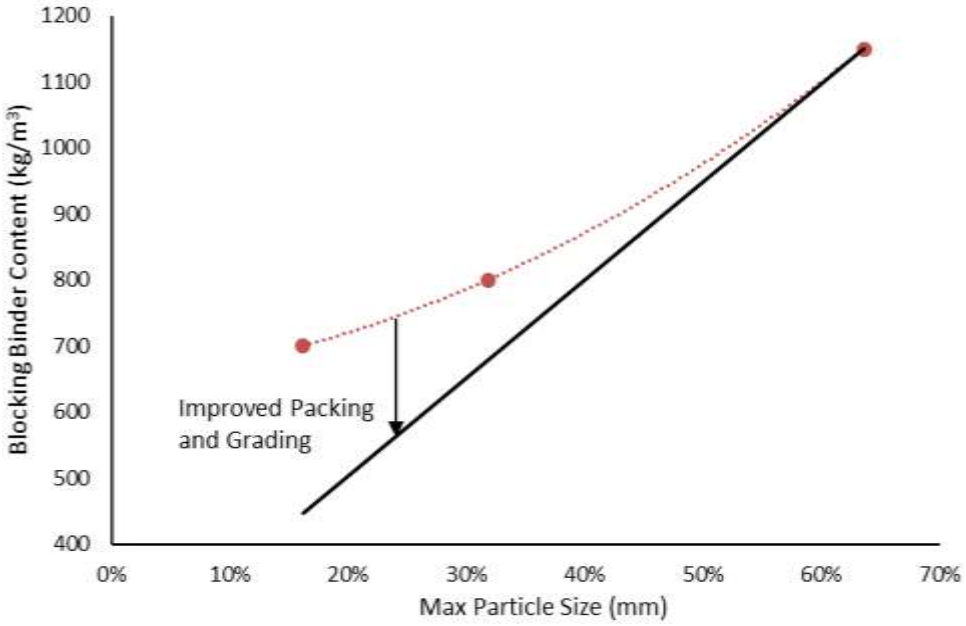

Figure 4.14. Conceptual Effect of improving Packing Density and Grading on Blockage

This concept could be applied to both the packing of sand particles, but also to the packing and particle size of the binder. Various SCM's and fillers such as fly ash, silica fume, and limestone fillers could be optimized for not only improvement of mechanical and durability properties, but also to reduce extrusion force and blockage.

Overall the blockage test proves to be useful for helping characterize and understand extrusion. The test lead to a successful selection of sand size, sand quantity, and binder quantity. The test method proves to be straightforward with no major issues in following the procedure described in Section 3.3. The blocking point can be evaluated

and can help to understand issues that might arise in mix designs before full scale testing when printing.

4.3. RHEOLOGICAL RESULTS

The following sections will discuss the calculation of rheological parameters and the results of the mixtures used for the extrusion tests. For Section 4.3.1 just the M-0.30 mixture is shown to describe the calculation process to transform the data to shear stress and plastic viscosity. Section 4.3.2 will show all of the results for the mixtures.

4.3.1. Transformation to Yield Stress and Plastic Viscosity. From the procedure described in Section 3.3 a data set of torque (N.m) and rotational velocities (rps) are found. These are first analyzed to evaluate if they are fully in equilibrium or if they are still undergoing a thixotropic breakdown. The points were plotted to see if each rotational velocity step levels off and then the average of the portion of the data that leveled off (or in equilibrium) was used to calculate the torque values for each rotational velocity. An example of the torque versus the number of measurements taken for each rotational velocity is shown below in Figure 4.15.

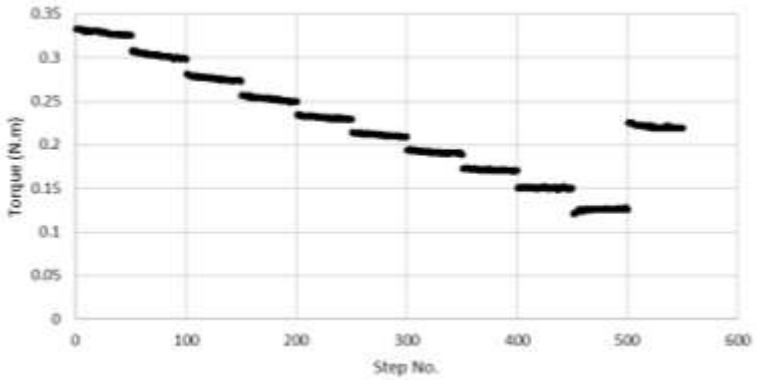

Figure 4.15. Torque versus Step to Check for Equilibrium

After the torque values in equilibrium were found, the torque (T) versus rotational velocity (N) was plotted. From this plot the intercept and slope values could be found. These values correspond to the variables G and H respectively. An example of this graph is shown below in Figure 4.16. After evaluating the data in Figure 4.16, it is clear that the closest fitting model is the Bingham Model due to the high linearity with an R^2 value of 0.997.

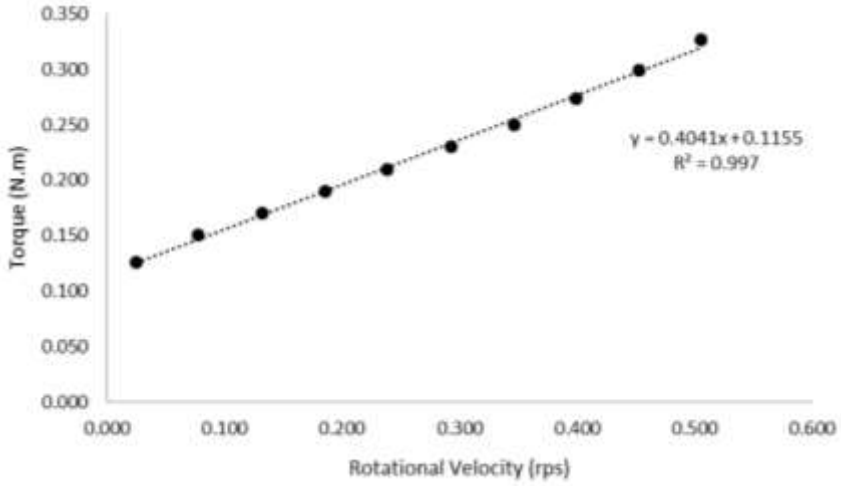

Figure 4.16. Torque versus Rotational Velocity for Rheology

The Reiner-Riwlin transformation equations were then used to convert the torque and rotational velocity. This transformation was chosen since it is one of the more accurate transformations for coaxial rheometers such as the Contec 6 [51]. This transformation uses the geometry of the rheometer and the G and H values to transform the data to a shear stress and shear rate equation rather than some transformations that do a point by point transformation. The equation for yield stress, τ_o, and plastic viscosity, μ_p, for the Reiner-Riwlin equation is shown below in Equation (7) and (8) respectively.

These equations would then be used to fit the terms in the Bingham model as described in Equation (1).

$$\tau_o = \frac{\left(\frac{1}{{R_i}^2} - \frac{1}{{R_o}^2}\right)}{4\pi h \ln\left(\frac{R_o}{R_i}\right)} G \tag{7}$$

$$\mu_p = \frac{\left(\frac{1}{{R_i}^2} - \frac{1}{{R_o}^2}\right)}{8\pi^2 h} H \tag{8}$$

In equation (7) and (8), R_i is the inner radius of the rheometer, R_o is the outer radius, h is the measured height of the mortar on the coaxial head of the rheometer, and G and H are the terms previously described from the torque versus rotational velocity graphs.

After calculating the initial rheological parameters, the data was checked to see if any of the points were in plug flow. This was done by if the plug radius R_p was less than the outer radius R_o. The lesser of these values would be used in calculations as R_s. The equation for calculating R_p is shown below in equation (9).

$$R_p = \sqrt{\frac{T}{2\pi\tau_o h}} \tag{9}$$

In equation (9), T is the torque for the point that is being checked for plug flow, τ_o is the yield stress calculated from the Reiner-Riwlin solution, and h is the height measured from the sample on the rheometer. If any of the points are in plug flow ($R_p < R_o$) then the an iterative process is used to adjust for the points in plug. By using the initial yield stress and plastic viscosity parameters, the shear rate can be adjusted according to equation (10).

$$\dot{\gamma}(R_i) = \frac{2}{{R_i}^2}\left(\frac{1}{{R_i}^2} - \frac{1}{{R_s}^2}\right)^{-1}\left[\omega + \frac{\tau_o}{\mu}\ln\left(\frac{R_s}{R_i}\right)\right] - \frac{\tau_o}{\mu} \tag{10}$$

Using the new shear rate calculated, the yield stress and plastic viscosity can then be calculated again as the intercept and slope of the data set. The difference between the initial and final rheological parameters are compared to find a difference. A solver function is then used to perform the iterations to minimize difference between the initial and final rheological parameters. This causes the correction for plug flow to converge to one set of yield stress and plastic viscosities. If the difference at the minimum point is sufficiently small, then plug flow is considered to be corrected for.

4.3.2. Results for Mixtures. Figure 4.17 shows the shear stress versus shear rate graph for both of the mixes without fibers (M-0.05-Low Workability and M-0.30-High Workability). From the graph, it is clear that the low workability mixture has a much higher yield stress, but a similar plastic viscosity as the high workability mixture. This makes sense as the difference between the two mixtures was just the difference in superplasticizer dosage which is known to drop the yield stress with an increase in dosage.

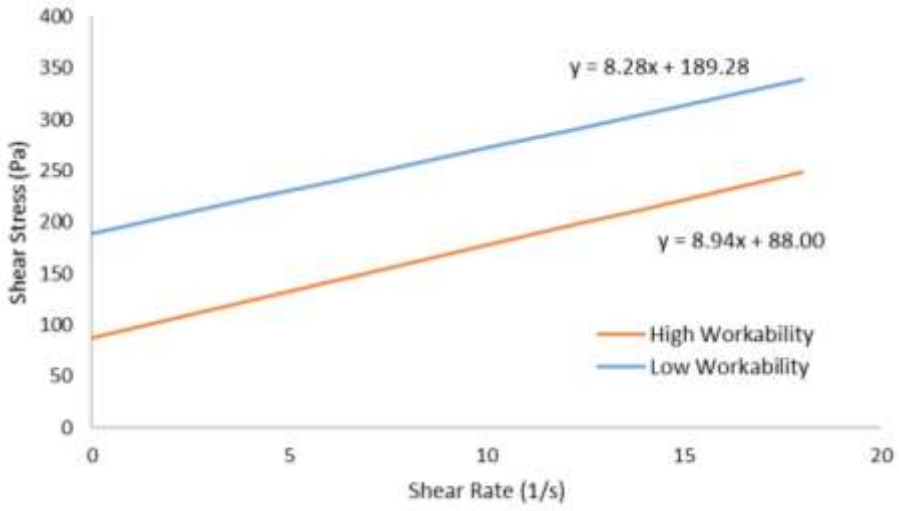

Figure 4.17. Shear Stress versus Shear Rate for M-0.05 and M-0.3

Figure 4.18 shows the shear stress versus shear rate for the two mixtures with fibers. It is known that measuring of rheology with fibers can be complicated due to the fibers aligning with the flow in the coaxial rheometer which makes for less accurate readings. It was still chosen to take the measurement for general comparison, however. The measurements for the rheology were also still taken even though these low fiber dosages blocked the syringe due to the rheological measurements taking place before the fiber blockage test occurred. When comparing the measurements, the plastic viscosity of the low workability fiber mixture was similar to those without fibers. The yield stress however still increased even with the probable fiber alignment. For the low workability fiber mixture, the yield stress and plastic viscosity was significantly lower. There could potentially be an experimental error in the mixing as the mini-slump was even significantly larger spread. The mixture was not remade and tested again due to the finding that it was not able to extrude due to the fibers blocking.

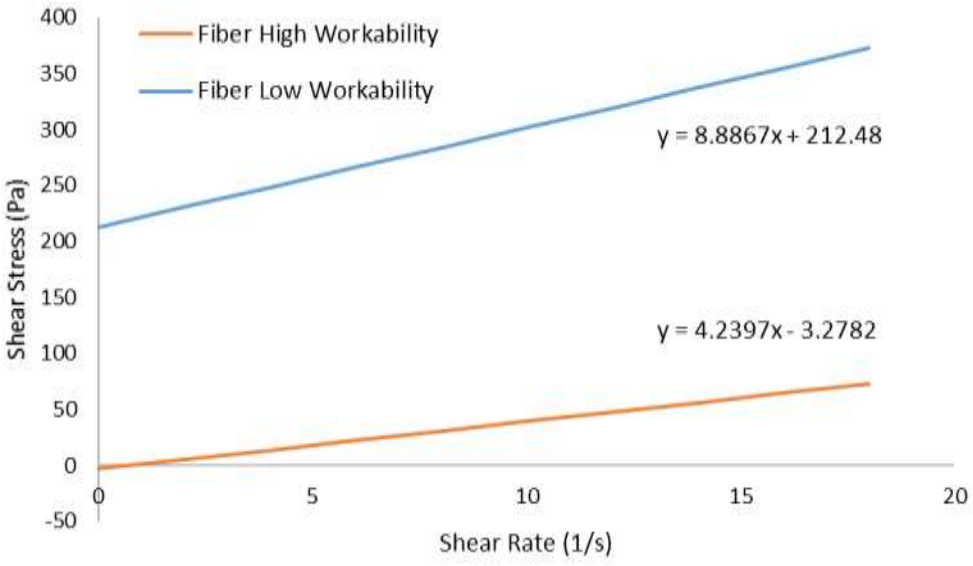

Figure 4.18. Shear Stress versus Shear Rate for MF-0.05 and MF-0.3

The results of the yield stress, plastic viscosity, and mini slump are shown below in Table 4.5. It should be noted that the low value of the mini slumps a flow table measurement was not used for comparison with the high workability mixtures. Since the low workability mixtures did not have a slump flow, the width of the top of the mini slump was measured. This was done so that a direct comparison could be made between the high workability mixtures that would flow on their own without the use of a flow table. All of the mini slump results correlated to the results of the rheometer in terms of yield stress.

Table 4.5. Summary of Rheological Parameters

	Yield Stress (Pa)	Plastic Viscosity (Pa.s)	Mini Slump (mm)
Low Workability	189.3	8.28	106
High Workability	88.0	8.94	172
Low Workability-with Fibers	212.5	8.89	104
High Workability-with Fibers	-3.28	4.24	245

4.4. EXTRUSION TESTING

This section includes the discussion of how the extrusion test was analyzed and the results from the ram extrusion test for printing. The nozzle to internal diameter ratio (d/D), extrusion rate, and effect of rheology are analyzed. Other quantitative and qualitative findings are also discussed to help describe the different phenomena that occur during extrusion.

4.4.1. Raw Results and Data from Extrusion Tests. As described in Section 3.4.3, after the test is complete the data from the serial monitor in the Arduino software is copied and saved as a text file. This data includes a list of points with the force values next to a time stamp. This data was then analyzed in Microsoft Excel. Since the load cell was programmed to read data points at every interval, it was assumed that if the distance of extrusion was known that the force readings would line up with the distance across equal increments throughout the test. For the test setup, the distance from start to finish was measured using dial calipers to get an accurate measurement of the extrusion distance for correlating the force readings to distance readings. For the testing parameters described in Section 3.4.2, the extrusion distance was 115.6 mm. Each distance point was calculated from the force data found using equation (11):

$$d_i = \frac{L_E}{N_t} n_i \tag{11}$$

In this equation, d_i is the distance for the n^{th} force measurement, L_E is the extrusion length, N_t is the total number of force measurements taken, and n_i is the n^{th} number data point from the beginning of the data set. Once the force was correlated to a distance, the force versus displacement graph could be found for the data set. Figure 4.19 shows an example of the raw data graphed in this way. The graph shows two measurements for an empty syringe, the two measurements taken for the syringe with mortar in it, and the average of the two measurements with mortar. From the raw data, several parameters were analyzed and are shown in Figure 4.20.

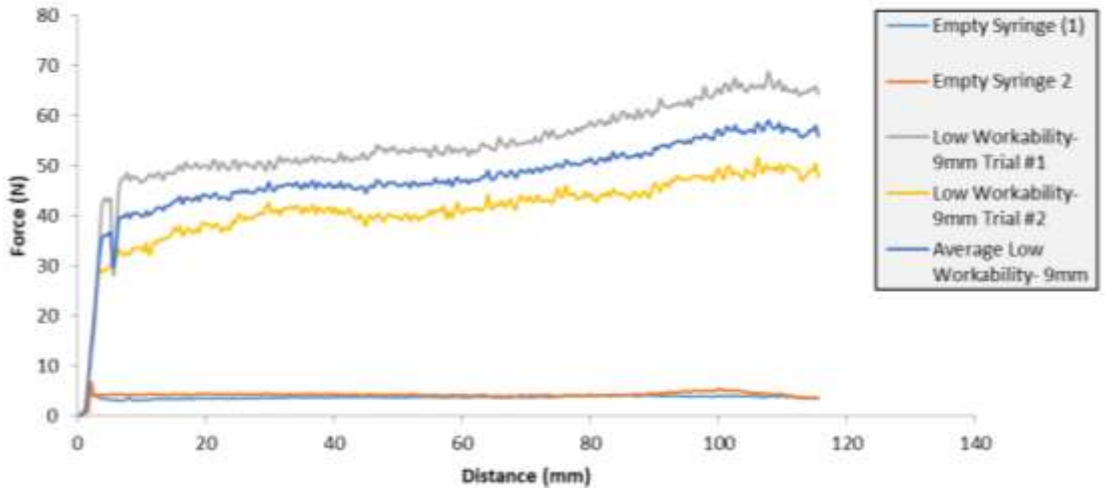

Figure 4.19. Example of Raw Data graphed for Extrusion Test

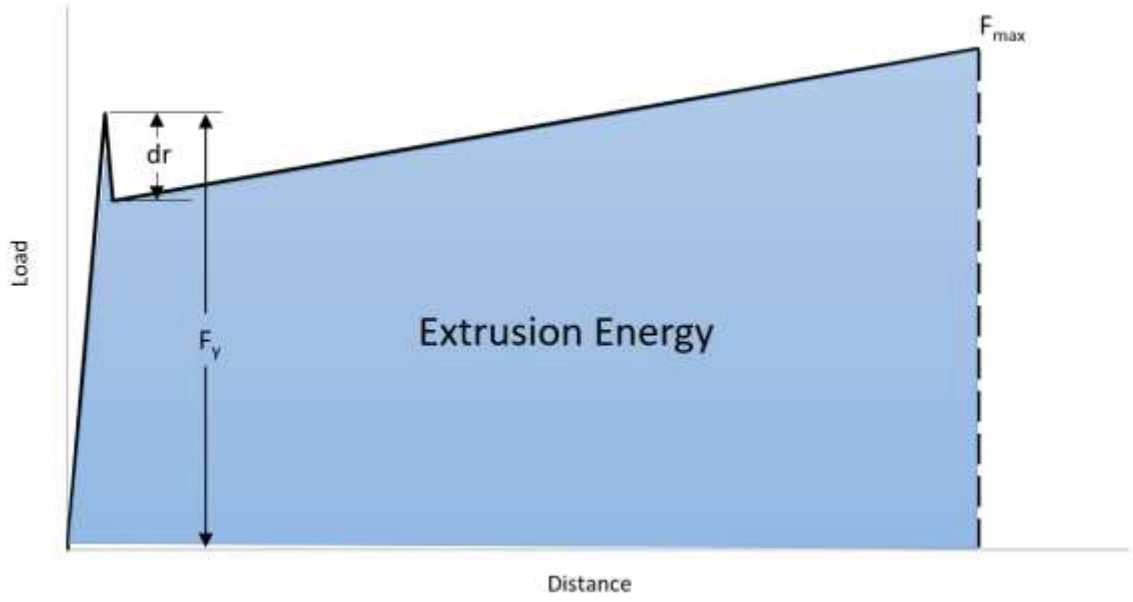

Figure 4.20. Extrusion Test Load versus Displacement Parameters

In the Figure 4.20, F_{max} is found at the maximum load for the load versus displacement graph. F_{max} is shown at the end of the graph, but it may also occur at other locations on the graph if the extrusion doesn't fit the a nice linear increase in force. This

was the case whenever extrusion forces were near the top or above the working capacity of the motor. It was found in several tests that that once the test started there was an initial height the force would reach, F_y, and then it would drop a certain distance, dr, before starting to increase again either below or above the F_y value. The presence of an Fy value followed by a drop, dr, shows that the material behaves with an initial static resistance and once the material starts to flow, the pushing force value it drops to the dynamic value of extrusion force needed to extrude. This concept is similar in relation to the rheological behavior as there is a static yield stress that drops the amount of shear force needed to shear the material which varies from the shear stress needed to move at a slow rate. It can also be compared to the tribological behavior as there is different coefficient of friction values for the static and dynamic cases. The extrusion energy was found by integrating the force versus displacement curve from the start to end of testing to calculate the area under the curve. This is shown mathematically using equation (12):

$$EE = \int_0^{L_E} F(x)dx \tag{12}$$

where EE is extrusion energy, F(x) is the function of the force displacement curve, and dx is the differential distance. To normalize the extrusion energy since the same amount might not always be extruded or if the motor would not be able to fully extrude the concrete the unit extrusion energy (UEE) can be calculated. This would be just the extrusion energy (EE) divided by the extrusion length (L_E).

The summarized results of the these parameters are shown below in Table 4.6. The effects of the nozzle size, extrusion rate, and rheology on these parameters will be discussed in detail in the following sections.

Table 4.6. Summarized Results from Extrusion Tests

	Low Workability (M-0.05)			High Workability (M-0.3)			Varying Speed (M-0.05)		
Nozzle Opening Size	**3.71 (mm)**	**6.32 (mm)**	**9.13 (mm)**	**3.71 (mm)**	**6.32 (mm)**	**9.13 (mm)**	**1.639 (mm/s)**	**1.513 (mm/s)**	**1.397 (mm/s)**
Max Load (N)	81.8	66.9	60.1	61.5	41.9	28.3	84.3	91.0	67.6
Extrusion Energy (N.mm)	5257	5665	5477	5949	3717	2575	1970	1970	6536
UEE (N.mm/mm)	66.3	49.0	47.4	51.5	32.2	22.3	70.5	77.6	56.6
Average Force (N)	67.2	49.1	47.5	51.6	32.3	22.5	70.6	77.7	56.6
F_y (N)	66.2	52.8	36.7	53.5	37.1	21.4	56.2	77.2	60.7
dr (N)	7.9	6.7	6.8	-	1.8	4.1	7.4	2.4	-

4.4.2. Effect of Nozzle Size. The three nozzle sizes used allowed for a varying d/D ratio to be tested to analyze the effect on extrusion. The 3mm, 6mm, and 9mm nozzle sizes thus lead to a d/D ratio of 0.094, 0.160, and 0.231 respectively. First the results were compared graphically using the load versus displacement graphs previously described. All the graphs described upcoming will be the average of the two readings as shown in Figure 4.19. Figure 4.21 shows the load versus displacement for varying d/D values for the low workability (M-0.05) mixture and Figure 4.22 shows the same, but for the high workability mixture (M-0.30).

From both Figure 4.21 and 4.22 the extrusion force needed is depending on the nozzle size or d/D ratio. The figures also show the variability that can take place during measurement. This variability could be due to a number of reasons from vibrations in the system from the motor to the motor struggling when reaching near the top of its working capacity to accumulation of sand particles around the nozzle getting partially clogged and unclogged. Taking this data the variation in average force, maximum force, and UEE was

calculated for the different d/D ratios. These are shown below in Figures 4.23, 4.24, and 4.25 respectively.

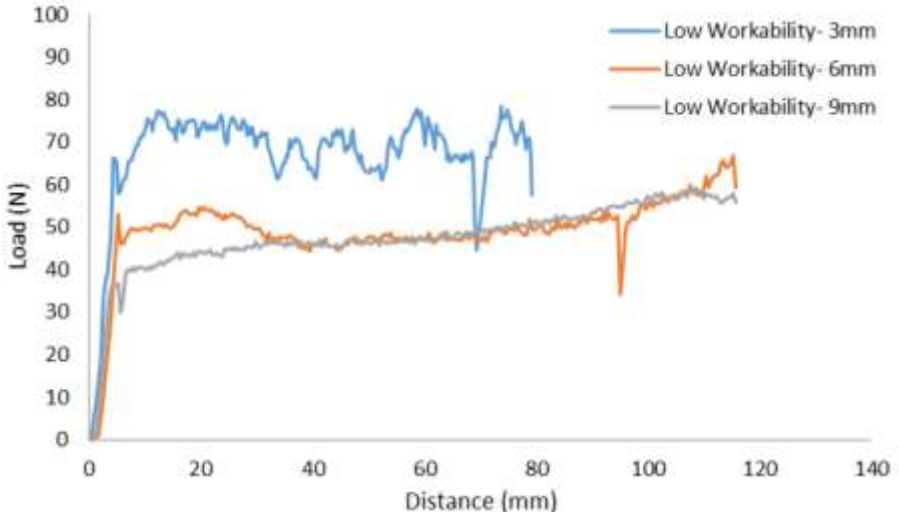

Figure 4.21. Low Workability (M-0.05) Extrusion Force versus Displacement

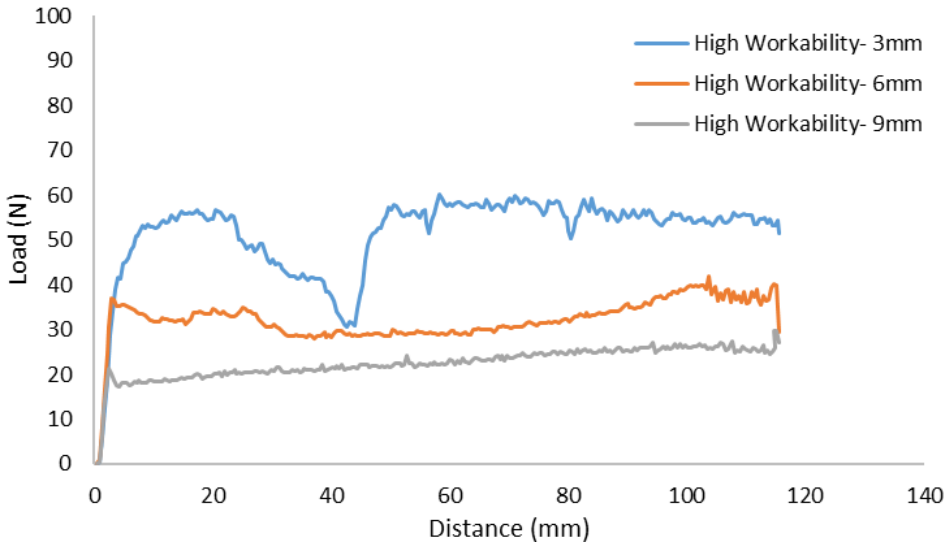

Figure 4.22. High Workability (M-0.3) Extrusion Force versus Displacement

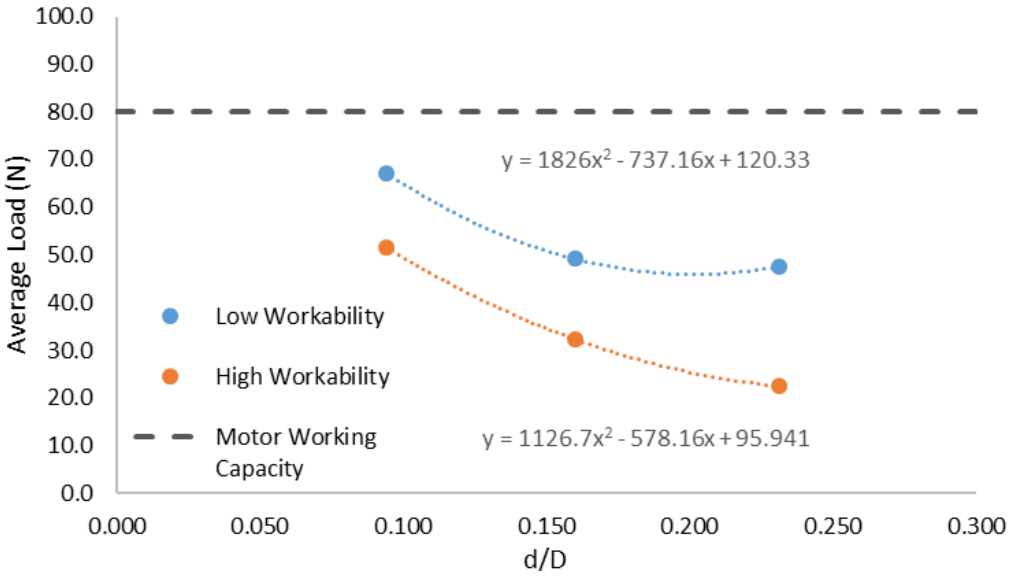

Figure 4.23. Average Extrusion Load versus d/D ratio

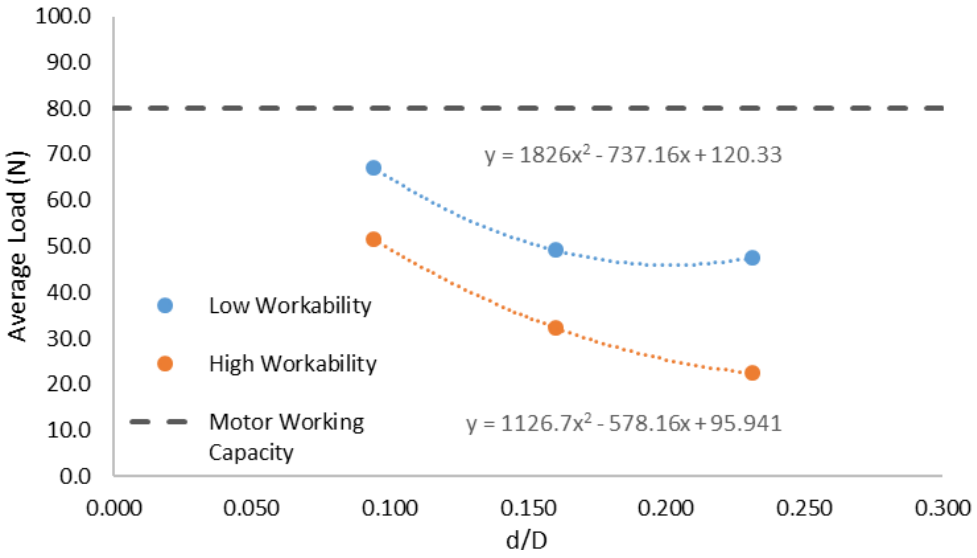

Figure 4.24. Maximum Extrusion Load versus d/D ratio

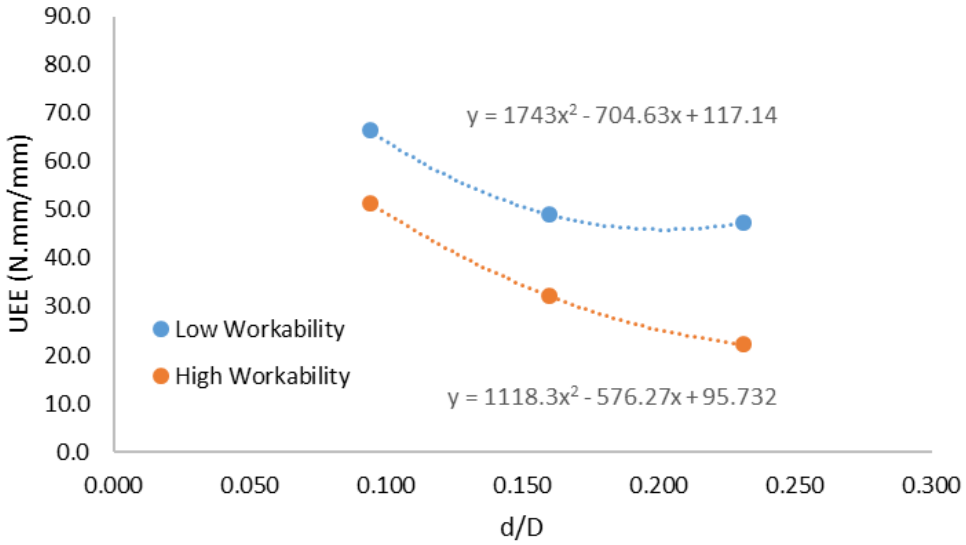

Figure 4.25. UEE versus d/D ratio

From the graphs it also verifies that the extrusion force decreases with a increasing d/D ratio. The extrusion energy also decreases with an increasing d/D ratio. For both the lower and higher workability mixtures seemed to show a similar behavior and shape when increasing the d/D ratio. This shows that the d/D ratio effect on the extrusion force or energy is independent of fluidity and yield stress of the concrete. Also, for the force and extrusion energy, the decrease starts to shows signs of leveling off. Once the extrusion force or energy would level off this would lead to a maximum d/D ratio to where any further increase would not change extrusion force. Physically this makes sense as at a certain point as the d/D ratio would increase, the concrete or mortar would want to flow or fall out of the extruder on its own due to gravity.

All of the graphs except for the M-0.3 high workability mixture with the 3mm nozzle had very distinct dr and F_y values. These values were analyzed to see if there were any relationship between each other or with a changing d/D ratio. The F_y value was found to have a linear relationship with the d/D ratio. This shows that the initial static energy or

force the extrusion system overcomes is also related to d/D. This relationship is shown in Figure 4.26.

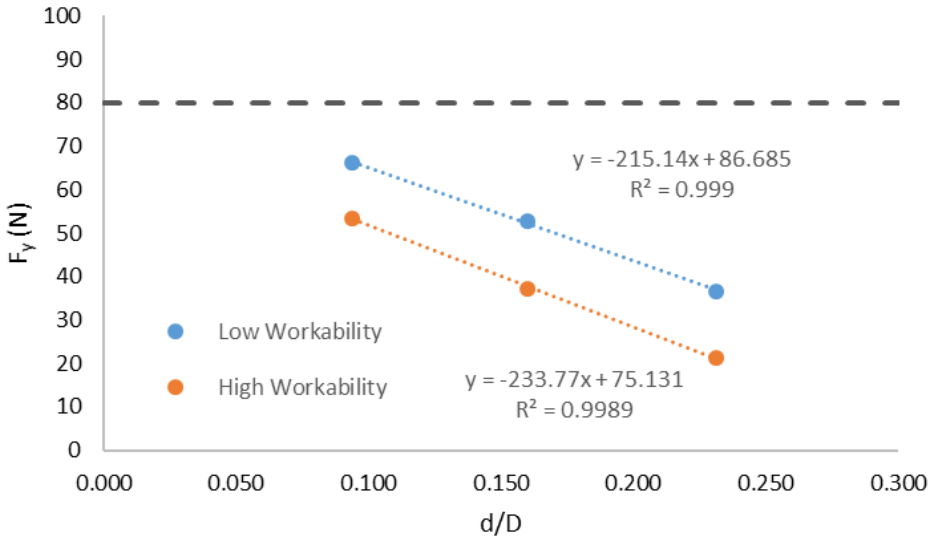

Figure 4.26. F_y versus d/D ratio

The relationship between dr and d/D and the ratio of dr/F_y and d/D was also investigated. There was no correlation found between either of these comparisons and for the current set of data it seems the dr is independent of F_y and the d/D ratio.

4.4.3. Effect of Extrusion Rate. For the M-0.05 mixture after the initial tests were done, three different extrusion rates were tested on the 9 mm syringe (d/D = 0.231). The different speeds tested were 1.39 mm/s, 1.51 mm/s, and 1.64 mm/s. The initial force versus displacement results of the test are shown in Figure 4.27.

As seen in the figure, the higher speeds did not extrude the full distance. This was due to the force required to extrude exceeding the working limit of 80 N of the motor. Once the force reached above this value then the motor was not able to rotate the

threaded rod and thus was not able to continue to move the syringe down to extrude. This caused the data to become more sporadic and the extrusion length shortened.

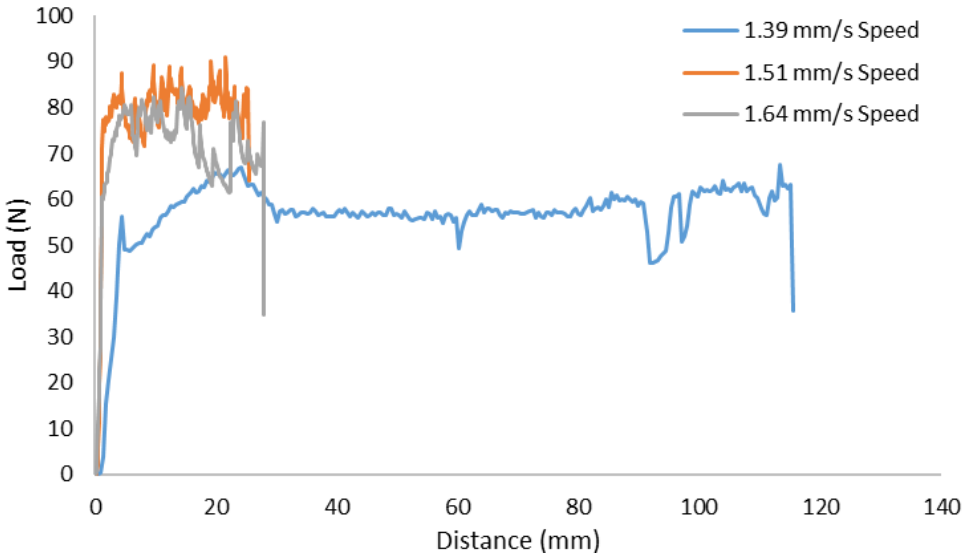

Figure 4.27. Extrusion Force versus Displacement for Varying Speeds

Even the small increase in speed was enough to bring the force needed above the motors capacity. Once the motion had completely stopped, even when the force slightly dipped below 80 N, the extrusion distance did not change but in very small magnitudes.

The average force, maximum force, and UEE were still analyzed for the experiment. These values are shown in Figures 4.28, 4.29, and 4.30. These show that the extrusion force and energy both increase with an increase in extrusion rate. However, once the threshold force that keeps the motor from rotating is reached, the results plateau off and are not able to be directly compared past this point as seen from the jump from 1.51 mm/s to 1.64 mm/s.

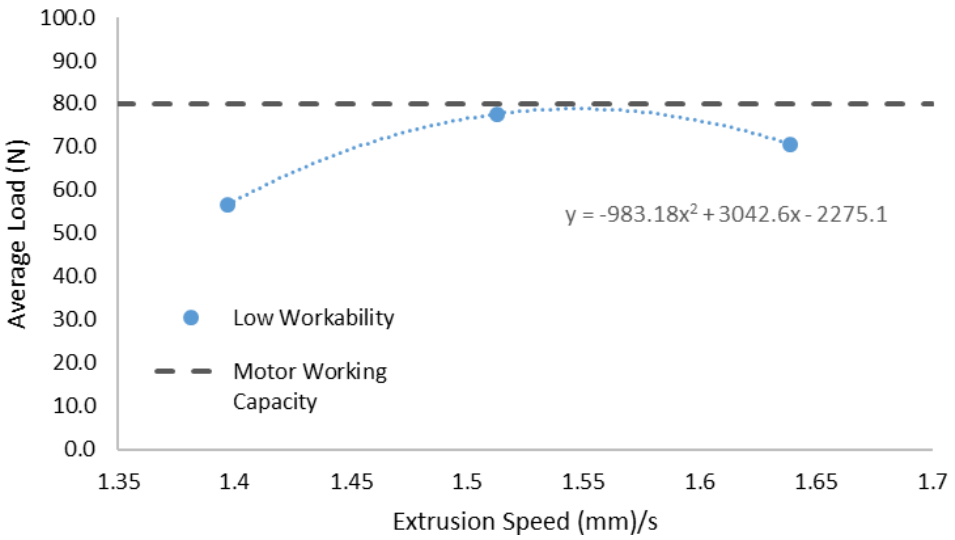

Figure 4.28. Average Extrusion Force versus Extrusion Speed

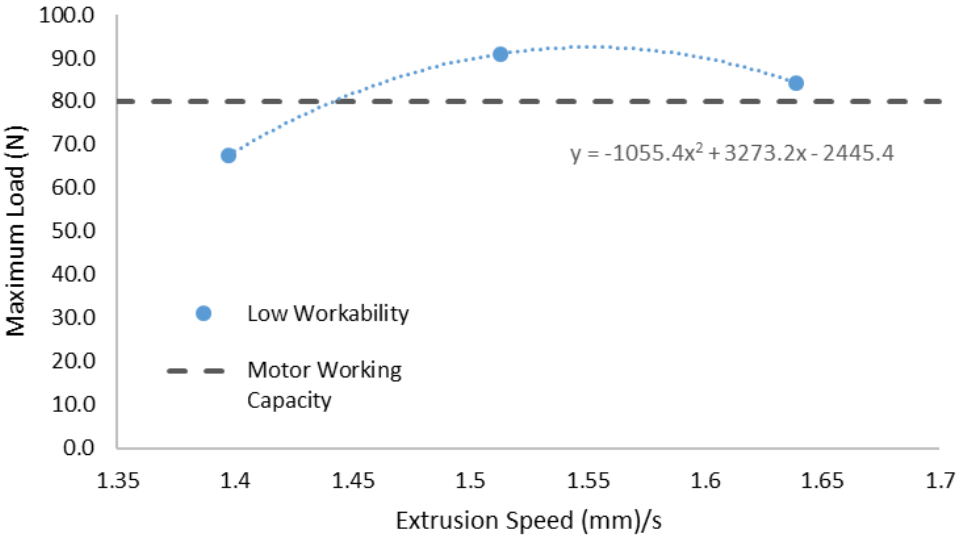

Figure 4.29. Max Extrusion Force versus Extrusion Speed

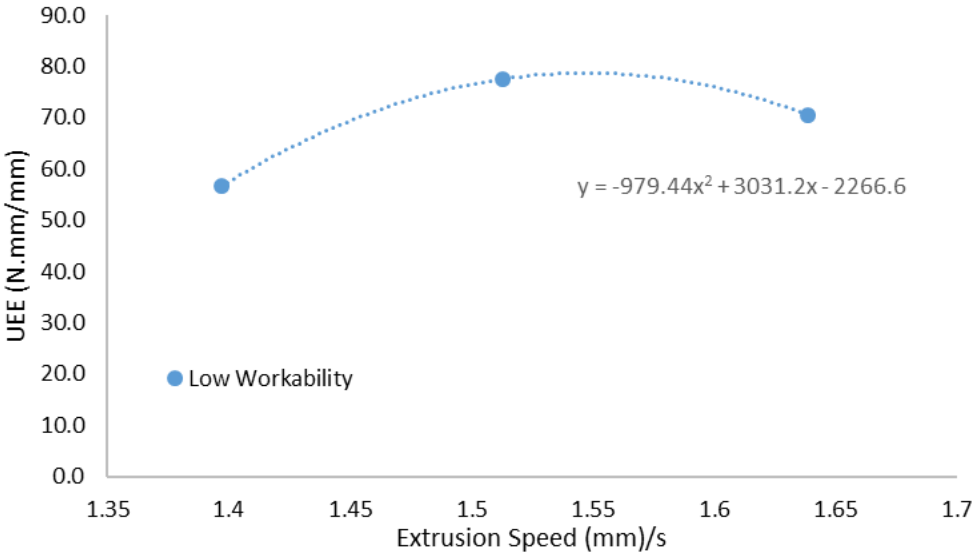

Figure 4.30. UEE versus Extrusion Speed

4.4.4. Effect of Workability on Extrusion. The effect of rheology was investigated by incorporating the rheological measurements from Section 4.3 with the extrusion measurements taken. First the load versus distance curves are compared for each of the three d/D ratios to directly compare the effect between the low (M-0.05) and high (M-0.3) mixtures. These are shown below in Figures 4.31, 4.32, and 4.33. From these figures, it is clear that the extrusion force was consistently less for the high workability mixture. Because the mixtures had a consistent viscosity, this means that the yield stress is directly related the amount of extrusion force necessary to extrude.

When comparing the average force, maximum force, UEE, and F_y in Figures 4.23-4.25 it is clear that all of these exhibit the same effect from between the two mixtures. As the yield stress is decreased, all of the curves shift vertically downward by the same ratio.

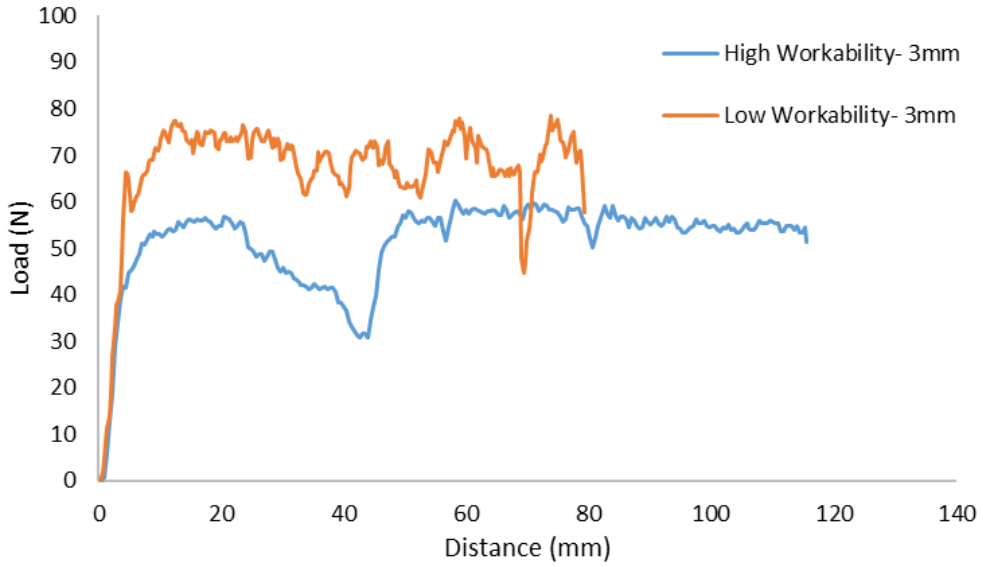

Figure 4.31. High versus Low Workability for 3 mm Opening

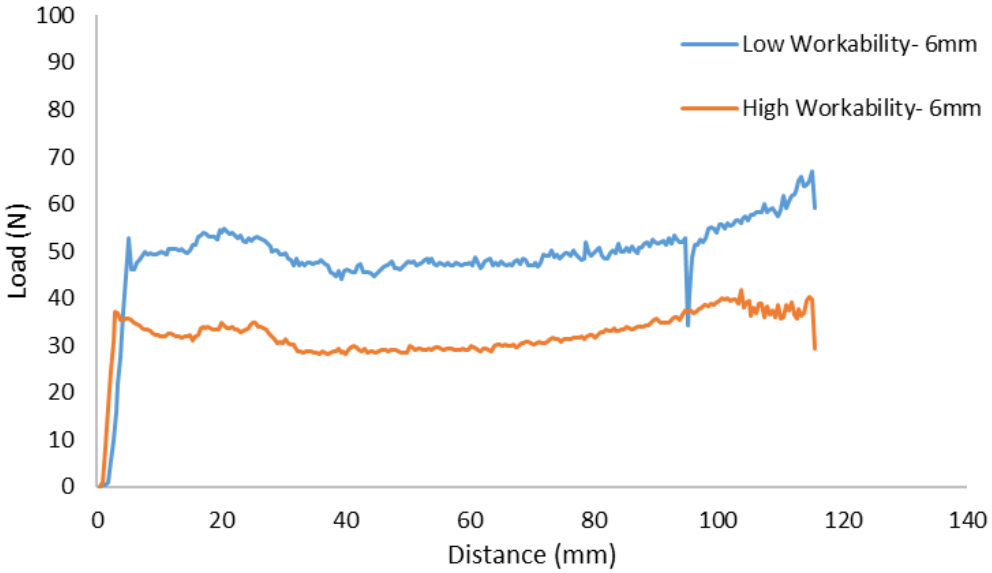

Figure 4.32. High versus Low Workability for 6 mm Opening

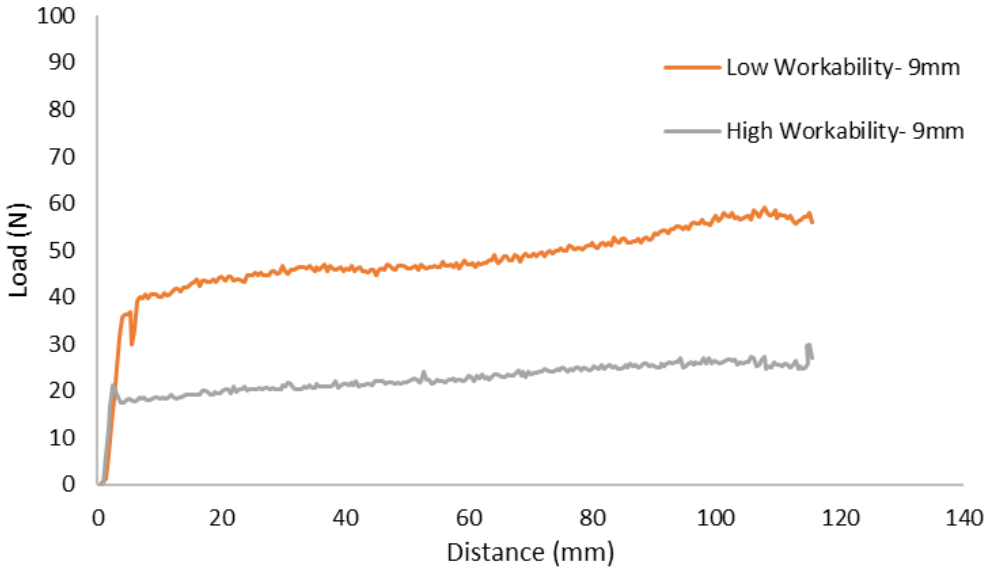

Figure 4.33. High versus Low Workability for 9 mm Opening

4.4.5. Effect of High Extrusion Pressure. When developing the extrusion test, several test mixtures were used to evaluate the system before the final device was built and the final mix designs were implemented. During these trials, qualitative findings were found when attempting to extrude for 3D printing. One finding was the negative effect on extrusion from high yield stress mixtures with small d/D ratios. One problem that arises for these combinations is the extrusion process does not act homogenous from beginning to end. With such high pressures in the capillary tube of the syringe, this caused more paste and bleed water to be extruded initially leaving the end of the syringe with a very stiff and dry mixture. The process acted similar to that of consolidation in a soil where more water was being forced out at prolonged high pressures. This artifact leads to the knowledge of balancing the d/D ratio, yield stress, and bleeding resistance within the mix design. Addressing any of the three items can help reduce pressure or bleeding in the mixture during extrusion. An example of this is shown below in Figure

4.34 where part of the concrete that was not extruded was retrieved out of the syringe showing it is no longer a plastic material but rather a frictional material similar to soil.

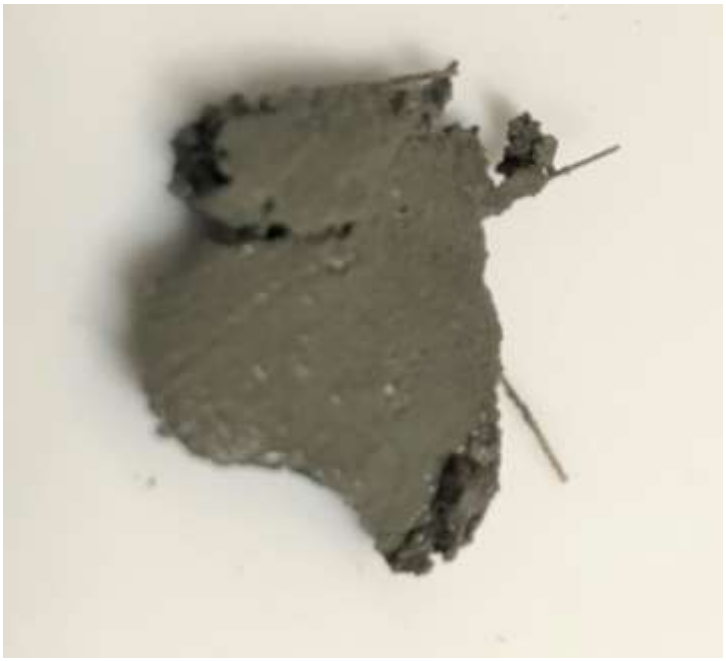

Figure 4.34. Dry Consolidated Mortar Due to High Extrusion Pressure

4.5. EFFECT OF PRINTING OF MECHANICAL PROPERTIES

The following section will describe the results between the manually printed and cast beams. The compression results are presented first to give the cast compressive strength of each mixture. This will give a baseline value of the strength and helped size the length chosen for the flexural test based upon estimated strength. The flexural results are then presented to compare the two methods.

4.5.1. Compressive Strength. Table 4.7 shows the results from the compression tests. The results shown are an average of the three cubes.

Table 4.7. Cube Compressive Strength Results

Mixture	Compressive Strength (MPa)	% Change from REF
REF	75.2	0%
F-0.25	69.1	-8.1%
F-0.50	70.3	-6.5%

The results match those in Section 4.1.2 in that the compressive strength of the mixtures with fibers do not improve compressive strength and slightly lower the value of the compressive strength. This decrease could be due to more the fibers increasing the ITZ throughout the matrix. The fibers did keep the cubes from completely breaking. The failure surface of the reference compared to the mixtures with the fibers is shown below in Figure 4.35.

Figure 4.35. Cube Compressive Failure Comparison

4.5.2. Flexural Results. Before analyzing the data from the three-point bending test, the cross-sections of the printed beams had to be analyzed in order to calculate the properties correctly. The properties found that are reported include the moment of inertia, distance to the centroid from the bottom of the beam, and the area. The radius of gyration, polar moment of inertia, perimeter, and product of inertia could also be found from the image analysis, but they are not needed for the analysis so they are not reported. Table 4.8 shows the summary of the results from the image analysis using AutoCAD.

Table 4.8. Printed Beam Geometric Properties from Image Analysis

Specimen	Area (cm^2)	Centroid (cm)	Moment of Inertia (cm^4)
Cast Beams	38.7	2.54	83.2
REF-1	29.7	2.11	42.1
REF-2	36.8	2.09	59.4
F-0.25-1	27.1	1.62	25.2
F-0.25-2	36.1	2.29	61.5
F-0.50-1	34.2	2.08	51.9
F-0.50-2	29.0	1.63	28.8

From the three-point bending test, the graphs of the load versus deflection for each specimen was found. From theses graphs, I_5, I_{10}, and I_{20} toughness indices, $R_{5,10}$ and $R_{10,20}$ residual strength values, total energy, and pre-peak energy can all be found. The

load-deflection graphs for all the tests are shown below in Figure 4.36. It should be noted that the magnitudes between the cast and printed beams can not be directly compared on the load-deflection diagrams due to the differences in cross-section dimensions. The results can also show the difference in fiber content on the behavior of the specimen, especially in the post-peak performance of the beams. Figures 4.37, 4.38, 4.39 show the load versus deflection for the REF, F-0.25, and F-0.50 mixes respectively for an easier comparison of the results and to look closer into the behavior differences between the cast and printed beams.

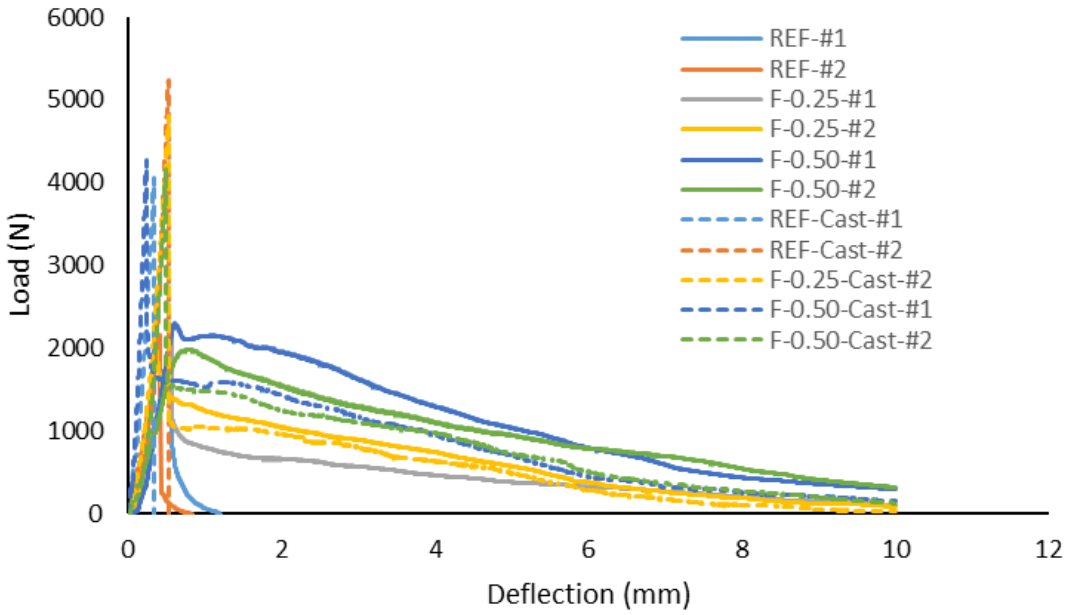

Figure 4.36. Load versus Deflection for Printed versus Cast Beams

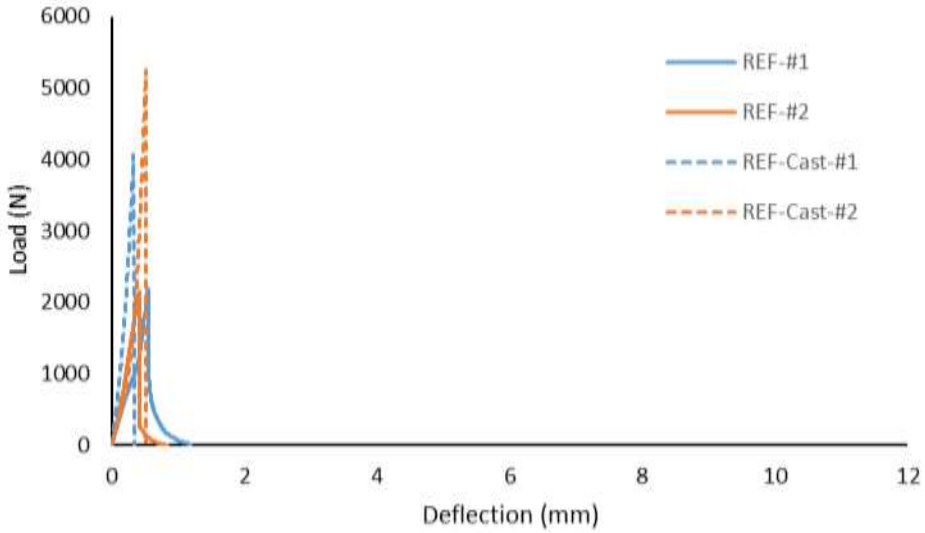

Figure 4.37. Load versus Deflection for REF (without fibers) Printed vs Cast Beams

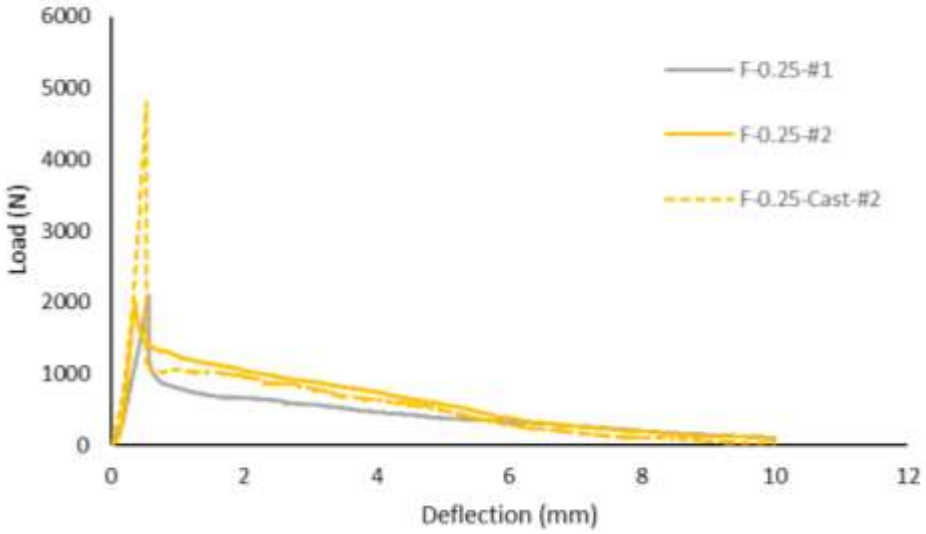

Figure 4.38. Load versus Deflection for F-0.25 Printed vs Cast Beams

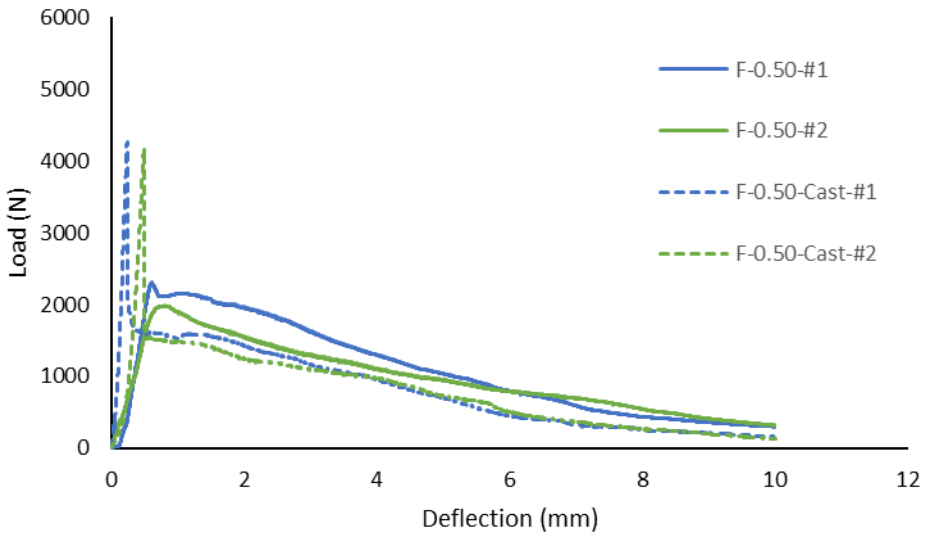

Figure 4.39. Load versus Deflection for F-0.50 Printed vs Cast Beams

Comparing the graphs, there is a noticeable difference in the peak load due to the cross-sectional difference, but the post-peak performance is similar between the two beams. The printed beams for most of the specimens even perform better than the cast beams in post-peak performance when comparing the graphs. To quantify the difference in performance of the beams the I_5, I_{10}, and I_{20} toughness values and $R_{5,10}$ and $R_{10,20}$ residual strength values were calculated as described in Section 4.1. The total energy and pre-peak energy was calculated as the total area under the graph and area under the graph until the LOP. The first crack stress was calculated differently than Section 4.1. Due to not being notched beams and having varying cross-sectional properties, the first crack stress was calculated using equation (6).

$$R = \frac{PL\bar{y}}{4I} \tag{13}$$

In equation (13), R is the first-crack stress, P is the load where the first crack forms, L is the length, $\bar{y}$ is the centroid distance from the bottom tension surface, and I is

the moment of inertia. L was a constant value of 200 mm. P was the found from analyzing the load versus deflection graphs, and $\bar{y}$ and I are found from Table 4.8. A summary of these results are shown in Table 4.9. A comparison in the change in the values caused by printing compared to the cast beams is shown in Table 4.10. It should be noted that for comparing the pre-peak and total energy, due to the difference in cross-section dimensions of the cast and printed beams, the values should not be directly compared when evaluating the performance between each other. The toughness indices and residual strength provide a better comparison due to them being based on the ratio of the area under the curve to the area under the pre-peak load.

Table 4.9. Print versus Cast Beam Flexural Properties

Specimen	First Crack Stress (MPa)	Pre-Peak Energy (N.mm)	Total Energy (N.mm)	I_5	I_{10}	I_{20}	$R_{5,10}$	$R_{10,20}$
REF-Printed	4.65	460	555	1.20	1.20	1.20	0	0
REF-Cast	7.21	684	691	1.01	1.01	1.01	0	0
F-0.25-Printed	5.28	363	5186	3.95	6.93	11.51	59.5	45.8
F-0.25-Cast	7.31	954	5500	2.16	3.43	5.10	25.5	16.7
F-0.50-Printed	5.20	745	10226	4.78	8.55	13.16	75.4	46.1
F-0.50-Cast	6.54	518	7850	3.17	5.55	9.56	47.7	40.1

Table 4.10. Percent Change in Flexural Properties from Printing

Specimen	First Crack Stress	Pre-Peak Energy	Total Energy	I_5	I_{10}	I_{20}	$R_{5,10}$	$R_{10,20}$
REF	-36%	-33%	-20%	+18%	+18%	+18%	-	-
F-0.25	-28%	-62%	-6%	+83%	+102%	+126%	+134%	+175%
F-0.50	-21%	-44%	+30%	+51%	+54%	+38%	+58%	+15%

For a visual comparison, the data from Table 4.9 was plotted as a bar graph to compare the first crack strength, toughness indices, and residual strength. The first comparison is between the first crack strength. This is shown below in Figure 4.40.

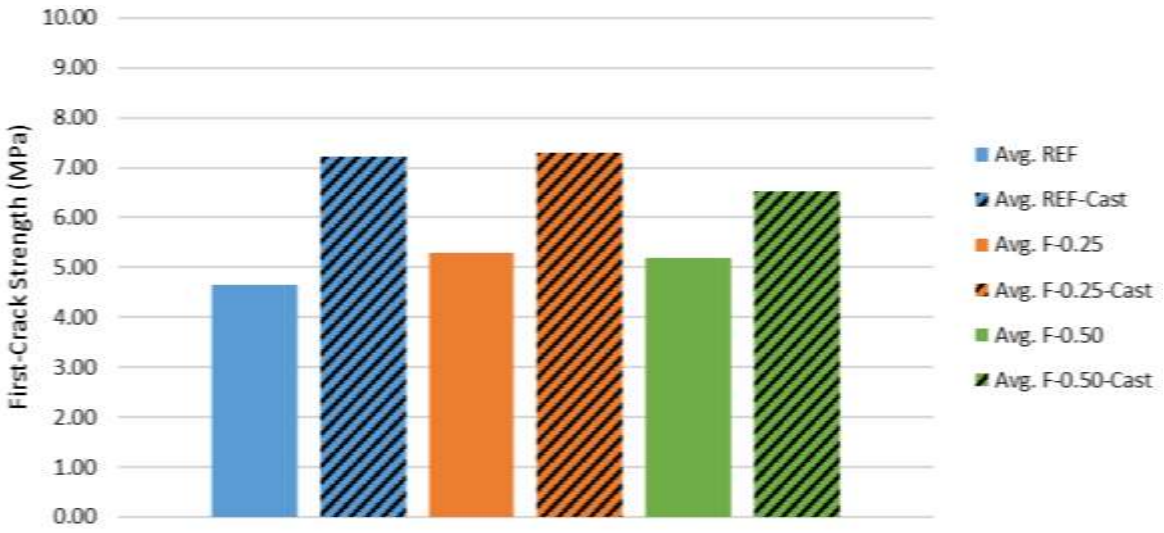

Figure 4.40. First-Crack Strength Comparison for Printed versus Cast Beams

When comparing the first-crack strength, the printed specimens all show to crack at a lower stress level. This lower strength from printing could be due to a couple different reasons. One might be that due to the inconsistency in manual printing. There could be gaps or macropores within the concrete layers or pockets of entrapped air if the layers were not entirely aligned with each other. This would lead to weakened zones within the specimen causing early cracking. An example of this is shown in one of the fractured cross sections in Figure 4.41. The lower strength could also be due to the weak interlayer bond between layers. It has been shown that at the micropores and microchannels form at interfacial regions in the direction of printing [30]. Since all of the layers were printed longitudinally, this would create weakened layers in direction of tensile stresses within the cross section. The printed and cast beams do not see much of an increase or decrease in first-crack strength with the addition of fibers. The reason for no major increase is that short fibers are the reinforcing system rather than long fibers. This matches what has been found in other research as short fibers are known to help improve post-crack properties and bridge micro-cracks while long fibers help improve the flexural strength and bridge macro-cracks [38], [39].

The I_5, I_{10}, and I_{20} toughness indices are compared below in Figures 4.42, 4.43, and 4.44 respectively. When comparing these results, the printed specimens show to improve the post-crack properties significantly. For all of the specimens the printed fibers outperformed the cast specimens. For the I_5 toughness value for the F-0.50, the toughness value is only slightly below 5.00. This shows that the response was close to elasto-plastic response for the early stages after the first-crack forms.

Figure 4.41. Printing Gaps in Cross Section

This shows that it would be likely to reach an elasto-plastic response or even strain hardening if the print could be designed to increase the fiber content slightly higher. This significant improvement in toughness in shows that the printing process can help improve the orientation of the fibers compared to the completely random orientation due to casting. This fiber orientation improvement is investigated and discussed in more detail later in this section.

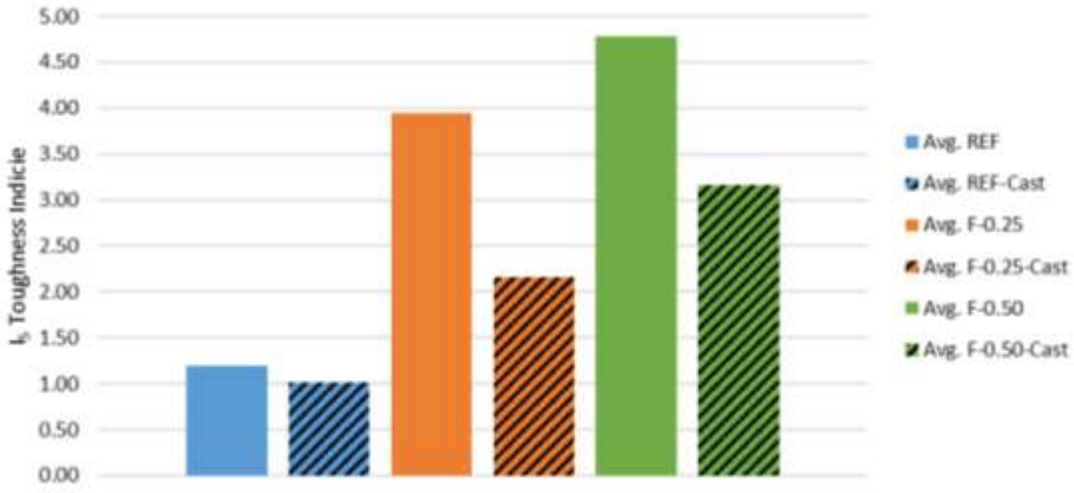

Figure 4.42. I_5 Toughness Comparison for Printed versus Cast Beams

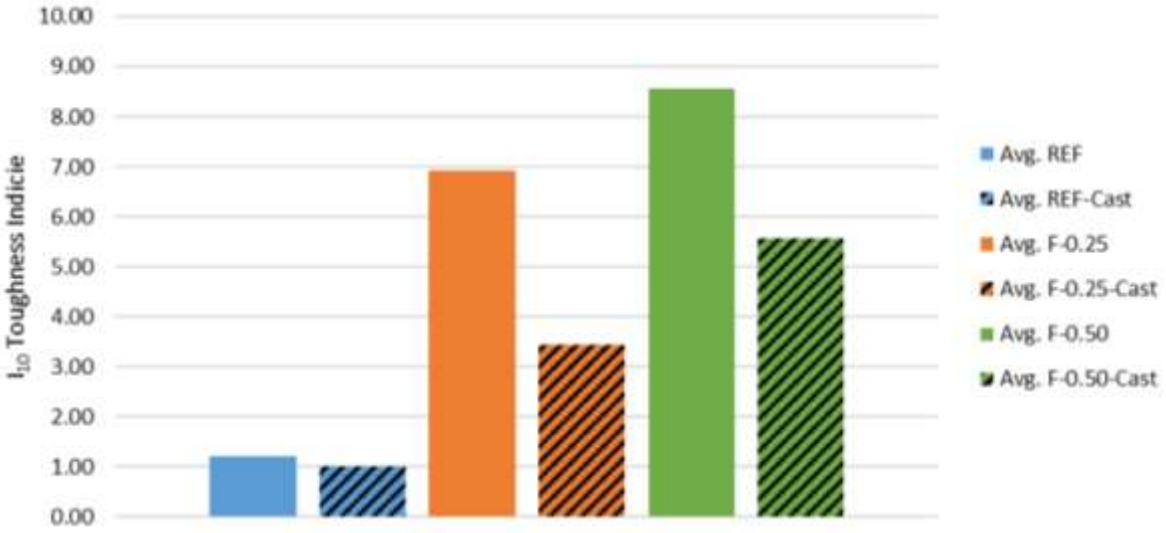

Figure 4.43. I_{10} Toughness Comparison for Printed versus Cast Beams

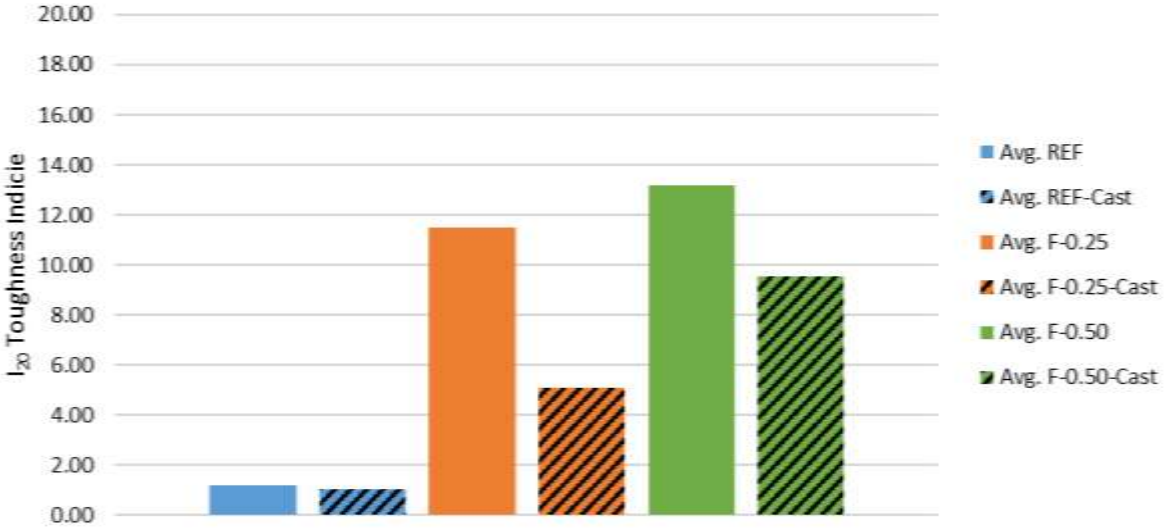

Figure 4.44. I_{20} Toughness Comparison for Printed versus Cast Beams

The $R_{5,10}$ and $R_{10,20}$ residual strength is compared in Figures 4.45 and 4.46. These results match the results found when comparing the toughness values between the cast

and printed beams. Again, an improved fiber orientation from the printing process would cause this increase.

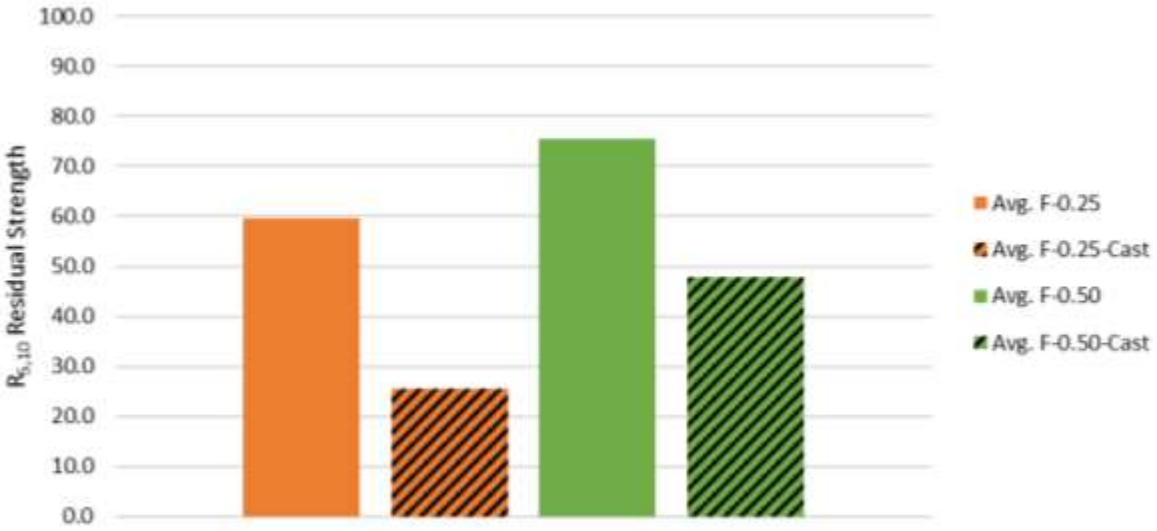

Figure 4.45. $R_{5,10}$ Residual Strength Comparison for Printed versus Cast Beams

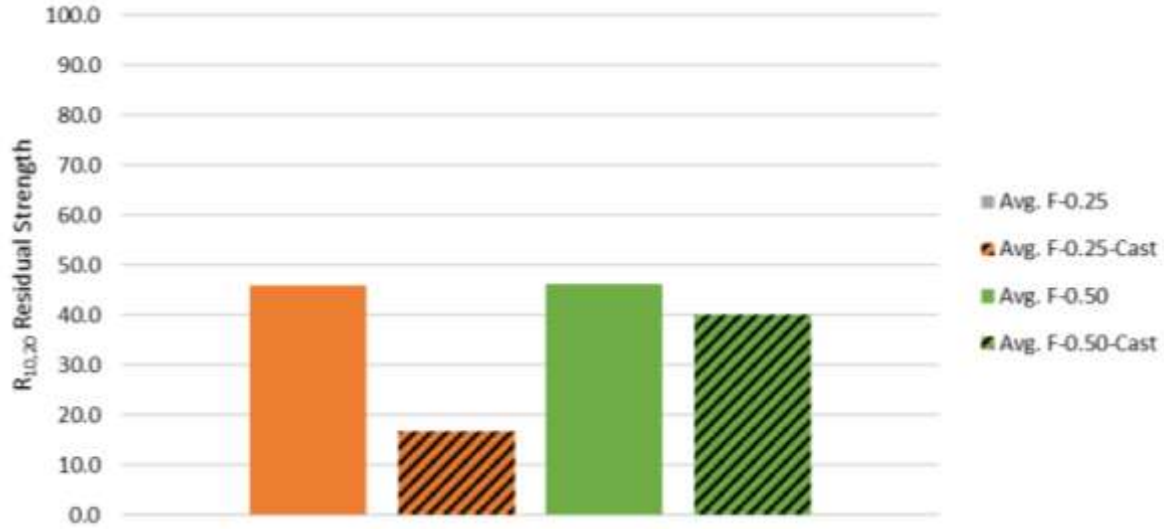

Figure 4.46. $R_{10,20}$ Residual Strength Comparison for Printed versus Cast Beams

After analyzing the results of the three-point bending test, the broken cross section was analyzed to directly compare the fiber orientation between the cast and

printed specimens. The calculation and procedure to find the fiber orientation are both described in Section 3.5.2. For both the F-0.25 and F-0.50 mixtures, the fiber orientation improved by printing the specimens. The results of these tests are shown in Figure 4.47. Printing the fibers increased the average fiber orientation from 0.19 to 0.21 for the 0.25% fibers and from 0.15 to 0.20 for the 0.50% fibers. This verifies that the extrusion process helps orient the fibers. If the extruder would have used a more pronounced reducer from the internal diameter to the nozzle, this may have even helped further increase the fiber orientation due to printing as the fibers would align themselves due to the boundary condition.

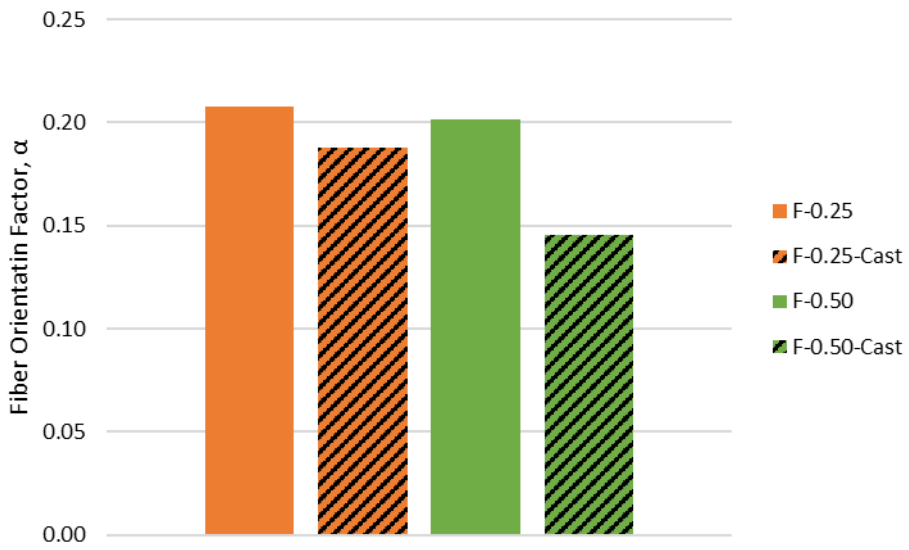

Figure 4.47. Fiber Orientation Factor for Printed versus Cast Beams

The failure-crack-pattern between the cast and printed beams also varied. For the cast beams, the crack was straight and continued to propagate vertically the entire time during loading. For the printed beams, the crack patterns slightly varied and were not 100% vertical. This variance in crack pattern was most likely due to the non-uniform

shape of the printed beam and the presence of multiple layers within the specimen. This nonuniformity caused differences in height across the beam and random locations of weakened layers due to the marco and micropores. When the crack would propagate, the internal cracks throughout the weakened sections would connect to form a curved crack pattern. The two main crack patterns observed for the printed beams are compared to the crack pattern of the cast beam in Figure 4.48. The crack pattern in (a) was consistent for all of the cast beams in which the crack propagation was vertical. The crack pattern in (b) was the most common crack pattern for the printed specimens in which the crack pattern had a degree of curvature as it propagated vertically. The crack pattern in (c) happened in a couple of the specimens. The cause for the crack pattern of (c) was most likely due to a weak bond in between layers which cause the crack to start propagating horizontally at the layer interface. A schematic is also shown in Figure 4.49.

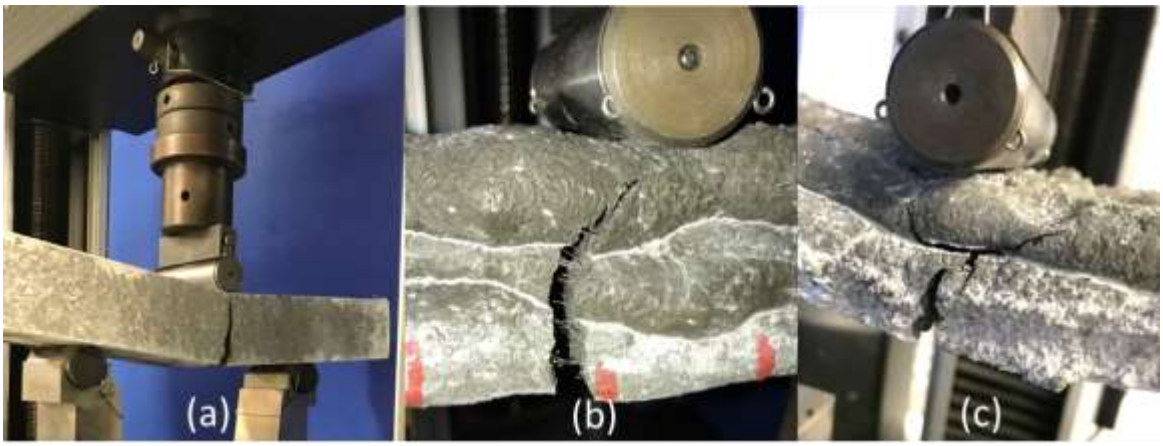

Figure 4.48. Crack Pattern Comparison Between Cast and Printed Beams

(a) Vertical Crack in Cast Beam

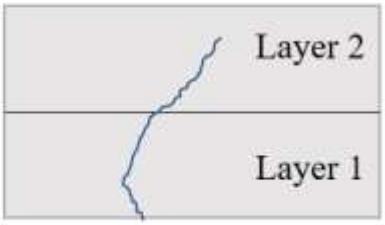

(b) Curved Crack Pattern

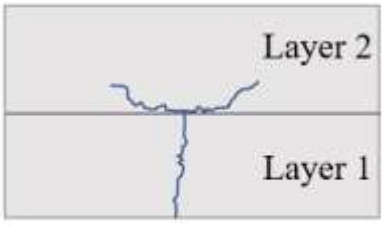

(c) Vertical Crack in Layer and Horizontal Crack at the Interface

Figure 4.49. Crack Pattern Schematic

5. CONCLUSION

5.1. SUMMARY

This study was done to take the first steps into developing a 3D printer for cement-based materials and create an understanding of some of benefits, challenges, and artifacts of printing, specifically in extrusion and flexural performance. First conventional cast-in-place fiber reinforced concrete was studied to understand the behavior, flexural properties, and post-crack properties. This study was done using both manufactured fibers and recycled fibers from scrap tires to look into an environmentally friendly option as a replacement for conventional manufactured fibers. Slump flow, compressive strength, modulus of elasticity, flexural strength, toughness, residual strength, and fracture energy were all investigated. The two fiber types were tested in three volume fractions and compared with a reference and hybrid mixture of the two fiber types.

After studying fiber-reinforced concrete, 3D printing was studied in detail investigating the current research and potential research areas. From this investigation, extrusion was chosen as the area of research due to it being the first process in printing and there being limited studies on extrusion for 3D printing cement-based materials. With fiber-reinforcement showing potential as reinforcement for printing, the flexural properties were also compared between printed and cast beams.

With limited studies on extrusion for printing, test methods were developed to investigate extrusion and the various parameters affecting extrusion. First, a blockage test was proposed to help develop successful mix design to look into the effects of extrusion. Blockage was studied by defining the blocking binder content for varying particle sizes

and workability. Fibers were attempted to be investigated, but the size of the current extrusion system led to blocking even at low fiber volumes. An extruder was designed and built for capabilities to test the extrudability of concrete and also be added as a modular head for a 1x1 meter 3D printer in the future. The extruder allowed for a ram extrusion test for 3D printing to be performed. A disc load cell measured the extrusion force throughout the constant displacement-controlled extrusion. Rheological properties were measured for the extrusion tests using a ConTec 6 Rheometer and mini-slump tests. This extrusion system allowed rheology, nozzle diameter size, and speed to be studied in terms of extrudability. Maximum extrusion force, average extrusion force, unit extrusion energy, and initial extrusion force were all analyzed for the three parameters stated. The extrusion process was also qualitatively looked at and issues faced during extrusion were described.

Flexural behavior was studied by comparing the behavior of cast-in-place beams to manually printed beams. The beams were tested using a three-point bending test. The beams were also analyzed after testing to compare the fiber orientation factor between the two methods. Flexural strength, toughness, residual strength, and fiber orientation were then compared between the beams.

5.2. CONCLUSIONS

From the study, several conclusions were able to be made about the use of recycled fibers as reinforcement, the extrusion test methods developed, blocking parameters, parameters effecting extrusion, and the flexural behavior of printed versus cast-in-place building methods.

1. Recycled Fiber versus Manufactured Fiber Behavior:
    a. The compressive strength of FRC for both the manufactured and recycled fibers did not improve, or slightly decreased the compressive strength of concrete.
    b. Both the use of manufactured fibers and recycled fibers do not affect the elastic modulus of concrete.
    c. The flexural behavior of FRC with recycled fibers showed a slight increase in flexural strength for the 0.75% mixture and slight decrease for the 0.50% and 0.25% mixtures. The main benefit of these fibers was in the increase in toughness and residual strength compared to the reference as expected. The recycled fibers compared similarly to the manufactured fibers in the post-peak performance. The toughness, residual strength, fracture energy, and CMOD behavior was within the same range as the manufactured fibers or even higher for some of the properties.
    d. For the hybrid mixture of manufactured and recycled fibers, the flexural performance outperformed the manufactured and recycled fiber mixtures with the same fiber volume fractions. This improvement in flexural properties could be due to the varying fiber size and length in the mixture that allows for a mixture of both micro, meso, and macro cracks to be bridged by the fibers.
2. Blockage Test Evaluation:
    a. The blockage test method proposed proves to successfully define blocking in an extruder by defining a maximum binder content that causes blocking. This

test can be used to develop successful mix designs for extrusion without blocking when comparing different particle sizes and workability levels.

b. Two different blocking mechanisms were noticed during testing. The first mechanism is a Homogenous Blocking Mechanism. This mechanism consists of a large quantity and accumulation of particle to cause blocking. The second mechanism is the Large Particle Blocking Mechanism. This mechanism consists of a couple large particles passing through the nozzle and causing blockage with a smaller number of particles. This mechanism causes the increase in binder content in the mix design to go from a linear to an exponential increase due to the random likeliness that a couple of large particles will block the extruder at lower binder contents.

c. For the current automated extrusion system (9 mm nozzle) the 13 mm long fibers could not be extruded even at low fiber volume fractions for high and low workability levels. Fibers longer than the nozzle opening cause blocking at the nozzle when oriented horizontally and diagonally as well as high accumulation of fibers oriented in the extrusion direction.

3. Ram Extrusion Test for Printing:

a. An extruder was successfully designed to be displacement controlled, use for variable size extruders up to 45 mm diameter, measure extrusion force, and have future capabilities to be added to a printing system. The extruder allowed for an investigation of effect of nozzle size, rheology, and extrusion rate on extrudability by comparing extrusion force and energy.

b. An increase in nozzle size or increase in nozzle size ratio (d/D) lead to decreased extrusion forces and unit extrusion energy. An increase in d/D ratio showed a high linear relationship when comparing the initial extrusion force F_y. This trend for extrusion force and energy was consistent for both high and low workability mixtures.

c. The effects of rheology on extrusion force and energy showed a direct correlation. The plastic viscosity between the low and high workability mixtures was about the same value, thus it can be concluded that the increase in yield stress increased the extrusion force and energy. This is shown by all of the graphs being shifted downward for the lower yield stress mixture while still following the same shape of the curve. With the initial extrusion force F_y showing a linear with similar slopes, it can also be noted that the F_y may be directly related to the yield stress of concrete. This would need to be further studied in a greater magnitude to verify.

d. An increase in extrusion rate lead to an increase in extrusion force and energy. With the increase in speed, the extrusion force was brought from a level that the extruder was able to extrude to a level where the motor could not extrude the mortar. Further testing would need to be done to quantify this increase from the change in extrusion rate by increasing the capacity the motor can push in the system or testing on a highly workable mixture.

e. High extrusion pressures due to low d/D ratios and high yield stress mixtures can lead to high rates of bleeding during extrusion. This can lead to a large increase in extrusion force and cause the mortar to go from a plastic to a soil

like consistency due to the consolidation from high pressures. This can be reduced by adjusting increasing the d/D ratio, lowering the yield stress, or increasing the bleeding resistance of concrete within the mix design.

4. Flexural Behavior between Cast and Printed Specimens
    a. The manually printed beams had a lower first-crack strength compared to the cast beams. This was due to increased voids due to the manual printing process as well as weakened bond between layers due to micopores and microchannels in the direction of bending as has been shown by Moini [30].
    b. The manually printed beams had an increased fiber orientation than the cast beams. This increased fiber orientation shows a benefit to printing and could even be further improved with a more precise extruder than the manual one used. Due to this increased fiber orientation, the printed beams had better toughness indices and residual strength. The high toughness and residual strength values of the show that fibers could be a good reinforcement in printing.

5.3. FUTURE WORK

This work being the initial startup on this 3D printing concrete project leads to several areas to further the work and studies on additive manufacturing. Future work contains two main areas that include further development of the 3D printing system and further studies into extrusion, blockage, and fiber reinforcement in printing.

1. Future Development of the 3D Printing System:

a. A 3D printing system using a XYZ linear motion table is being developed with the capability of adding the extruder to the system. Currently the 3D printing controller board and XYZ linear motion table is purchased. The 1x1 meter table is being set up and the controller board is being programmed to allow for printing.
b. The extruder is also being optimized. The steel plates are being replaced with equivalent aluminum plates to reduce the weight of the systems. Development work could also be done to create a graphic user interface (GUI) to allow for easier use of the extruder without knowledge of how the program works. Work could also be done to increase the capacity of the motor either with a different motor or addition of a gear system that would raise the working limit of the system and allow for higher yield stress materials or higher extrusion rates to be worked with.

2. Extrusion, Blockage, and Fiber Reinforcement:
    a. One area for future study would be to investigate the effect of packing density on extrusion and blockage to see how it effects extrusion force and if it would change the blocking point for a mixture.
    b. A workability box could also be made for extrusion to define the rheological properties that allow for extrusion. This would then also help characterize the effects of different constituents within the mix design on extrudability.
    c. Extrusion rate could be studied in more detail to quantify the effect in more detail by increasing the capacity of the system and lowering the extrusion force.

d. The effect of fibers on extrusion and characterizing the extrudability of FRC could be done by altering the current system to allow for printing fibers or using a different type of fiber.
e. Flexural properties could further be studied by looking at the effects of different types of fibers to see if the fiber orientation and post-crack properties also increase.
f. Beyond the study of extrudability and fibers as reinforcement, a transition from looking at extrudability to buildability could be done to tie the results together to get the full picture of 3D printing concrete in the fresh state.

APPENDIX A.

EXTRUDER DESIGN

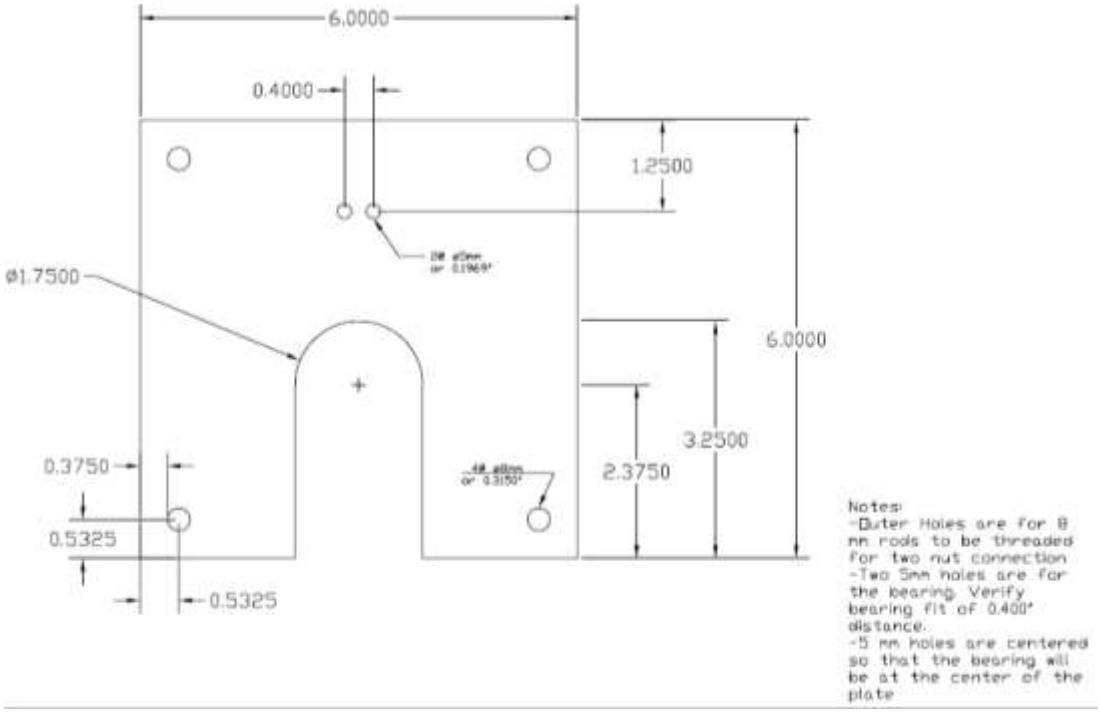

Figure A.1. Bottom Plate Design

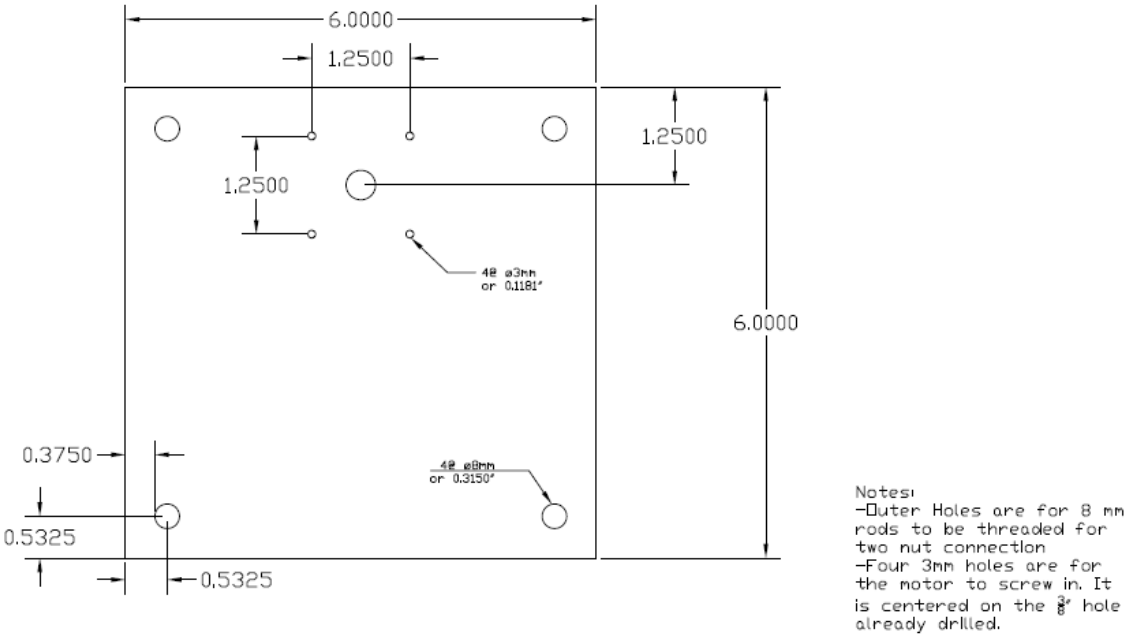

Figure A.2. Top Plate Design

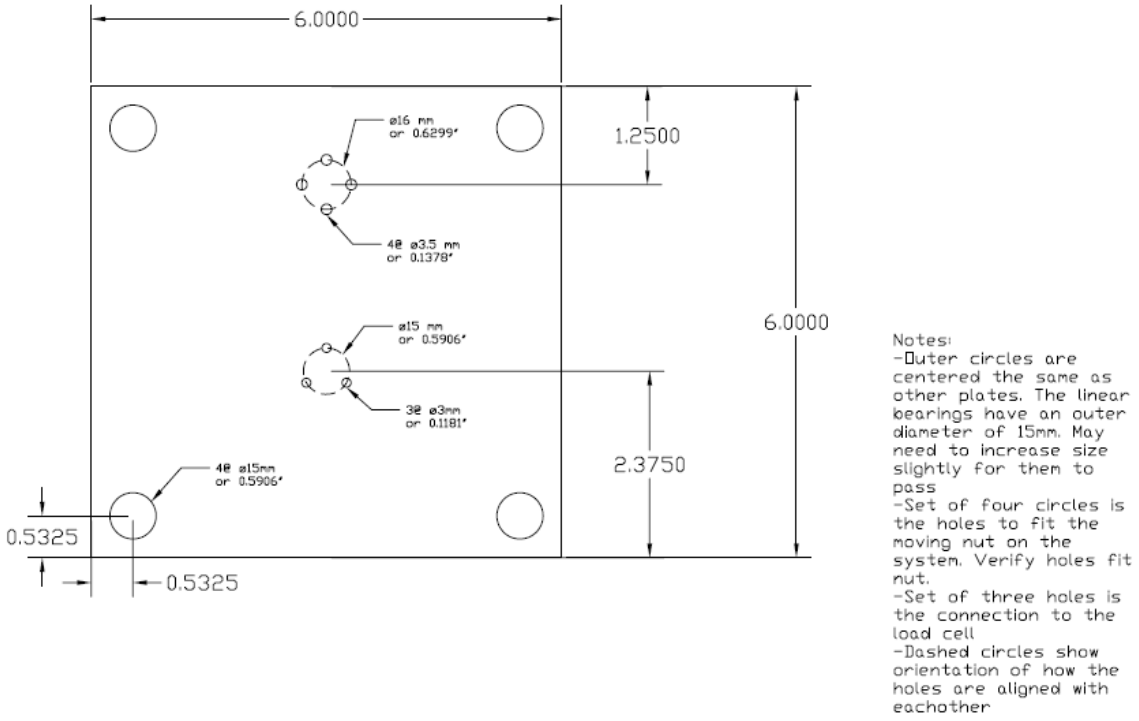

Figure A.3. Moving Plate Design

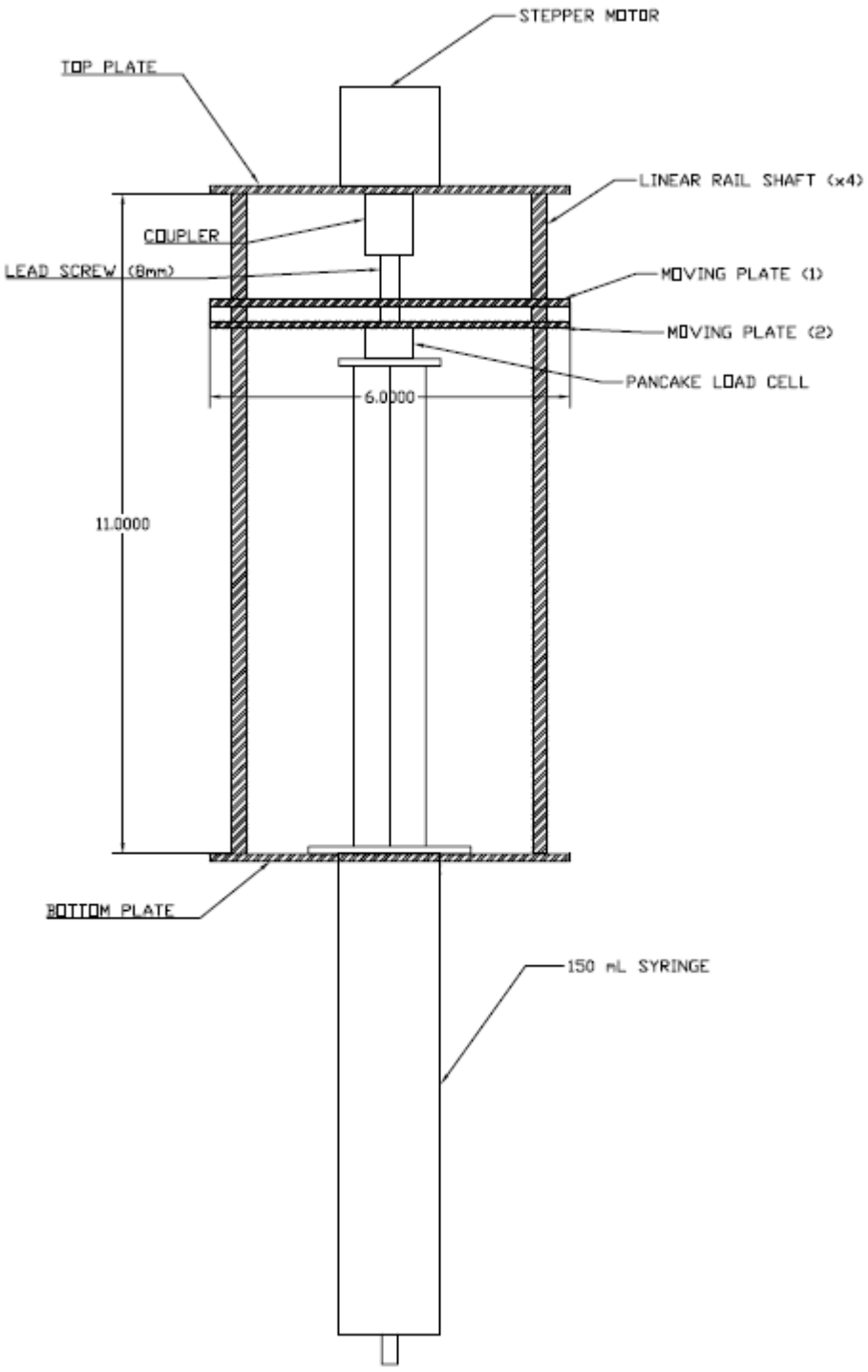

Figure A.4. Extruder Front View

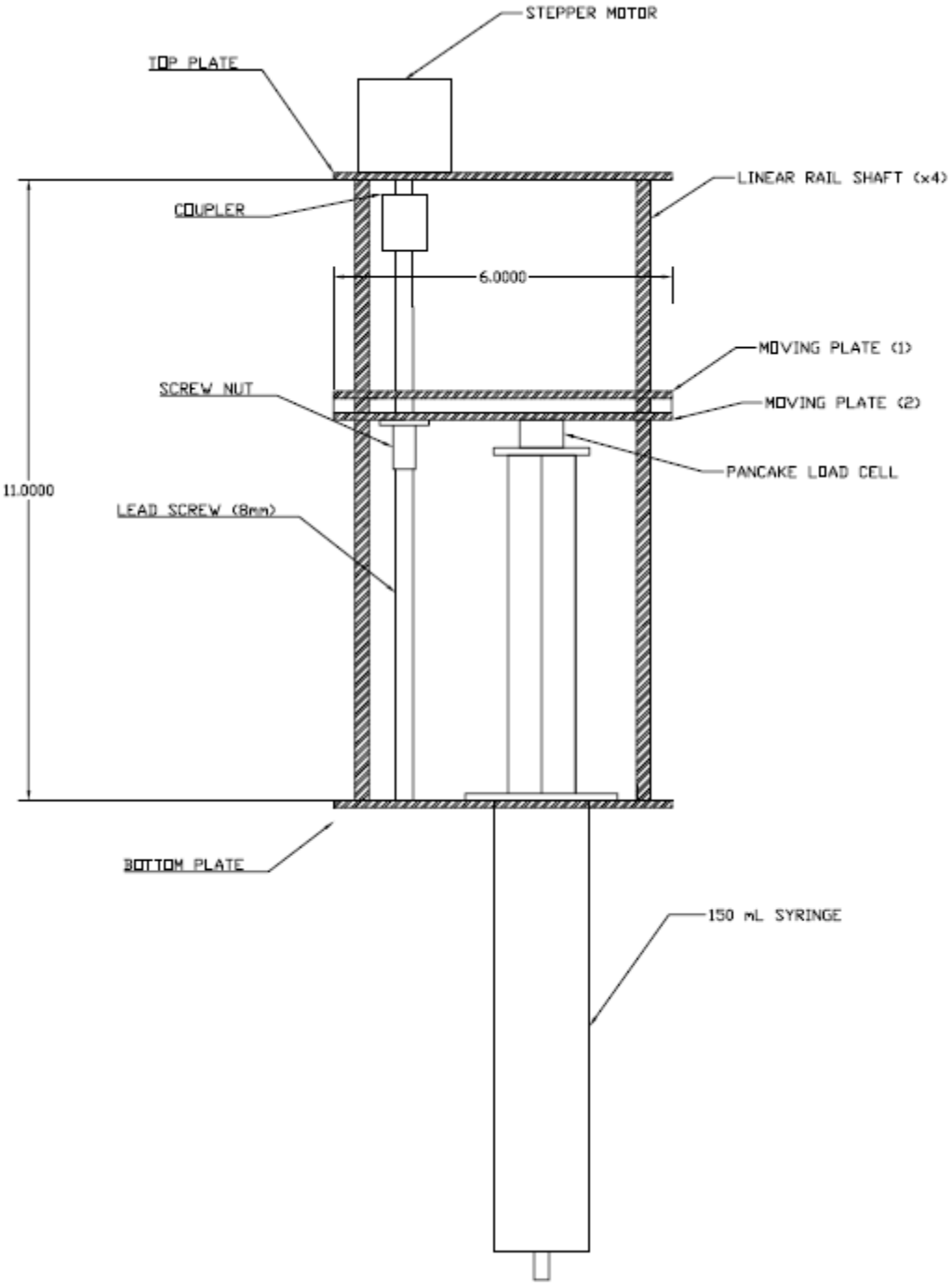

Figure A.5. Extruder Side View

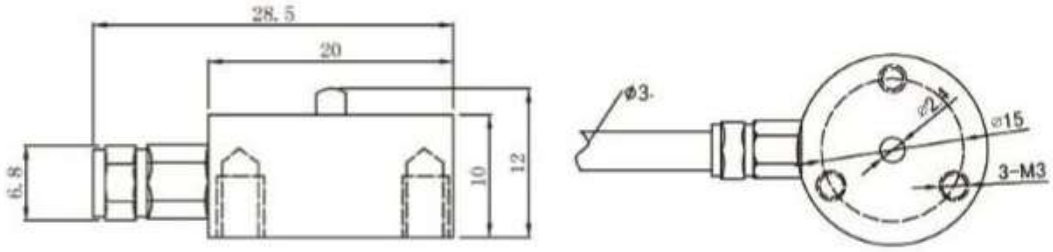

Specifications:		
capacity	kg	5,10,20,30,50,100,200,300,500
safe overload	%FS	120
ultimate overload	%FS	150
rated output	mV/V	1.5±0.5
excitation voltage	Vdc	5~15
combined error	%FS	±0.3
zero balance	%FS	± 0.1
non-linearity	%FS	± 0.3
hysteresis	%FS	± 0.3
repeatability	%FS	± 0.3
creep	%FS/30min	± 0.1
input resistance	Ω	385 ± 35
output resistance	Ω	350 ± 3
insulation resistance	MΩ	≥ 2000
operating temperature range	℃	-20 ~ +65
compensated temperature range	℃	-10 ~ +40
temperature coefficient of SPAN	%FS/10℃	± 0.3
temperature coefficient of ZERO	%FS/10℃	± 0.3
Electrical connection	cable	4 core shielded PVC cable, Ø3.0 × 2m
Wires connection	Excitation +: Red , Excitation -: Black, Output +:Green, Output-:White	

Figure A.6. Load Cell Specifications

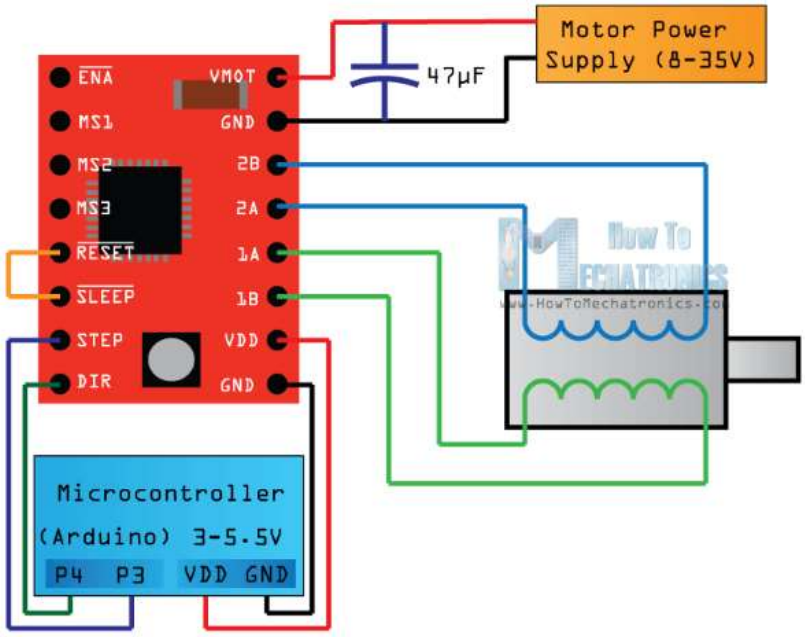

Figure A.7. Stepper Motor Circuit Diagram from [86]

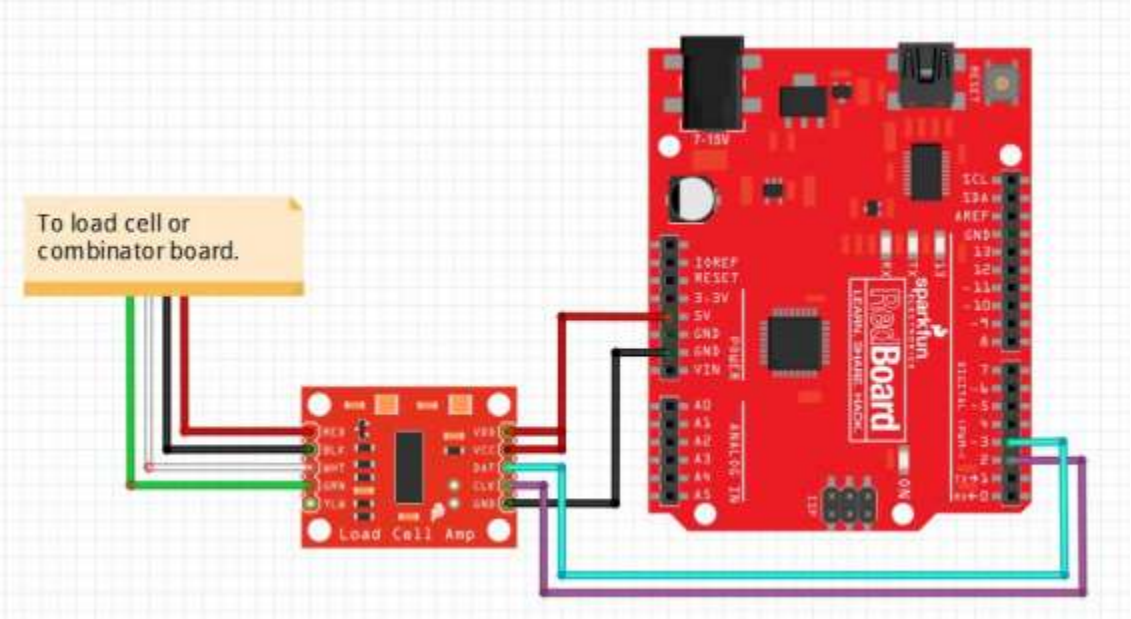

Figure A.8. Load Cell Circuit Schematic from [87]

APPENDIX B.

EXTRUDER CODE

Motor Control Code:

```
// defines pins numbers
const int stepPin = 3;
const int dirPin = 4;

void setup() {
  // Sets the two pins as Outputs
  pinMode(stepPin,OUTPUT);
  pinMode(dirPin,OUTPUT);

  //*****************************************************
  // input variables
  int motorSpeed = 14000; //speed for test 14000
  double angleOfRotation = 5250; // units are in degree (5250 for test)
  int direction1 = 1; // 0 is LOW and goes back towards the motor, 1 is HIGH and goes
forward to push the syringe

  //*****************************************************
  // code
  int rotation = int(angleOfRotation/360*200);
  digitalWrite(dirPin,1); // Enables the motor to move in a particular direction
  // Makes 200 pulses for making one full cycle rotation
  for(int x = 0; x < rotation; x++) {
    digitalWrite(stepPin,HIGH);
    delayMicroseconds(motorSpeed);
    digitalWrite(stepPin,LOW);
    delayMicroseconds(motorSpeed);
  }
  digitalWrite(dirPin,0); //Moves motor back to starting position
  for(int x = 0; x < rotation; x++) {
    digitalWrite(stepPin,HIGH);
    delayMicroseconds(1000);
    digitalWrite(stepPin,LOW);
    delayMicroseconds(1000);
  }
}
void loop() {
}
```

Load Cell Calibration Code [87]

```
#include "HX711.h"
#define DOUT  3
#define CLK  2

HX711 scale(DOUT, CLK);

float calibration_factor = -40900; //-7050 worked for my 440lb max scale setup

void setup() {
  Serial.begin(9600);
  Serial.println("HX711 calibration sketch");
  Serial.println("Remove all weight from scale");
  Serial.println("After readings begin, place known weight on scale");
  Serial.println("Press + or a to increase calibration factor");
  Serial.println("Press - or z to decrease calibration factor");

  scale.set_scale();
  scale.tare(); //Reset the scale to 0

  long zero_factor = scale.read_average(); //Get a baseline reading
  Serial.print("Zero factor: "); //This can be used to remove the need to tare the scale.
Useful in permanent scale projects.
  Serial.println(zero_factor);
}
void loop() {
  scale.set_scale(calibration_factor); //Adjust to this calibration factor

  Serial.print("Reading: ");
  Serial.print(scale.get_units(), 3);
  Serial.print(" lbs"); //Change this to kg and re-adjust the calibration factor if you follow
SI units like a sane person
  Serial.print(" calibration_factor: ");
  Serial.print(calibration_factor);
  Serial.println();
  if(Serial.available())
  {
    char temp = Serial.read();
    if(temp == '+' || temp == 'a')
      calibration_factor += 10;
    else if(temp == '-' || temp == 'z')
      calibration_factor -= 10;
  }
}
```

Load Cell Measurement Code

```
#include "HX711.h"

#define calibration_factor -42060.0 //This value is obtained using the
SparkFun_HX711_Calibration sketch

#define DOUT  3
#define CLK  2

HX711 scale(DOUT, CLK);

void setup() {
  Serial.begin(9600);
  Serial.println("HX711 scale demo");

  scale.set_scale(calibration_factor); //This value is obtained by using the
SparkFun_HX711_Calibration sketch
  scale.tare(); //Assuming there is no weight on the scale at start up, reset the scale to 0

  Serial.println("Readings:");
}

void loop() {
  delay(300);
  Serial.print("Reading: ");
  Serial.print(scale.get_units(), 2); //scale.get_units() returns a float
  Serial.print(" lbs"); //You can change this to kg but you'll need to refactor the
calibration_factor
  Serial.println();
}
```

BIBLIOGRAPHY

[1] "What is 3D Printing," 2019. [Online]. Available: https://3dprinting.com/what-is-3d-printing/.

[2] T. Wangler *et al.*, "Digital Concrete: Opportunities and Challenges," *RILEM Tech. Lett.*, vol. 1, p. 67, 2016.

[3] G. De Schutter, K. Lesage, V. Mechtcherine, V. N. Nerella, G. Habert, and I. Agusti-Juan, "Vision of 3D printing with concrete-Technical, economic, and environmental potentials," *Cem. Concr. Res.*, vol. 91, pp. 399–404, 2017.

[4] T. Salet, F. Bos, R. J. . Wolfs, and Z. Ahmed, "3D concrete printing- a structural engineering perspective," *High Tech Concr. where Technol. Eng. meet*, pp. xliii–lvii, 2017.

[5] R. A. Buswell, W. R. Leal de Silva, S. Z. Jones, and J. Dirrenberger, "3D printing using concrete extrusion: A roadmap for research," *Cem. Concr. Res.*, vol. 112, no. October 2017, pp. 37–49, 2018.

[6] T. A. M. Salet, Z. Y. Ahmed, F. P. Bos, and H. L. M. Laagland, "Design of a 3D printed concrete bridge by testing," *Virtual Phys. Prototyp.*, vol. 13, no. 3, pp. 222–236, 2018.

[7] "Contour Crafting," 2019. [Online]. Available: http://contourcrafting.com/.

[8] "Advanced Sustainable Material Management: 2014 Tables and Figures," 2016. [Online]. Available: www.epa.gov.EPA.

[9] T. R. Naik and F. Asce, "Sustainability of Concrete Construction," vol. 13, no. May, pp. 98–103, 2008.

[10] A. Kazemian, X. Yuan, E. Cochran, and B. Khoshnevis, "Cementitious materials for construction-scale 3D printing: Laboratory testing of fresh printing mixture," *Constr. Build. Mater.*, vol. 145, pp. 639–647, 2017.

[11] Y. Zhang, Y. Zhang, G. Liu, Y. Yang, M. Wu, and B. Pang, “Fresh properties of a novel 3D printing concrete ink,” *Constr. Build. Mater.*, vol. 174, pp. 263–271, 2018.

[12] A. Pierre, A. Perrot, and D. Rangeard, “Structural built-up of cement-based materials used for 3D- printing extrusion techniques,” *Mater. Struct.*, pp. 1213–1220, 2016.

[13] Y. W. D. Tay, G. H. A. Ting, Y. Qian, B. Panda, L. He, and M. J. Tan, “Time gap effect on bond strength of 3D-printed concrete,” *Virtual Phys. Prototyp.*, vol. 14, no. 1, pp. 104–113, 2019.

[14] T. T. Le, S. A. Austin, S. Lim, R. A. Buswell, A. G. F. Gibb, and T. Thorpe, “Mix design and fresh properties for high-performance printing concrete,” *Materials and Structures/Materiaux et Constructions*, vol. 45, no. 8. pp. 1221–1232, 2012.

[15] R. Lediga and D. Kruger, “Optimizing Concrete Mix Design for Application in 3D Printing Technology for the Construction Industry,” *Solid State Phenom.*, vol. 263, pp. 24–29, 2017.

[16] Y. Weng, M. Li, M. J. Tan, and S. Quian, “Design 3D printing cementitious materials via Fuller Thompson theory and Marson-Percy model,” *Constr. Build. Mater.*, no. 163, pp. 600–610, 2018.

[17] B. Boulekbache, M. Hamrat, M. Chemrouk, and S. Amziane, “Flowability of fibre-reinforced concrete and its effect on the mechanical properties of the material,” *Constr. Build. Mater.*, vol. 24, no. 9, pp. 1664–1671, 2010.

[18] M. Hambach and D. Volkmer, “Properties of 3D-printed fiber-reinforced Portland cement paste,” *Cem. Concr. Compos.*, vol. 79, pp. 62–70, 2017.

[19] B. Panda, S. Chandra Paul, and M. Jen Tan, “Anisotropic mechanical performance of 3D printed fiber reinforced sustainable construction material,” *Mater. Lett.*, vol. 209, pp. 146–149, 2017.

[20] J. Yu and C. K. Y. Leung, “Impact of 3D printing direction on mechanical performance of strain-hardening cementitious composite (SHCC),” *RILEM Bookseries*, vol. 19, pp. 255–265, 2019.

[21] S. Christ, M. Schnabel, E. Vorndran, J. Groll, and U. Gbureck, “Fiber reinforcement during 3D printing,” *Mater. Lett.*, no. 139, pp. 165–168, 2015.

[22] D. G. Soltan and V. C. Li, “A self-reinforced cementitious composite for building-scale 3D printing,” *Cement and Concrete Composites*, vol. 90. pp. 1–13, 2018.

[23] H. Ogura, V. N. Nerella, and V. Mechtcherine, “Developing and Testing of Strain-Hardening Cement-Based Composites (SHCC) in the Context of 3D-Printing,” *Materials (Basel).*, vol. 11, no. 1375, pp. 1–18, 2018.

[24] R. Kuo and R. Rael, “ARC Fellows: 3D Printed Concrete for Building Structure and Construction,” 2016. [Online]. Available: http://arts.berkeley.edu/arc-fellows-3d-printed-concrete-for-building-structure-and-construction/.

[25] W. R. Leal da Silva, “3D Concrete Printing-Technological issues in concrete mix design and extrusion,” *Danish Technological Institute*, 2017. [Online]. Available: https://www.dti.dk/projects/3d-printed-buildings/36993.

[26] V. N. Nerella, M. Nather, A. Iqbal, M. Butler, and V. Mechtcherine, “Inline quantification of extrudability of cementitious materials for digital construction,” *Cem. Concr. Compos.*, 2018.

[27] S. Lim *et al.*, “Development of a Viable Concrete Printing Process,” pp. 665–670.

[28] R. J. M. Wolfs, F. P. Bos, and T. A. M. Salet, “Early age mechanical behaviour of 3D printed concrete: Numerical modelling and experimental testing,” *Cem. Concr. Res.*, vol. 106, no. January, pp. 103–116, 2018.

[29] B. Zareiyan and B. Khoshnevis, “Effects of interlocking on interlayer adhesion and strength of structures in 3D printing of concrete,” *Autom. Constr.*, vol. 83, no. August, pp. 212–221, 2017.

[30] M. Moini, J. Olek, B. Magee, P. Zavattieri, and J. Youngblood, “Additive manufacturing and characterization of architectured cement-based materials via X-ray micro-computed tomography,” *RILEM Bookseries*, vol. 19, pp. 176–189, 2019.

[31] M. Moini, J. Olek, J. P. Youngblood, B. Magee, and P. D. Zavattieri, “Additive Manufacturing and Performance of Architectured Cement-Based Materials,” *Adv. Mater.*, vol. 30, no. 43, 2018.

[32] N. A. Libre, M. Shekarchi, M. Mahoutian, and P. Soroushian, “Mechanical properties of hybrid fiber reinforced lightweight aggregate concrete made with natural pumice,” *Constr. Build. Mater.*, vol. 25, no. 5, pp. 2458–2464, 2011.

[33] R. S. Olivito and F. A. Zuccarello, “An experimental study on the tensile strength of steel fiber reinforced concrete,” *Compos. Part B Eng.*, vol. 41, no. 3, pp. 246–255, 2010.

[34] A. G. Graeff, K. Pilakoutas, K. Neocleous, and M. V. N. N. Peres, “Fatigue resistance and cracking mechanism of concrete pavements reinforced with recycled steel fibres recovered from post-consumer tyres,” *Eng. Struct.*, vol. 45, pp. 385–395, 2012.

[35] H. Tlemat, K. Pilakoutas, and K. Neocleous, “Stress-strain characteristic of SFRC using recycled fibres,” *Mater. Struct. Constr.*, vol. 39, no. 287, pp. 365–377, 2006.

[36] K. Neocleous, H. Tlemat, and K. Pilakoutas, “Design Issues for Concrete Reinforced with Steel Fibers, Including Fibers Recovered from Used Tires,” *J. Mater. Civ. Eng.*, vol. 18, no. 5, pp. 677–685, 2006.

[37] H. Zhu, C. Li, M. Wu, M. Yan, and Z. Jiang, “Persistence of Strength/Toughness in Modified-Olefin-Fiber- and Hybrid-Fiber-Reinforced Concrete,” *J. Test. Eval.*, vol. 45, no. 6, p. 20150313, 2017.

[38] H. R. Pakravan, M. Latifi, and M. Jamshidi, “Hybrid short fiber reinforcement system in concrete: A review,” *Constr. Build. Mater.*, vol. 142, pp. 280–294, 2017.

[39] Y. Mohammadi, S. P. Singh, and S. K. Kaushik, “Properties of steel fibrous concrete containing mixed fibres in fresh and hardened state,” *Constr. Build. Mater.*, vol. 22, no. 5, pp. 956–965, 2008.

[40] N. Buratti, C. Mazzotti, and M. Savoia, “Post-cracking behaviour of steel and macro-synthetic fibre-reinforced concretes,” *Constr. Build. Mater.*, vol. 25, no. 5, pp. 2713–2722, 2011.

[41] G. Centonze, M. Leone, and M. A. Aiello, “Steel fibers from waste tires as reinforcement in concrete: A mechanical characterization,” *Constr. Build. Mater.*, vol. 36, pp. 46–57, 2012.

[42] E. Martinelli, A. Caggiano, and H. Xargay, “An experimental study on the post-cracking behaviour of Hybrid Industrial/Recycled Steel Fibre-Reinforced Concrete,” *Constr. Build. Mater.*, vol. 94, pp. 290–298, 2015.

[43] O. Sengul, “Mechanical behavior of concretes containing waste steel fibers recovered from scrap tires,” *Constr. Build. Mater.*, vol. 122, pp. 649–658, 2016.

[44] A. Caggiano, H. Xargay, P. Folino, and E. Martinelli, “Experimental and numerical characterization of the bond behavior of steel fibers recovered from waste tires embedded in cementitious matrices,” *Cem. Concr. Compos.*, vol. 62, pp. 146–155, 2015.

[45] ASTM C1018-97, “Standard Test Method for Flexural Toughness and First-Crack Strength of Fiber-Reinforced Concrete (Using Beam With Third-Point Loading),” vol. 04, no. October, pp. 1–8, 1998.

[46] N. Roussel *et al.*, *Understanding the rheology of concrete*. Woodhead Publishing, 2012.

[47] A. Gregori, Z. Sun, and S. P. Shah, “Rheological Method to Evaluate Structural Buildup,” *ACI Mater. J.*, vol. 104, no. 3, pp. 242–250, 2007.

[48] O. H. Wallevik and J. E. Wallevik, “Rheology as a tool in concrete science: The use of rheographs and workability boxes,” *Cem. Concr. Res.*, vol. 41, no. 12, pp. 1279–1288, 2011.

[49] S. C. Paul, “Properties of 3D Printable Concrete,” *ProfAM Conf.*, no. January, pp. 16–19, 2017.

[50] D. Feys, R. Cepuritis, S. Jacobsen, K. Lesage, E. Secrieru, and A. Yahia, “Measuring Rheological Properties of Cement Pastes: Most common Techniques, Procedures and Challenges,” *RILEM Tech. Lett.*, vol. 2, pp. 129–135, 2017.

[51] O. H. Wallevik, D. Feys, J. E. Wallevik, and K. H. Khayat, “Avoiding inaccurate interpretations of rheological measurements for cement-based materials,” *Cem. Concr. Res.*, vol. 78, pp. 100–109, 2015.

[52] A. Yahia and K. H. Khayat, “Applicability of rheological models to high-performance grouts containing supplementary cementitious materials and viscosity enhancing admixture,” *Mater. Struct.*, vol. 36, no. July, pp. 402–412, 2003.

[53] N. Roussel and P. Coussot, “‘ Fifty-cent rheometer ’ for yield stress measurements :,” *J. Rheol. (N. Y. N. Y).*, vol. 49, no. 3, pp. 705–718, 2005.

[54] N. Roussel, “Correlation between yield stress and slump : Comparison between numerical simulations and concrete rheometers results,” *Mater. Struct.*, pp. 501–509, 2006.

[55] R. Le Roy and N. Roussel, “The Marsh Cone as a viscometer: theoretical analysis and practical limits,” vol. 38, pp. 25–30, 2005.

[56] K. H. Khayat and Y. Roussel, “Testing and performance of fiber-reinforced, self-consolidating concrete,” *Mater. Struct. Constr.*, vol. 33, no. July, pp. 391–397, 2000.

[57] L. Martinie, P. Rossi, and N. Roussel, “Rheology of fiber reinforced cementitious materials: classification and prediction,” *Cem. Concr. Res.*, vol. 40, no. 2, pp. 226–234, 2010.

[58] A. Emdadi, I. Mehdipour, N. A. Libre, and M. Shekarchi, “Optimized workability and mechanical properties of FRCM by using fiber factor approach: theoretical and experimental study,” *Mater. Struct. Constr.*, vol. 48, no. 4, pp. 1149–1161, 2015.

[59] I. Mehdipour and N. A. Libre, “Linking fiber factor to material performance of fiber-reinforced self-consolidating cement-based materials,” *ACI Mater. J.*, vol. 114, no. 1, pp. 77–91, 2017.

[60] D. Malaszkiewicz, “Influence of polymer fibers on rheological properties of cement mortars,” *Open Eng.*, vol. 7, no. 1, pp. 228–236, 2017.

[61] G. Krage and O. H. Wallevik, “Rheology of Synthetic-Fiber Reinforced Scc,” in *5th International RILEM Symposium on Self-Compacting Concrete*, 2007, no. September, pp. 347–352.

[62] Y. Ding, S. Liu, Y. Zhang, and A. Thomas, “The investigation on the workability of fibre cocktail reinforced self-compacting high performance concrete,” *Constr. Build. Mater.*, vol. 22, no. 7, pp. 1462–1470, 2008.

[63] T. Ponikiewski and J. Katzer, “Fresh mix characteristics of self-compacting concrete reinforced by fibre,” *Period. Polytech. Civ. Eng.*, vol. 61, no. 2, pp. 226–231, 2017.

[64] N. Roussel, “Rheological requirements for printable concretes,” *Cem. Concr. Res.*, vol. 112, no. May, pp. 76–85, 2018.

[65] K. G. Kuder and S. P. Shah, “Rheology of extruded cement-based materials,” *ACI Mater. J.*, vol. 104, no. 3, pp. 283–290, 2007.

[66] N. Roussel and F. Cussigh, “Distinct-layer casting of SCC : The mechanical consequences of thixotropy,” vol. 38, pp. 624–632, 2008.

[67] A. Perrot, C. Lanos, P. Estellé, and Y. Melinge, “Ram extrusion force for a frictional plastic material: Model prediction and application to cement paste,” *Rheol. Acta*, vol. 45, no. 4, pp. 457–467, 2006.

[68] A. Perrot, Y. Mélinge, D. Rangeard, F. Micaelli, P. Estellé, and C. Lanos, “Use of ram extruder as a combined rheo-tribometer to study the behaviour of high yield stress fluids at low strain rate,” *Rheol. Acta*, vol. 51, no. 8, pp. 743–754, 2012.

[69] A. Perrot, D. Rangeard, Y. Melinge, P. Estelle, and C. Lanos, “Extrusion Criterion for Firm Cement-Based Materials,” *Appl. Rheol.*, vol. 19, no. 5, 2009.

[70] Z. Toutou, N. Roussel, and C. Lanos, “The squeezing test: A tool to identify firm cement-based material’s rheological behaviour and evaluate their extrusion ability,” *Cem. Concr. Res.*, vol. 35, no. 10, pp. 1891–1899, 2005.

[71] Y. Chen, L. J. Struble, and G. H. Paulino, “Extrudability of Cement-Based Materials,” *Am. Ceram. Soc. Bull.*, pp. 9101–9104, 2006.

[72] A. Peled and S. Shah, “Processing Effects in Cementitious Composites: Extrusion and Casting,” *J. Mater. Civ. Eng.*, vol. 15, no. 2, pp. 192–199, 2003.

[73] ASTM C403/C403M-16, “Standard Test Method for Time of Setting of Concrete Mixtures by Penetration Resistance.” ASTM, pp. 1–7, 2016.

[74] ASTM C33-03, “Standard Specification for Concrete Aggregates,” *ASTM Int’l*, 2003.

[75] ASTM C39-04a, “Compressive Strength of Cylindrical Concrete Specimens,” pp. 1–14, 2007.

[76] ASTM C469-02, “Standard Test Method for Static Modulus of Elasticity and Poisson ’ s Ratio of Concrete,” vol. 04, pp. 1–5, 2002.

[77] ASTM C494/C494M-17, “Standard Specification for Chemical Admixtures for Concrete,” pp. 1–10, 2017.

[78] ASTM C136/C136M-14, “Standard Test Method for Sieve Analysis of Fine and Coarse Aggregates,” pp. 1–5, 2014.

[79] ASTM C1437-15, “Standard Test Method for Flow of Hydraulic Cement Mortar,” *ASTM Int’l*, pp. 6–7, 2015.

[80] S. Printing, “Discov3ry Paste Extruder,” 2019. [Online]. Available: https://www.structur3d.io/discov3ry-2-complete.

[81] ASTM C305-14, “Standard Practice for Mechanical Mixing of Hydraulic Cement Pastes and Mortars of Plastic Consistency,” pp. 14–16, 2014.

[82] ASTM C109-16a, “Standard Test Method for Compressive Strength of Hydraulic Cement Mortars (Using 2-in . or [50-mm] Cube Specimens),” *ASTM Int’l*, pp. 1–10, 2019.

[83] ASTM C78-02, “Standard Test Method for Flexural Strength of Concrete (Using Simple Beam with Third-Point Loading).” pp. 1–3.

[84] RILEM TC 50, “Determination of the fracture energy of mortar and concrete by means of three-point bending on notched beams.” .

[85] T. Almusallam, S. M. Ibrahim, Y. Al-Salloum, A. Abadel, and H. Abbas, “Analytical and experimental investigations on the fracture behavior of hybrid fiber reinforced concrete,” *Cem. Concr. Compos.*, vol. 74, pp. 201–217, 2016.

[86] Dejan, “How To Control a Stepper Motor with A4988 Driver and Arduino,” *How To Mechatronics*. [Online]. Available: https://howtomechatronics.com/tutorials/arduino/how-to-control-stepper-motor-with-a4988-driver-and-arduino/.

[87] N. Seidle, “Load Cell Amplifier HX711 Breakout Hookup Guide,” *Sparkfun*. [Online]. Available: https://learn.sparkfun.com/tutorials/load-cell-amplifier-hx711-breakout-hookup-guide/all#introduction.

VITA

Jonathan Thomas Kuchem was born in Washington, Missouri. He graduated with his Bachelors of Science degree in Civil Engineering in May of 2018 from Missouri University of Science and Technology. He continued his education at Missouri University of Science and Technology and graduated with his Masters of Science in Civil Engineering with an emphasis in Structural Engineering in July of 2019. Jonathan was a Greenberg Scholar, which allowed him to earn his Master's degree in an accelerated program.